

**UCLA**

**UCLA Electronic Theses and Dissertations**

**Title**

Electrowetting, Electrodeposition, and Electronic Control System for Digital Microfluidics

**Permalink**

<https://escholarship.org/uc/item/8h29k7ff>

**Author**

Li, Jia

**Publication Date**

2019

Peer reviewed|Thesis/dissertation

UNIVERSITY OF CALIFORNIA

Los Angeles

Electrowetting, Electrodeposition, and Electronic Control System for Digital Microfluidics

A dissertation submitted in partial satisfaction of the  
requirements for the degree Doctor of Philosophy  
in Mechanical Engineering

by

Jia Li

2019

© Copyright by

Jia Li

2019

## ABSTRACT OF THE DISSERTATION

Electrowetting, Electrodeposition, and Electronic Control System for Digital Microfluidics

by

Jia Li

Doctor of Philosophy in Mechanical Engineering

University of California, Los Angeles, 2019

Professor Chang-Jin Kim, Chair

For electrowetting-on-dielectric (EWOD) devices, which are most commonly used for digital (droplet) microfluidics, the reliability issues, such as electric breakdown of the dielectric layer, electric charging of the hydrophobic topcoat, and uniformity of the device surface, make their applications and commercialization much more challenging and expensive than originally anticipated. While trying to overcome the reliability issues of EWOD, we discover a new microscale liquid handling mechanism, which we name “electrodeposition”, that works in a manner opposite to electrowetting. Without the need of dielectric layer or hydrophobic topcoat, electrodeposition is not only free from the reliability issues of EWOD but also much simpler to fabricate. Using only 5 V, we were able to move, split, merge, and generate droplets on an open device configuration in air without using the cover plate or oil environment.

The history of EWOD research and commercialization over the last two decades has shown that a success requires not only proper background and expertise in the science and engineering of EWOD but also adequate resources and facilities for fabricating and operating EWOD devices. Unfortunately, these resources and facilities are not available to most researchers and groups, especially outside engineering. To help EWOD realize its inherent potential and boost the field of digital microfluidics for wide acceptance, in this dissertation we propose and start what we call “cybermanufacturing ecosystem” that will empower the mass, who know little about EWOD design, fabrication, and operation, to utilize digital microfluidics through webservices. The goal of the cybersystem is for a user to design an EWOD device within hours instead of weeks and order their design to be fabricated as an actual device by a foundry service. For testing the EWOD devices, we have developed an electronic control system with which users can not only operate but also debug their EWOD devices.

The dissertation of Jia Li is approved.

Pei-Yu Chiou

Xiaochun Li

Chih-Kong Ken Yang

Chang-Jin Kim, Committee Chair

University of California, Los Angeles

2019

# TABLE OF CONTENT

ABSTRACT OF THE DISSERTATION .....	ii
TABLE OF CONTENT .....	v
LIST OF FIGURES .....	viii
LIST OF TABLES .....	xi
ACKNOWLEDGEMENTS .....	xii
VITA .....	xiv
Chapter 1 Introduction .....	1
1.1 The birth and the growth of EWOD .....	1
1.2 The commercialization status of EWOD .....	2
1.2.1 The liquid lens .....	3
1.2.2 The reflective display .....	4
1.2.3 Digital microfluidics for biochemical assays .....	6
1.2.4 Other companies and products .....	9
1.2.5 Summarize for commercialization status of EWOD .....	10
1.3 Bottlenecks limit a stronger growth of EWOD digital microfluidics .....	11
1.4 Scope of research: two approaches for solving the limitations of EWOD.....	12
1.5 References .....	13
Chapter 2 Electrodewetting .....	17
2.1 Introduction .....	17
2.1.1 Eliminate the dielectric and hydrophobic layer of an EWOD device .....	17
2.1.2 The concept of “electrodewetting” .....	18
2.1.3 The electrically-induced dewetting phenomenon.....	19
2.2 Electrodewetting mechanism .....	19
2.2.1 The surfactant-mediated electrodewetting mechanism .....	19
2.2.2 Verification of the mechanism by three experiments.....	20
2.2.3 Surfactant distribution on substrate .....	25
2.3 Key performance of electrodewetting .....	26
2.3.1 High reversibility .....	26
2.3.2 Resistance to high current.....	27
2.3.3 Bistability.....	29
2.4 Characterization of electrodewetting .....	32

2.4.1 Effect of surfactant type, surfactant concentration and voltage .....	32
2.4.2 Other working conditions .....	37
2.4.3 Contact angle measurement method.....	39
2.5 Electrodewetting Device .....	42
2.5.1 Open air device configuration .....	42
2.5.2 Electrodewetting device made on silicon .....	44
2.5.3 Electrodewetting device made on glass.....	46
2.6 Summary .....	47
2.7 References .....	48
Chapter 3 Cybermanufacturing Ecosystem for Digital Microfluidics .....	51
3.1 The background and motivation.....	51
3.2 Cybermanufacturing ecosystem architecture .....	52
3.3 The EWOD CAD .....	54
3.4 The EWOD foundry service.....	56
3.5 The online portal (the design) .....	57
3.6 Summary .....	64
3.7 References .....	64
Chapter 4 A USB-powered smartphone-size electronic control system for digital microfluidics devices   66	
4.1 The market need.....	66
4.2 Approaches for EWOD control circuits .....	67
4.3 The electronic control system developed.....	69
4.3.1 Overall description of the system .....	69
4.3.2 The control circuits and PCB.....	71
4.3.3 The alignment and interfacing of EWOD device .....	72
4.3.4 The graphic user interface (GUI).....	74
4.4 Summary .....	76
4.5 References .....	77
Chapter 5 Low-cost and Low-topography Fabrication of Multilayer Interconnections for Microfluidic Devices .....	79
5.1 Introduction .....	79
5.2 Fabrication processes .....	80
5.3 Confirmation of partial and full anodization.....	84



5.4 Application to EWOD microfluidic devices .....	86
5.5 Summary .....	90
5.6 References .....	91
Chapter 6 Summaries and Future Directions .....	92
6.1 Dissertation Summaries.....	92
6.2 Future research directions .....	93

## LIST OF FIGURES

Figure 1-1. The numbers of search result in Google Scholar for the term “electrowetting” in papers and patents. ....	2
Figure 1-2. History of the liquid lens business. ....	4
Figure 1-3. History of electrowetting-based reflective display business. ....	6
Figure 1-4. History of digital microfluidics business. ....	7
Figure 1-5. Technical barrier and reliability issues are two major bottlenecks that limit the growth of electrowetting community. ....	11
Figure 2-1. The concept of electrodedewetting. ....	18
Figure 2-2. The surfactant-mediated electrodedewetting mechanism proposed and studied with a wire-inserted sessile drop on a conductive, hydrophilic substrate. ....	20
Figure 2-3. Confocal microscopic images showing redistribution of fluorescent ionic surfactant (R18) under electrodedewetting voltage ....	21
Figure 2-4. Steam condensation images reveal the wettable state of the substrate after blowing away (in the direction of the blue arrow) a water droplet containing DTAB. ....	22
Figure 2-5. Surfactant concentration on substrate surface during electrodedewetting and reverse electrodedewetting revealed by a blow-off test. ....	24
Figure 2-6. The condensation test result matches the fluorescent test result. ....	26
Figure 2-7. Setup for electrodedewetting longevity test. ....	26
Figure 2-8. Screenshots of a droplet that was under electrodedewetting switching for over $10^4$ cycles, or 6 hours. ....	27
Figure 2-9. Despite usual operating current is small ( $3\ \mu\text{A}$ ), electrodedewetting still works under 1000X current ( $3\ \text{mA}$ ) when significant electrolysis occurs on the needle and the substrate. ....	28
Figure 2-10. EWOD depends on electric field builds up across the dielectric layer while the electrodedewetting depends on electric field builds up across the droplet. ....	29
Figure 2-11. Switching between electrodedewetting, neutral, and actively-recovered wetting state experimentally confirmed for droplets containing DTAB (cationic surfactant) and SDS (anionic surfactant) on a bare silicon wafer. ....	31
Figure 2-12. For cationic surfactant such as DTAB, the autophobing effect is eliminated at low pH. ....	33

Figure 2-13. Effect of surfactant concentration and actuation voltage on electrodedewetting. ....	35
Figure 2-14. Effect of surfactant concentration and actuation voltage (i.e., Figure 2-13) shown separately for each surfactant to include error bars or all data.....	37
Figure 2-15. Electrodedewetting confirmed for a variety of liquids on bare silicon.....	37
Figure 2-16. The effect of pH on electrodedewetting, obtained for DTAB. ....	38
Figure 2-17. Contact angle measurement setup with a wire-droplet system for the current study. ....	41
Figure 2-18. Method for detecting droplet-substrate-contact-line for automatic contact angle measurement.....	42
Figure 2-19. A droplet over two electrodes is moved by electrodedewetting.....	43
Figure 2-20. Electric actuation of a droplet atop two adjacent electrodes explained with an imaginary top wire, assuming a cationic surfactant. ....	43
Figure 2-21. Fabrication process of the electrodedewetting device used to demonstrate the digital microfluidic operations in this study (drawn not to scale). ....	45
Figure 2-22. Droplet generation, transportation, and splitting realized by electrodedewetting. ....	46
Figure 2-23. Fabrication process of transparent electrodedewetting device. ....	47
Figure 2-24. Sequential images showing a droplet of surfactant-containing DI water being split on the transparent device (with no cover plate) in air. ....	47
Figure 3-1. Inspired by how the operating systems (OS) of Windows and Macintosh flourished the PC industry, the cybermanufacturing ecosystem (also referred to as “cybersystem” in this manuscript) aims to boost the field of digital microfluidics by letting people, who know little about EWOD design, fabrication and operation, utilize digital microfluidics as a convenient liquid handling platform.....	52
Figure 3-2. The architecture of cybermanufacturing ecosystem. ....	53
Figure 3-3. Our current version of EWOD CAD greatly reduces the time needed in designing an EWOD device by offering pre-defined EWOD electrode shapes and auto-routing of the traces.....	55
Figure 3-4. A mock page for the portal website which clearly lists and links to the major services of the cybermanufacturing system: the EWOD CAD, foundry service and EWOD electronic control system.....	59
Figure 3-5. A mock page displaying the thumbnails of the design files generated by different users.....	60

Figure 3-6. A mock page where a user is able to configure the order before sending it for manufacturing.....	61
Figure 3-7. A mock page of the online storefront for the EWOD control system and the general-purpose EWOD device made on glass (bottom left) and on silicon substrate (bottom right). .....	63
Figure 4-1. The control circuits allow users to provide DC or AC signals (with tunable amplitude and frequency) to the individual electrodes independently.....	68
Figure 4-2. Our electronic control system for digital microfluidics consists of three major components: the control circuits, the device interface, and GUI. ....	70
Figure 4-3. The electronic circuits and device interfaces revealed by removing the aluminium chassis from the system. ....	71
Figure 4-4. The system includes a unique mechanism to align the device to system quickly and conveniently for accurate interfacing. ....	73
Figure 4-5. The system can operate devices with a range of thicknesses and sizes. ....	74
Figure 4-6. User can custom the mapping between the buttons on the GUI and the electrodes on a EWOD device.....	75
Figure 4-7. An actuation sequence contains thousands of states. The states are executed sequentially.....	76
Figure 5-1. Process flow to fabricate the proposed multilevel interconnections, drawn for three layers. ....	82
Figure 5-2. Resistance measurement for each layer. ....	86
Figure 5-3. The proposed multilayer interconnection technology applied to EWOD devices as a demonstration. ....	88
Figure 5-4. Digital microfluidic operations on an EWOD device with 3-layer interconnections.	89

## **LIST OF TABLES**

Table 3-1. Comparison between EWOD devices made of various substrates..... 57

## ACKNOWLEDGEMENTS

I would like to express my deepest thanks to my Ph.D. advisor, Professor CJ Kim. In my early years under his guidance, I always admired his capability to quickly identify key issues in one's presentation and initiate profound discussions. Later on, especially in the 5<sup>th</sup> year, I was delighted to find out that I could do the same. I am very grateful that in a continuous effort by Prof. CJ Kim, I gradually grew to be a mature researcher and a thinker. His relentless spirit in research resonated with mine and made me shooting for higher goals with pure joy and enthusiasm. During my 6 years at UCLA, we had over 2200 folded emails in exchange and I am so proud and lucky to have a mentor who's willing to invest so much in his student.

I would like to pay my gratitude to Professor Jia Zhou (Fudan University) for leading me to the field of digital microfluidics in early 2011. I would like to thank my teachers in University of Electronic Science and Technology of China (UESTC). The skill set I learned there still benefits me today.

Many thanks go to my colleague Dr. Muchen Xu, who provided generous help and guidance for me to adapt to the new research environment at the beginning of my Ph.D. life. I thank Dr. Supin Chen, who initiated the multilayer EWOD device project which became part of my Ph.D. research topic. I thank Ryan Freeman for his company during my study of the MEMS courses. I pay thanks to Dr. Tingyi "Leo" Liu, who provided critical suggestions to my electrodedwetting experiments. I give thanks to James Jenkins, Lian-Xin "Coco" Huang, Ning Yu, Jeong-Won Lee, Gintare Kerezyte, Dr. Guangyi Sun, and Dr. Janet Hur for their company and help during my research.

I would like to thank my research partners. Their hard work, responsibilities, and fast responses inspired me. I pay thanks to Professor R. Michael van Dam and his student Dr. Noel Ha

for their contribution to electrodedwetting project. I thank Professor Tsung-Yi Ho and his student Chichun Liang (National Taiwan University, Taiwan) for their contribution to EWOD CAD. I thank Professor Kwanwoo Shin (Sogang University, S. Korea) for his help in supplying paper EWOD devices.

I would like to acknowledge the National Science Foundation for their support for the electrodedwetting project and the cybermanufacturing project.

I devote my earnest thankfulness to my father Xiaoming Li, my mother Sue Yu, and my mother-in-law Shuwen Peng. They provided me tremendous care and support during my Ph.D. life. At last, I'd like to give my sincere thanks to my wife Jing Yang for her unconditional love and support.

## VITA

- 2011 B. E., Electrical Engineering  
University of Electronic Science and Technology of China, Chengdu, China
- 2012 Visiting Student Researcher  
University of California, Los Angeles, USA
- 2013-2018 Graduate Student Researcher  
Teaching Fellow  
Mechanical and Aerospace Engineering Department  
University of California, Los Angeles

## JOURNAL PUBLICATIONS

J. Li and C.-J. Kim, Electrodewetting for digital microfluidics (*Under review*)

## CONFERENCE PUBLICATIONS & PRESENTATIONS

J. Li and C.-J. Kim\*, Electro-dewetting on transparent substrate: device fabrication and demonstration, *Proc. IEEE Int. Conf. MEMS*, Seoul, Korea (2019), **Oral**.

C.-J. Kim\* and J. Li, The commercialization state of electrowetting-on-dielectric (EWOD), *Bio-IT Healthcare Initiative Workshop & the 15th Korea-U.S.A. Joint Symposium on N/MEMS and Bioengineering*, Daejeon, S. Korea (2018), **Oral**.

J. Li and C.-J. Kim\*, Cybermanufacturing ecosystem for expanding electrowetting community, *International Meeting on Electrowetting*, Enschede, Netherlands (2018), **Oral**.

J. Li\* and C.-J. Kim, Digital microfluidics starter kit, *Droplets Workshop*, Los Angeles, USA (2017), **Oral**.

J. Li and C.-J. Kim\*, Electrodewetting, *International Meeting on Electrowetting*, Taipei, Taiwan (2016), **Oral**.

J. Li, S. Chen, and C.-J. Kim\*, A convenient method to fabricate multilayer interconnections for microdevices, *Proc. IEEE Int. Conf. MEMS*, Estoril, Portugal, pp. 265-267 (2015), **Poster**.

J. Li and C.-J. Kim\*, Development of handheld digital microfluidic systems, *Proc. Int. Conf. Miniaturized Systems for Chemistry and Life Sciences ( $\mu$ TAS)*, Gyeongju, Korea, 1199-1201 (2015), **Poster**.

J. Li\* and C.-J. Kim, Shrinking down the electronics for handheld digital microfluidic systems, *International Meeting on Electrowetting*, Cincinnati, USA (2014), **Poster**.



(\* indicates the presenter)

## **PATENT**

J. Li and C.-J. Kim, Device and method for aligning sample substrate to cover substrate having protruding pins, US Provisional No. 62/675,414. (2018).

C.-J. Kim and J. Li, Methods for fluid manipulation by electrodedewetting, International application No. PCT/US2017/014073. (2017).

# Chapter 1 Introduction

## 1.1 The birth and the growth of EWOD

Akin to the electrocapillarity by Lippmann [1], electrowetting makes a liquid appear more wetting on a surface than the inherent level of wetting by applying an electrically field. However, the conventional electrowetting, first described in 1983 for a liquid electrolyte on metal by Beni and Hackwood [2], was not strong enough (e.g., contact angle change too small) for engineering applications. The electrowetting effect became stronger in around 1993 when a dielectric layer added on the metal surface allowed application of high voltages [3]. Coined as electrowetting-on-dielectric (EWOD) [4], [5] to differentiate it from the conventional electrowetting [2] and continuous electrowetting [6], [7], EWOD was shown capable of not only switching a sessile droplet between beading and wetting by University of Joseph Fourier in 1997 [8] but also moving a liquid along desired paths on a surface by Nanolytics, UCLA, and Duke University in 2000 [9], [10], [11]. Soon, EWOD was shown to generate water droplets from an on-chip reservoir as well as move, split, and merge them, establishing the four essential microfluidic operations [12] in air (as well as in oil) and convincing digital microfluidics and lab-on-a-chip will someday be possible. The field of electrowetting has taken off, as the growing number of publications (including patents) in Figure 1-1 indicates.

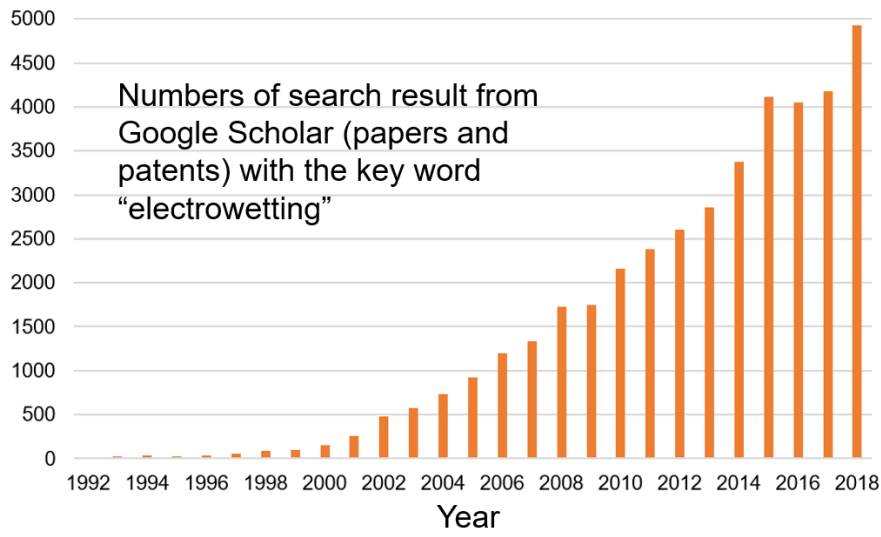


Figure 1-1. The numbers of search result in Google Scholar for the term “electrowetting” in papers and patents.

## 1.2 The commercialization status of EWOD

Realizing the promising utility of EWOD for applications since year 2000, startups began to emerge mainly for optical and biomedical applications while academic researchers continued exploring additional applications areas [13], [14], [15]. In optical applications, Varioptic has pioneered a liquid lens and introduced a collection of products in the market, and Liquavista successfully prototyped a reflective display based on the video-speed display initiated by Philips Research [16]. In biomedical, Advanced Liquid Logic has developed a DNA preparation instrument, and GenMark Diagnostics and Babies introduced molecular diagnostics instruments in recent years. These successes led to a flurry of acquisitions involving multinational companies (e.g., Corning, Amazon, and Illumina) and attracted a slew of additional startups. Although some of the products had a setback or are currently hindered by the well-known reliability issues of EWOD, the persisting success of liquid lenses and the recent FDA approvals of molecular

diagnostics instruments testify that EWOD is a powerful and versatile technology with a wide and far-reaching potential for the years to come.

### **1.2.1 The liquid lens**

University of Joseph Fourier (Grenoble, France) filed a patent of variable focus lens consisting of a sessile drop in an immiscible liquid actuated by EWOD in 1997 [8], and its inventor Bruno Berge founded Varioptic (Lyon, France) in 2002. Compared with the conventional motorized lens, the liquid lens has many advantages: (i) no wear and silent operation, (ii) fast actuation ( $< 50$  ms), (iii) high mechanical shock resistance ( $> 2000$  g), and (iv) low power consumption ( $< 20$  mW with driver) [17]. In addition to controlling the focal length by EWOD, the company developed additional functions such as variable tilt and image stabilization. They also found optical aberration can be greatly reduced by adding a resistive layer between the insulation layer [18] and electrodes dielectric failure under DC voltage can be significantly alleviated by adding multivalent salt in conductive liquid [19]. The company began its first shipment of the liquid lens in 2007 produced by Creative Sensor (Nanchang, China) but later partnered with Seiko Instruments (Chiba, Japan) for mass manufacturing. Today, Varioptic's liquid lens is implemented in a wide range of products, including machine barcode readers [20], intraoral cameras [21], cell counters [22], ophthalmology [23], biometrics [24], low visions devices [25].

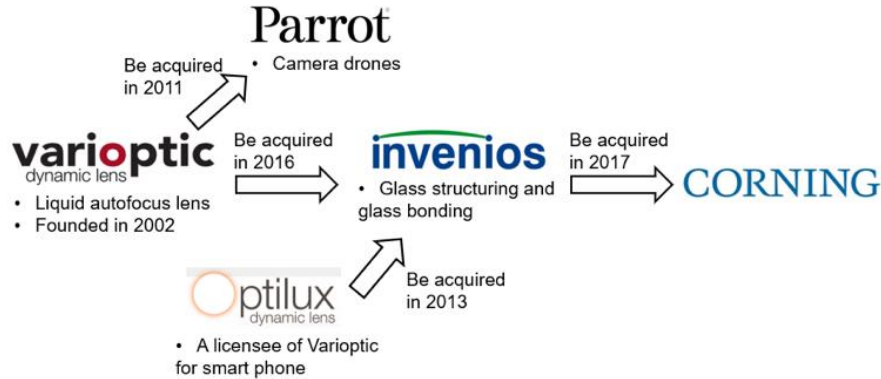


Figure 1-2. History of the liquid lens business. Varioptic has been the world leader in liquid lens technology and the first example of successful commercialization for electrowetting.

Varioptic has gone through several changes in the 2010s, as visually summarized in Figure 1-2. In 2011, Varioptic was acquired by Parrot (Paris, France), a company well known for camera drones. At the same time, Optilux (Santa Barbara, USA) was founded with an exclusive right to use the liquid lens in smart phones and tablets. Then, as an interesting turn of events, Invenios (Santa Barbara, USA), a microfabrication foundry specializing in glass-based gene sequencing chip and microfluidic devices, acquired Optilux in 2013 and Varioptic from Parrot in 2016, only to be acquired immediately (in 2017) by Corning, a Fortune (Global) 500 Company specializing in glass and ceramics. Currently the Varioptic liquid lens is marketed as Corning Varioptic Lenses.

Following the Invenios' acquisition of Varioptic, the founder Bruno Berge founded Laclarée (Lyon, France) in 2016 to apply the liquid lens for prescription eyeglasses. In the meantime, Verily Life Sciences, formerly Google Life Sciences and a subsidiary of Alphabet (Mountain View, USA), is actively developing electrowetting based contact lens with multiple patents filed since 2017 [26], [27]. Despite the long and winding path to the status today, the competition does not seem fierce as almost every company is working on different applications.

### 1.2.2 The reflective display

Philips Research (Eindhoven, the Netherlands) filed an electrowetting display patent in 2002 [28], and its inventors Johan Feenstra and Robert Hayes founded a spinoff Liquavista (Eindhoven, the Netherlands) in 2006. Compared with an electrophoretic display (E-ink), their electrowetting-powered display was fast enough to play video contents [16]. They moved forward to commercialize the display by improving its contrast, brightness, saturation, speed, power consumption, and reliability while achieving grayscale, full-color, and trans-reflective displays. Liquavista was acquired by Samsung Electronics (Suwon, S. Korea) in 2010 and the technology matured [29], but soon Amazon (Seattle, U.S.A.) purchased the business from Samsung in 2013 to apparently improve its e-reader, which is monochrome and has slow refresh rate. Amazon was building a production team in Shenzhen, China as late as 2016 [30], but it shut down Liquavista in 2018. Although the reason for the shutdown is not known, one can imagine the challenges of commercializing a display for consumer market (e.g., every pixel of the display should function over millions of voltage cycles for years without degradation) including fierce competitions (e.g., CLEARink with another video-speed reflective display technology).

Consumer market is not the only playing field for reflective displays. As Liquavista was being founded, Hans Feil founded Miortech (Eindhoven, the Netherlands) in 2006 as a spinoff of Liquavista and formed Etulipa (Eindhoven, the Netherlands) as a subsidiary of Miortech in 2013 to develop outdoor digital signage using electrowetting. Reflective displays are attractive for outdoor signage not only because of its readability in bright light but also because they do not create light pollution. Because digital signs – much larger than electronic paper – require assembling of multiple tiles, Etulipa added an optical waveguide on top of electrowetting display tiles to make them visibly seamless [31]. Unique challenges are to assure superior reliability to withstand the harsh outdoor conditions, such as flying particles, rain, temperature cycles, and sun

radiation. While maturing the technology for a wide range of outdoor applications, their first application is an electronically changeable copy board (eCCB) named Carbon, boasting clear black digital lettering. The tiles that constitute the copy board are manufactured in United Radiant Technology (Taichung, Taiwan). Figure 1-3 visually summarizes the history of reflective display business until today.

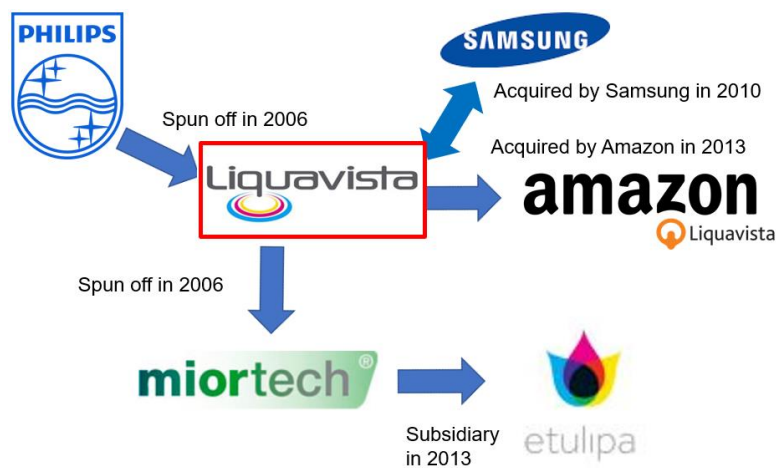


Figure 1-3. History of electrowetting-based reflective display business. Liquavista has pioneered electronic paper but saw the utilities expanding to outdoor applications.

Recently, a team led by GuoFu Zhou and Alexander Henzen (former Philips employees who had earlier founded IREX Technologies, an electronic paper company spun off from Philips) is also commercializing electrowetting display in South China Normal University (China) and Shenzhen Guohua Optoelectronics (Shenzhen, China). It is still to be seen how the above three will overcome the challenges and bring the products to the market.

### 1.2.3 Digital microfluidics for biochemical assays

Alex Shenderov filed a patent for a device capable of manipulating droplets on a surface by EWOD actuation in 1999 [32] and founded Nanolytics (Raleigh, U.S.A.). Independently, UCLA (Los Angeles, U.S.A.) filed a similar patent in 2000 [33], and its inventor CJ Kim founded Core MicroSolutions (Los Angeles, U.S.A.) in 2002. Based on the collaborative research between Nanolytics and Richard Fair’s lab in Duke University [11], Michael Pollack and Vamsee Pamula founded Advanced Liquid Logic (Morrisville, U.S.A.) in 2004. All the three companies explored to commercialize EWOD digital microfluidics for a wide range of applications but mostly biomedical, such as accelerating drug discovery process by replacing robotic manipulations of liquids with EWOD digital microfluidic manipulations. Eventually, the Advanced Liquid Logic acquired Nanolytics in 2007 and Core MicroSolutions in 2009 before being acquired by Illumina (San Diego, U.S.A.) in 2013.

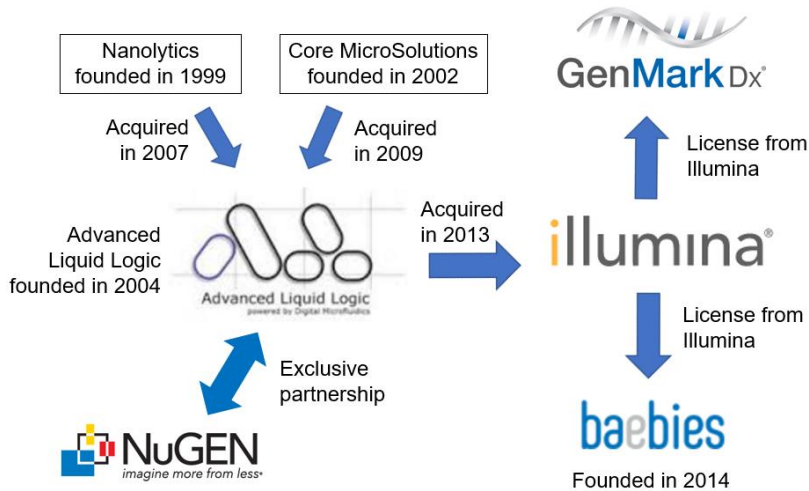


Figure 1-4. History of digital microfluidics business. Advanced Liquid Logic has played a key role for the two main products of today: GenMark’s ePlex system for molecular diagnostics and Baebies’ SEEKER for enzymatic assays for newborns.

Prior to the above acquisition, NuGEN Technologies (Redwood City, U.S.A, now part of Decan Group in Männedorf, Switzerland) introduced a digital microfluidics-based DNA library preparation instrument called Mondrian SP Workstation [34] in 2011 in partnership with Advance



Liquid Logic. After the 2013 acquisition, Illumina launched a similar, expanded product called NeoPrep Library Prep System in 2015. Performing the majority of steps automatically (e.g., magnetic bead-based operations, thermal cycling, and optical detection) by EWOD, the system completed sample preparation in ~30 min automatically instead of the 4-5 hours of manual operation by users. Unfortunately, this system was discontinued in 2017 for undisclosed reasons, which are generally understood as reliability problems [35] likely caused by underestimating the challenges of engineering and manufacturing (the authors' opinion). The above setback did not discourage other sequencing companies from employing the EWOD digital microfluidic technology for similar goals. Oxford Nanopore Technologies (Oxford, United Kingdom) launched VolTRAX V2 for DNA/RNA library preparation in 2018. Their consumables (the TFT based EWOD devices [36]) are supplied by Aqdrop (Oxford, United Kingdom), a company jointly formed by Sharp and Foxconn. Compared with NeoPrep, VolTRAX V2 has several advantages for better reliability. First, its EWOD device is made of glass substrate using LCD manufacturing method instead of the PCB substrate employed for NeoPrep's EWOD device. Compared with the PCB-based, the glass-based EWOD device has a smoother (i.e., less surface topology) surface, allowing a thinner dielectric layer and ensuring better control of the liquid volume. Second, a feedback detection of liquid volumes is implemented in the system, allowing the users to dispense exact volumes of liquids into the device. Third, by reducing the number of libraries running at a time, their cartridge has a smaller chance to fail than the NeoPrep's cartridge that runs 16 libraries in parallel.

Advanced Liquid Logic was working with GenMark Diagnostics (Carlsbad, U.S.A.) to explore a fully integrated in-vitro diagnostic platform that detects DNA/RNA targets using the eSensor of GenMark before the 2013 acquisition by Illumina. GenMark obtained a license and

continued the development to complete ePlex System, which is built to operate multiplex panels each for a certain disease. Their ePlex System and the first panel (the respiratory pathogen or RP panel) were FDA cleared in 2017, and two other panels (the blood culture identification for Gram positive organisms or BCID-GP panel and the blood culture identification for fungal organisms or BCID FP panel) were FDA cleared in 2018 with additional panels in the pipeline. Currently, the GenMark ePlex system with its panels is considered the most sophisticated and versatile electrowetting product in the market.

In collaboration with the Neonatal-Perinatal Research Institute of Duke University, Advance Liquid Logic developed a molecular diagnostic system to detect lysosomal storage disorders (LSDs) for newborn babies. After the 2013 Illumina acquisition, Vamsee Pamula and Richard West obtained the license and formed Baebies (Durham, U.S.A.) in 2014 to continue commercializing the LSDs screening system and screening services for newborns. Their instrument SEEKER was FDA approved in 2017.

#### **1.2.4 Other companies and products**

In recent years, more companies or products based on electrowetting started to emerge as novel applications continued to be discovered. One example is e-Maldi (Enschede, the Netherlands) founded by Frieder Mugele in 2012 as a spinoff of the University of Twente (Enschede, the Netherlands) based on a pending patent [37]. By oscillating the liquid-solid-air contact lines by electrowetting actuation, their active target plate led to ~100x more sensitive signals for than the existing practice for matrix-assisted laser desorption ionization mass spectrometry (MALDI-MS). Another example is Aqdrop, a joint venture founded by Sharp (Sakai, Japan) and Hon Hai Precision Industry (a.k.a. Foxconn) (Taipei, Taiwan) in 2017. They are currently supplying the

TFT thin-film based EWOD devices to Oxford Nanopore Technologies but also exploring a wide range of biochemical applications in genomics, proteomics, cellomics, and synthetic biology. Founded in 2016, Digi.Bio (Amsterdam, the Netherlands) is currently in an accelerator program hosted by Merck, one of the world's largest pharmaceutical companies. Targeting biochemical applications as well, they are currently working with levels diagnostics for fighting antimicrobial resistance.

### **1.2.5 Summarize for commercialization status of EWOD**

We summarized the history and status of the major commercialization activities of electrowetting technologies, covering liquid lens, electronic displays, and various biochemical applications. The big picture reveals a few trends and teaches some good lessons. First, almost every electrowetting company worked on unique applications quite different from others even if the underlying technologies are similar. Focusing on different applications and pursuing different markets, the competition is still relatively weak. Second, while some of the ambitious products have experienced setbacks (Liquavista's electronic paper and Illumina's DNA/RNA library preparation system), they did not discourage others from continuing to pursue similar goals. Instead, others learned valuable lessons and adjusted their strategies to improve the product reliability or shift the target market. Third, the success of Advanced Liquid Logic suggests that collaborating with mature biochemical companies is important to explore biochemical applications – easy to say than do in practice. Fourth, now approximately 20 years after the first electrowetting company was founded, we started to see a surge of startup companies formed and being formed and new products being developed and launched, as new applications continue to be discovered. Understanding the practical limitations of EWOD devices better and also learning how to design

and manufacture more reliable EWOD product, the chances of success have been increasing for new companies and new product, allowing them to harvest from the wide potential of electrowetting and EWOD technologies.

### 1.3 Bottlenecks limit a stronger growth of EWOD digital microfluidics

As an elegantly simple platform technology for microfluidics, EWOD digital microfluidics has enjoyed exponential advancement during the past 20 years (Chapter 1.1) and has culminated in many commercial applications (Chapter 1.2). Despite the success, however, we suspect two main bottlenecks have been preventing many potential researchers from joining and flourishing in the field: technical barriers and reliability issues, as illustrated in Figure 1-5.

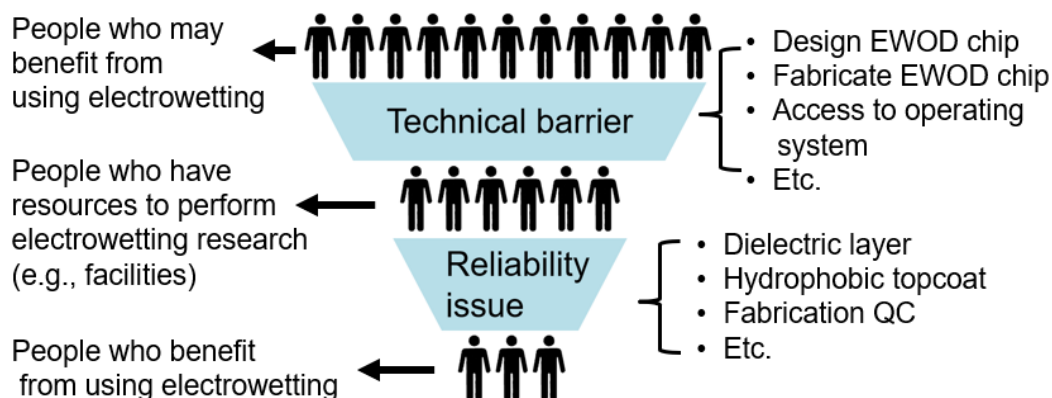


Figure 1-5. Technical barrier and reliability issues are two major bottlenecks that limit the growth of electrowetting community.

Technical barriers refer to the fabrication of EWOD devices (chips or plates), which often require special facilities and knowledge [38], and the building of control electronics and software to operate the devices [39]. Reliability issues refer to the major failure mechanisms of the devices during usage: First, since the voltage applicable on a given dielectric material is proportional to

the thickness and the electrowetting force is proportional to the voltage squared [5], [40], one would prefer a reasonably thick dielectric to make the EWOD devices more robust (especially important for commercial product) despite a relatively high voltage required. However, since deposition of a defect-free thin film is challenging, especially across the relatively large area of some devices, the dielectric layer often experiences electric leakage or even breakdown [41], resulting in the notoriously well-known device failure by electrolysis [38]. Second, the top surface needs to be hydrophobic so that a droplet is naturally dewetted on it and has a sufficient room for significant induced wetting by electrowetting. However, since most materials, including the added dielectric layer, are hydrophilic, a low-energy material is coated on top to render the final surface hydrophobic. Unfortunately, this hydrophobic topcoat, e.g., polytetrafluoroethylene (PTFE), is susceptible to charging under electric field [42] and prone to protein fouling [43], not to mention its material and deposition costs. Despite the associated problems, the dielectric layer and hydrophobic topcoat (i.e., EWOD) were the critical advances that made the once-obscure concept of electrowetting practical for applications, leading to the digital microfluidics of today.

#### **1.4 Scope of research: two approaches for solving the limitations of EWOD**

We focus on addressing the reliability issue and technical barrier of EWOD in this dissertation. In chapter 2, we report an ionic surfactant-mediated mechanism “electro-dewetting” which does not require hydrophobic coating and dielectric layer, eliminating the reliability issues of EWOD. We investigated the underlying mechanism and performed characterization study of electro-dewetting. The electro-dewetting device demonstrated high reversibility, reliability against electrolysis and is bistable. Chapter 3 represent the overview of a cybermanufacturing ecosystem which allows users to (i) design own digital microfluidic devices using dedicated CAD tools, (ii)

order fabrication of the designed devices from foundry services, (iii) obtain a device operating system, and (iv) help build an online portal by sharing their designs. With the cybermanufacturing system in place, users can focus on their own ideas and applications without the engineering and manufacturing burdens of digital microfluidics. Chapters 4 and 5 are two important parts of the cybermanufacturing ecosystem. Chapter 4 represents an electronic control system which allows people in a wide range of disciplines and technical levels to develop and debug EWOD devices. Chapter 5 represents a low cost and low surface topography fabrication method for multilayer EWOD devices. Due to the simplicity of this method, the device has the potential to be a better-quality alternative to the PCB EWOD devices and a low-cost alternative to the active matrix TFT EWOD devices.

## 1.5 References

- [1] Gabriel Lippmann, Relation entre les phénomènes électriques et capillaires. *Ann. Chim. Phys.*, **5**, 494 (1875)
- [2] Beni, G. & Hackwood, S. Electro-wetting displays. *Appl. Phys. Lett.* **38**, 207–209 (1981).
- [3] B. Berge, Électrocapillarité et mouillage de films isolants par l'eau, C. R. Acad. Sci. Paris, t. **317**, Série II, 157-163 (1993).
- [4] Lee, J., Moon, H., Fowler, J., Kim, C.-J. & Schoellhammer, T. Addressable micro liquid handling by electric control of surface tension. *Technical Digest. 14th IEEE International Conference on Micro Electro Mechanical Systems*, 499–502 (2001).
- [5] Lee, J., Moon, H., Fowler, J., Schoellhammer, T. & Kim, C.-J. Electrowetting and electrowetting-on-dielectric for microscale liquid handling. *Sensors Actuators A Phys.* **95**, 259–268 (2002).
- [6] Beni, G., Hackwood, S. & Jackel, J. L. Continuous electrowetting effect. *Appl. Phys. Lett.* **40**, 912–914 (1982).
- [7] Junghoon Lee & Chang-Jin Kim. Surface-tension-driven microactuation based on continuous electrowetting. *J. Microelectromechanical Syst.* **9**, 171–180 (2000).

- [8] Berge, Bruno, and Jerome Peseux. Lens with variable focus. U.S. Patent No. 6,369,954. (2002).
- [9] Shenderov, Alexander David. Actuators for microfluidics without moving parts. U.S. Patent No. 6,565,727. (2003).
- [10] Kim, Chang-Jin, and Junghoon Lee. Electrowetting-driven micropumping. U.S. Patent No. 8,529,743. (2013).
- [11] Pollack, M. G., Fair, R. B. & Shenderov, A. D. Electrowetting-based actuation of liquid droplets for microfluidic applications. *Appl. Phys. Lett.* **77**, 1725–1726 (2000).
- [12] Sung Kwon Cho, Hyejin Moon & Chang-Jin Kim. Creating, transporting, cutting, and merging liquid droplets by electrowetting-based actuation for digital microfluidic circuits. *J. Microelectromechanical Syst.* **12**, 70–80 (2003).
- [13] Sen, P. & Chang-Jin Kim. A Liquid–Solid Direct Contact Low-Loss RF Micro Switch. *J. Microelectromechanical Syst.* **18**, 990–997 (2009).
- [14] Nelson, W. C., Kavehpour, H. P. & Kim, C.-J. “CJ”. A miniature capillary breakup extensional rheometer by electrostatically assisted generation of liquid filaments. *Lab Chip* **11**, 2424 (2011).
- [15] Hale, R. S. & Bahadur, V. Electrowetting-based microfluidic operations on rapid-manufactured devices for heat pipe applications. *J. Micromechanics Microengineering* **27**, 075004 (2017).
- [16] Hayes, R. A. & Feenstra, B. J. Video-speed electronic paper based on electrowetting. *Nature* **425**, 383–385 (2003).
- [17] <http://www.chronix.co.jp/chronixjp/products/picture/varioptic/pdf/Varioptic%20presentation%20v6.0%20-%20V2.pdf> (visited in March, 2019)
- [18] Berge, Bruno, et al. Optical electrowetting device. U.S. Patent No. 8,649,102. (2014).
- [19] Berge, Bruno, and Mathieu Maillard. Electrowetting optical device with low power consumption. U.S. Patent Application No. 14/394,753.
- [20] <https://microscan.com/en-us>
- [21] <https://www.carestreamdental.com/en-us/>
- [22] <https://logosbio.com/automated-cell-counters/brightfield/luna-1l>
- [23] <http://www.tomey.com/tomeycorp/product.html>
- [24] <https://usa.morpho.com/>
- [25] <https://www.esighteyewear.com/>

- [26] Kuiper, Stein, and Daniel Otts. Electrowetting lenses having oleophobic surfaces. U.S. Patent Application No. 16/107,823.
- [27] Otts, Daniel, and Stein Kuiper. situ filling and sealing of electrowetting intraocular lenses. U.S. Patent Application No. 15/945,880.
- [28] Feenstra, Bokke, Robert Hayes, and Menno Prins. Display device. U.S. Patent Application No. 10/504,708.
- [29] <https://the-digital-reader.com/2012/03/21/samsung-electrowetting-screen-tech-to-hit-mass-production-next-year/#.UEDIeI5VVy4>
- [30] <https://goodereader.com/blog/e-paper/amazon-is-building-a-production-team-in-china-for-liquavista-displays>
- [31] Feil, Hermanus, and Doeke Jolt Oostra. Optical seam reduction. U.S. Patent Application No. 15/027,215.
- [32] Shenderov, Alexander David. Actuators for microfluidics without moving parts. U.S. Patent No. 6,565,727. 20 (2003).
- [33] Kim, Chang-Jin, and Junghoon Lee. Electrowetting-driven micropumping. U.S. Patent No. 8,529,743. 10 (2013).
- [34] <https://www.youtube.com/watch?v=niGt2q7CKfw>
- [35] <http://omicsomics.blogspot.com/2017/02/illumina-drops-neoprep.html>
- [36] Hadwen, B. et al. Programmable large area digital microfluidic array with integrated droplet sensing for bioassays. *Lab Chip* 12, 3305 (2012).
- [37] Eral, Huseyin Burak, Mampallil Augustine Dileep, and Frieder Mugele. Method for treating a drop of liquid. U.S. Patent Application No. 13/697,870.
- [38] Nelson, W. C. & Kim, C.-J. Droplet actuation by electrowetting-on-dielectric (EWOD): a review. *J. Adhes. Sci. Technol.* **26**, 1747-1771 (2012).
- [39] Gong, J. Portable Digital Microfluidic System: Direct Referencing EWOD Devices and Operating Control Board. Ph.D. Thesis Ph.D. Thesis, University of California, Los Angeles (2007).
- [40] Moon, H., Cho, S. K., Garrell, R. L. & Kim, C.-J. Low voltage electrowetting-on-dielectric. *J. Appl. Phys.* **92**, 4080–4087 (2002).
- [41] Raj, B., Dhindsa, M., Smith, N. R., Laughlin, R. & Heikenfeld, J. Ion and liquid dependent dielectric failure in electrowetting systems. *Langmuir* **25**, 12387–12392 (2009).



- [42] Verheijen, H. J. J. & Prins, M. W. J. Reversible electrowetting and trapping of charge: model and experiments. *Langmuir* **15**, 6616–6620 (1999).
- [43] Latip, E. N. A. et al. Protein droplet actuation on superhydrophobic surfaces: a new approach toward anti-biofouling electrowetting systems. *RSC Adv.* **7**, 49633–49648 (2017).

## Chapter 2 Electrodewetting

### 2.1 Introduction

#### 2.1.1 Eliminate the dielectric and hydrophobic layer of an EWOD device

The reliability issues of EWOD device (Chapter 1.3) originate from its dielectric and hydrophobic layer. There have been interesting attempts in recent years to achieve effective electrowetting without the dielectric layer and hydrophobic surface. One approach is to use special surfaces featuring an extremely small contact-angle hysteresis. With little resistance of pinning on the surface, even the small electrowetting force of the conventional electrowetting – or called EWOC [1] in contrast to EWOD – can induce an appreciable decrease in contact angle. A significant contact-angle change was achieved with EWOC on newly cleaved basal planes of highly oriented pyrolytic graphite in oil (as well as air) [1]. However, the small electrowetting forces would make it difficult to overcome disturbances, such as gravity, vibration, and imperfections, which are inevitable in realistic conditions. Another approach is to use two immiscible electrolytic solutions (ITIES) [2]. In this electrolyte-in-electrolyte system on a conductive surface, electrowetting can be achieved by applying a very small voltage applied between the two electrolytes. Yet another approach is to replace the dielectric coating with the native oxide of a liquid-metal electrode [3], making the device robust both for fabrication and usage. However, this native oxide approach also requires a two-liquid system, as it demands a small hysteresis and the help of oil-based surfactant. Without the hydrophobic layer, a device surface becomes more hydrophilic. This situation would be more favorable to a mechanism that can increase the contact angle under voltage, thus the electrodewetting.

## 2.1.2 The concept of “electrowetting”

We propose to use term “electro-dewetting” or “electrodewetting” to describe phenomenon that acts in an opposite manner to electrowetting, i.e., electrically repels a droplet on substrate under voltage (shown in Figure 2-1) and the phenomenon should be effectively enough to support digital microfluidics.

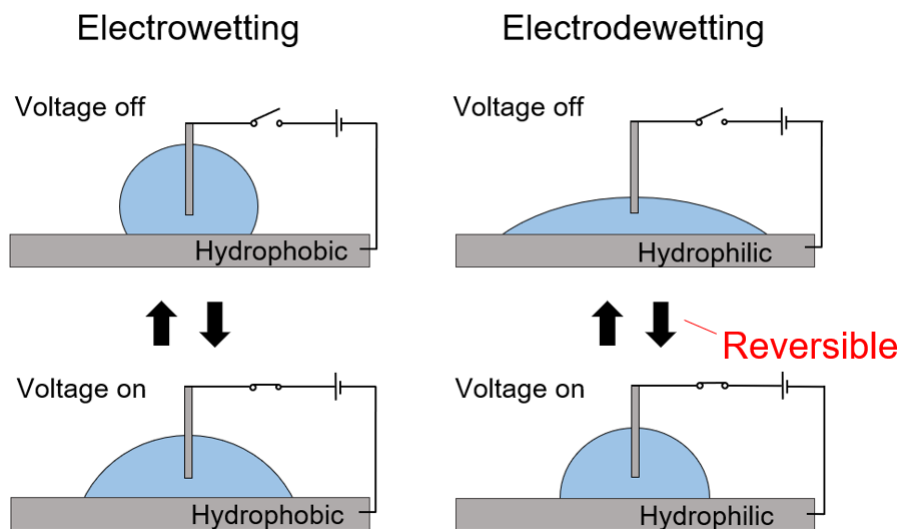


Figure 2-1. The concept of electrodewetting. The electrodewetting method should be reversible and to match the effectiveness of electrowetting to serve digital microfluidics.

Although there's previous article use the term “electro-(de)wetting”, i.e., “Electro-(de)wetting on Superhydrophobic Surfaces”, Langmuir, 2013, 13, 13346, it has a different meaning. They make a droplet wet a superhydrophobic surface by electrowetting (into Wenzel state) and agitate the system to let the impaled droplet jump up onto the superhydrophobic surface again (into Cassie-Baxter State). This is similar to several other methods that provide an energy for the impaled droplet to jump from a more stable state (Wenzel) to a less stable state (Cassie-Baxter), e.g., vibrating the experiment table, boiling the liquid, etc. Regretfully, we feel it is bit too much a

stretch to claim this Cassie-to-Baxter transition by an external energy input is an electrodedwetting phenomenon. We require electrodedwetting to match the effectiveness of EWOD.

### **2.1.3 The electrically-induced dewetting phenomenon**

Although there are several electrically-induced dewetting phenomenon reported, none of them were effective for common microfluidics because they are based on irreversible processes [4], [5] or special conditions [6], studies involving surfactants have shown that reversibility may be possible. For example, electrically-initiated dewetting of an aqueous film on derivatized gold electrodes has been demonstrated using redox-active surfactants [7]. Recently, by using ionic surfactants, the coefficient of a lubricated friction was switched in a solid-liquid-solid configuration [8], and boiling bubble nucleation was modulated in a liquid-vapor-solid system [9]. Furthermore, an organic droplet was translated on a conjugated polymer electrode in an aqueous electrolyte [10]. However, they have not led to a microfluidic platform technology, which would require an electric actuation that is reversible, repeatable, strong, and easily applicable to a liquid-fluid-solid system [11].

We found a surfactant-mediated mechanism that can dewet droplets on hydrophilic substrate in a highly reliable and reversible manner. Using only  $\pm 2.5$  V and a few  $\mu\text{A}$ , we were able to generate, move, split, and merge water droplets in open air. The compatibility is further validated with a variety of liquids, including common buffers and organic solvents, showing potential in wide applications. We proposed to name this phenomenon as “electrodedwetting”.

## **2.2 Electrodedwetting mechanism**

### **2.2.1 The surfactant-mediated electrodedwetting mechanism**

The droplet contains an ionic surfactant, which consists of a charged hydrophilic “head” group and a neutral hydrophobic “tail” region. Depending on the polarity applied and the type of surfactant, the electric field inside the conductive (resistive) liquid drives the ionic surfactant molecules towards or away from the liquid-solid interface, making the drop dewet the surface (Figure 2-2a) or wet it again (Figure 2-2b).

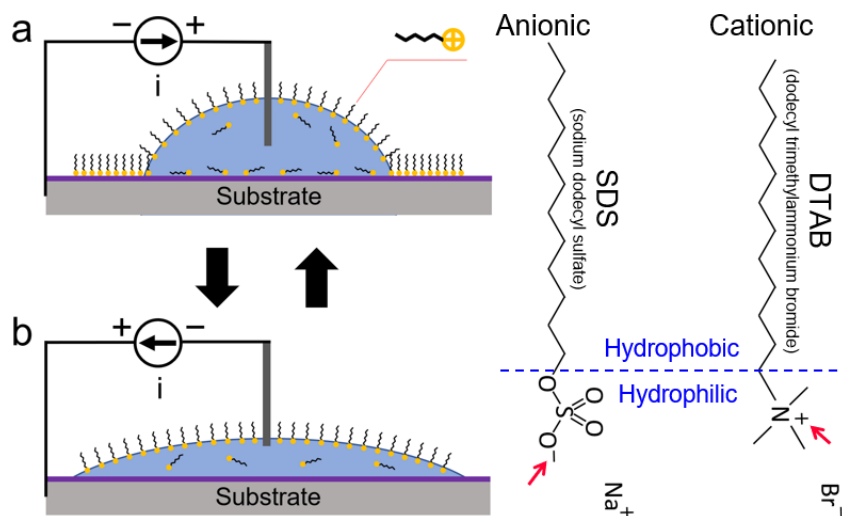


Figure 2-2. The surfactant-mediated electrodedwetting mechanism proposed and studied with a wire-inserted sessile drop on a conductive, hydrophilic substrate. **a**, For electrodedwetting, the electric field inside the liquid between the substrate and wire, established by the small current across a thin oxide (purple line) and through the liquid (blue), draws the ionic surfactant molecules (cationic surfactant is shown) onto the liquid-solid interface, making the droplet dewet (bead up on) the substrate. **b**, For wetting by active recovery, the opposite electric field by the reverse current removes the ionic surfactant away from the surface, making the droplet wet (spread on) the substrate. For most cases, wetting is also possible by passive recovery, i.e., simply removing the electric signal.

### 2.2.2 Verification of the mechanism by three experiments

Three experiments, combined, provide evidence to support the proposed mechanism of reversible electrodedwetting.

Experiment 1 to visualize the electric migration of surfactant: The first set of experiments was done under a confocal microscope, using a droplet of solution containing a fluorescent

surfactant R18, to visualize the cationic surfactant electrophoretically driven to the surface by the electric field inside the liquid droplet when actuated. Confocal microscopy was performed with an SP8-SMD inverted confocal microscope (Leica Microsystems Inc., IL, USA), using XZ scan mode, 1.38 fps, 400  $\mu\text{m}$  x 400  $\mu\text{m}$  field of view, 0.992  $\mu\text{m}$  optical section,  $\sim 471$  nm excitation, and 625 nm (571-685 nm window) emission at the Advanced Light Microscopy and Spectroscopy Laboratory (ALMS) in the California NanoSystems Institute (CNSI) of UCLA. Though the temporal resolution of confocal imaging ( $\sim 0.7$  sec) was too low to show the gradual evolution of an electrodedwetting event ( $\sim 0.5$  sec total duration), we could still obtain images right before and right after (separated in time by  $\sim 0.7$  sec) the application of the electrodedwetting voltage. The two images of a vertical slice of a droplet in Figure 2-3 reveal the surfactant molecules to be originally located on/near the liquid-air interface and then populating on/near the liquid-solid interface upon actuation.

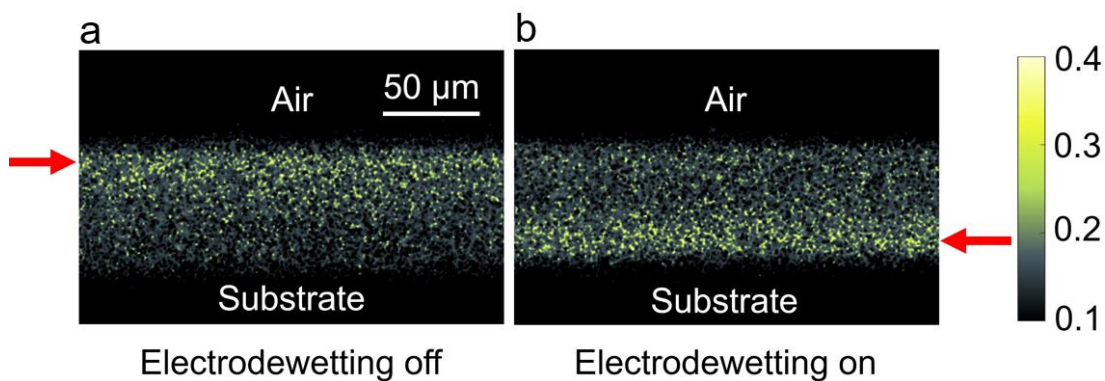


Figure 2-3. Confocal microscopic images show that a fluorescent ionic surfactant (R18) is concentrated near the air-liquid interface of the droplet before actuation (see the red arrow), and becomes concentrated near the solid-liquid interface during the electrodedwetting actuation (see the red arrow), corroborating that surfactant is driven to the substrate by electrodedwetting.

Experiment 2 to confirm the adsorption of surfactant: Experiment 1 showed the surfactant molecules are migrated to the substrate by the electrodedwetting actuation but does not necessarily confirm the surfactant molecules are “deposited” (adsorbed) on the surface. To assess the

surfactant deposition illustrated in Figure 2-2, Experiment 2 was performed using DTAB. The surfactant adsorbed on the solid surface around and under the droplet can be maintained reasonably well after physically blowing the droplet off of the surface. The blowing gas flow was roughly horizontal on the substrate from a nitrogen gun positioned ~1 cm away from the droplet center. The level of surfactant concentration on the droplet-free surface can then be revealed by condensing steam on the surface or using fluorescent microscopy. To acquire the hydrophilicity map by steam condensation, we boiled DI water in an electric hotpot and directed its steam over to the sample surface through a plastic tube.

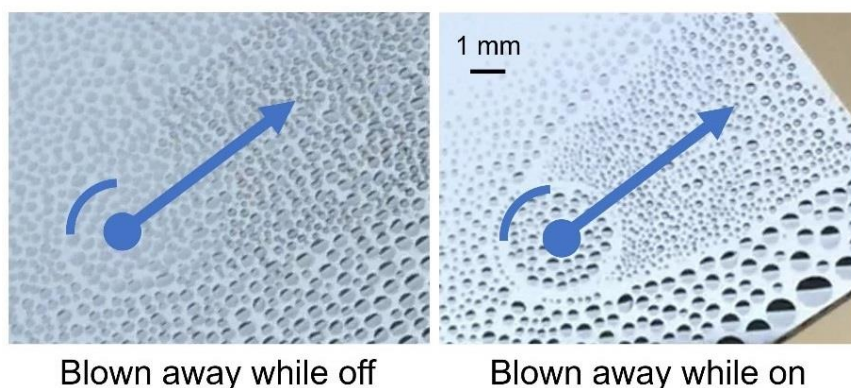


Figure 2-4. Steam condensation images reveal the wettability state of the substrate after blowing away (in the direction of the blue arrow) a water droplet containing DTAB. Unlike the unactuated droplet (left), the electrodedewetted droplet leaves a dewettable area (right), corroborating that electrodedewetting deposits surfactant on the surface.

If the droplet is placed on a fresh silicon surface and blown away with a nitrogen gun without electrodedewetting actuation, one can expect a surface essentially the same as bare silicon. When steam was directed onto this hydrophilic surface, the steam condensed everywhere, leaving only a faint pattern of where the droplet had been located, as shown in the left picture of Figure 2-4. In comparison, when the droplet was blown away while being electrodedewetted, there was a clearly noticeable ring of no condensation right outside where the electrodedewetted droplet had been

located, as shown in the right picture of Figure 2-4. This ring pattern of subdued condensation visualizes the DTAB-adsorbed ring pattern.

These two sets of experiments in Figure 2-3 and Figure 2-4 corroborate that ionic surfactant molecules are driven to and adsorbed on the substrate surface by electrodedwetting actuation.

Experiment 3 to verify the desorption of surfactant: Experiments 1 and 2 could be performed in reverse order to assess the reverse actuation of electrodedwetting. However, to strengthen the support for the reversal of electrodedwetting, which determines the repeatability and real-world applicability, we have performed Experiment 3 for the surfactant desorption using fluorescent ionic surfactant R18, which would provide somewhat quantitative data. Unlike a sessile droplet containing a regular ionic surfactant, a sessile droplet containing the amphiphilic fatty acid R18 electrodedweted and recovered to wetting with poor axisymmetry and repeatability. The droplet moved around despite the wire, and the contact line did not recede (dewet) and advance (rewet) around a fixed central position on the surface when repeated. Thus, in Figure 2-5 we show only three steps towards three states. The surface outside the droplet has a high concentration of surfactant (yellow) because, unfortunately, R18 spontaneously spreads upon droplet deposition due to autophobing, leaving a large R18-covered field. Step 1: reverse actuation actively cleaned up much of the R18 molecules deposited by autophobing, bringing the droplet to a wetting state not to be influenced by the autophobing anymore (as far as the droplet does not venture out to the yellow region again). Step 2: electrodedwetting actuation actively deposited new R18 molecules by electrodedwetting, bringing the droplet to a dewetting state. Step 3: reverse actuation actively cleaned up much of the R18 molecules deposited by electrodedwetting, bringing the droplet to a wetting state. Despite the difference (i.e., R18 has autophobing behavior, but the other surfactants in this paper did not exhibit autophobing), the fluorescent intensities in Figure 2-5 indicates the



reverse actuation does clean up the surfactant molecules left outside the droplet during the preceding step, i.e. surfactant deposited by either dewetting (Step 2) or autophobing (prior to Step 1) almost completely. Despite the poor electrodedwetting performance with R18, this three-step exercise nevertheless provides evidence that the reverse actuation removes the deposited surfactant off the surface and returns an electrodedwelled surface back to the natural, wetted state.

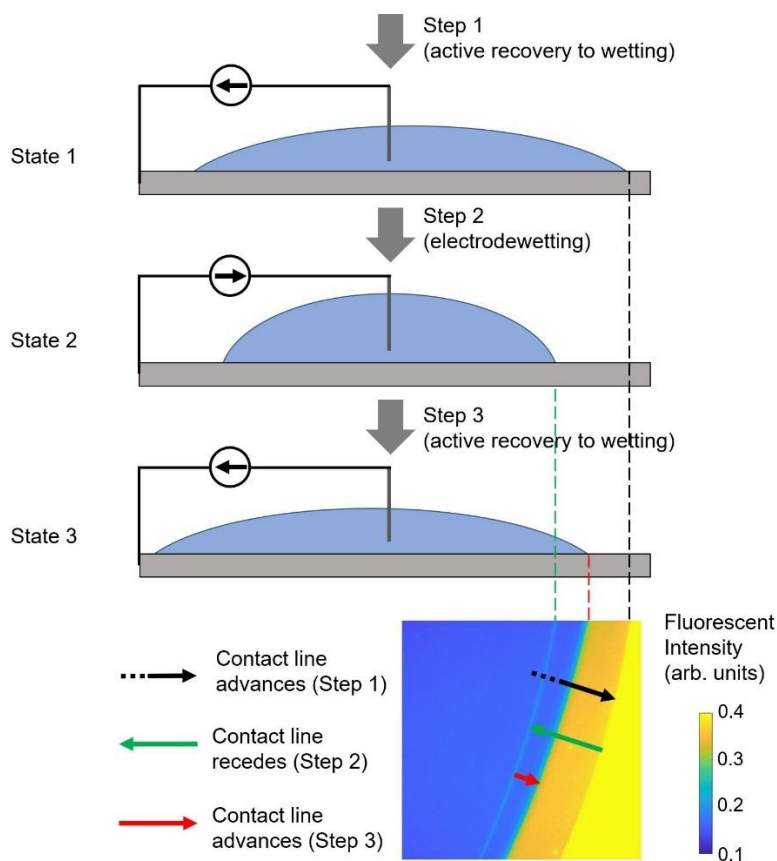


Figure 2-5. Surfactant concentration on substrate surface during electrodedwetting and reverse electrodedwetting revealed by a blow-off test. A water droplet with ionic fluorescent surfactant was electrically actuated to wet, dewet, and wet the surface successively, as illustrated in the three sideview schematics (top portion of the figure). The top-view fluorescent image (bottom right) reveals the surfactant molecules left on the substrate surface after the droplet was blown away while actuation was on. The fluorescent image is color-enhanced. The surface outside the droplet has a high concentration of surfactant due to autophobing after the droplet was initially placed on the fresh surface. Step 1 lets the droplet wet the surface, i.e., natural state, by applying reverse electrodedwetting. The contact line advances to the black dashed line drawn in the sideview schematics, corresponding to the black arrow in the fluorescent image. Step 2 lets the droplet dewet the surface by applying electrodedwetting. The contact line retreats to the green

dashed line drawn in the sideview schematics, corresponding to the green arrow in the fluorescent image. Step 3 lets the droplet wet the surface again by applying reverse electrodedewetting. The contact line advances to the red dashed line drawn in the sideview schematics, corresponding to the red arrow in the fluorescent image.

### **2.2.3 Surfactant distribution on substrate**

On the silicon substrate surface, we defined two surface regions – region I (always inside droplet) and region II (outside droplet during electrodedewetting but inside during wetting). Figure 2-6a is obtained using similar method described in experiment 2 in chapter 2.2.2. The droplet was blown away while being electrodedewetted. Since we were using DTAB surfactant at pH 2.3, there is no autophobic effect, meaning there is no surfactant deposited outside the droplet when it is dispensed on the silicon. Accordingly, the “Si” region has tiny droplets spreading out in Figure 2-6a. In comparison, region II.C has tiny droplets beading up, suggesting there’re surfactants left on the surface. Meantime, in region I.C the tiny droplets bead up less than region II.C, indicating there is less surfactant molecules deposited in region I.C than in region II.C. Above conclusion is double confirmed with the fluorescent intensity scale obtained (in Figure 2-6) using method similar to experiment 3 in chapter 2.2.2. Region II.C shows higher fluorescent intensity than I.C, suggesting there’s more surfactant in II.C. Also, it is worth to note that the region II.D and I.D has similar intensity compare to fresh silicon surface, meaning reverse voltage can clean up the surfactant on the surface, ensuring the reversibility.

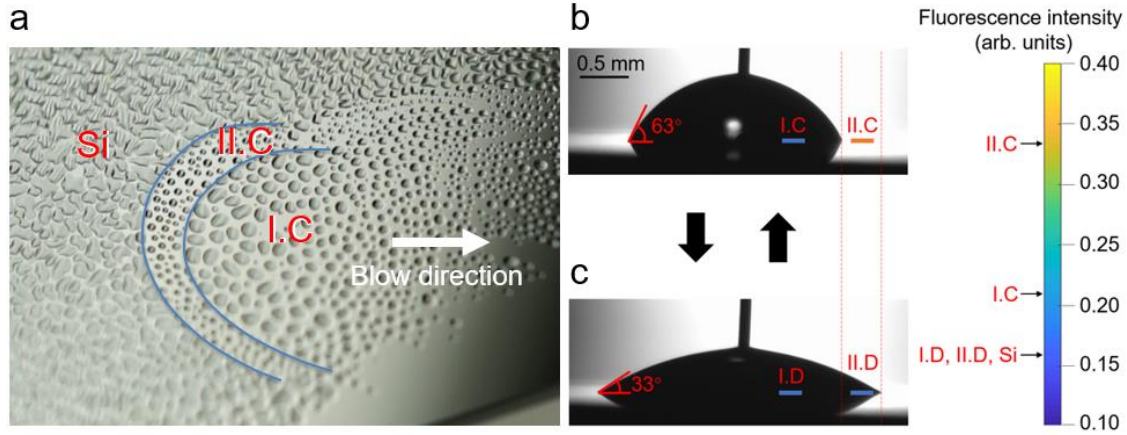


Figure 2-6. The condensation test and the fluorescent test all revealed that region II.C (outside droplet during electrodedwetting) has more surfactant than region I.C (inside droplet during electrodedwetting). Fluorescent test also showed that region I.D and II.D has similar fluorescent intensity compared to fresh silicon surface, suggesting reverse voltage can clean up the surfactant on the surface.

## 2.3 Key performance of electrodedwetting

### 2.3.1 High reversibility

By devising a setup that minimizes droplet evaporation (shown in Figure 2-7), electrodedwetting switching could be repeated for over  $10^4$  cycles, or 6 hours that the droplet lasted without significant evaporation, with no hint of deterioration (shown in Figure 2-8).

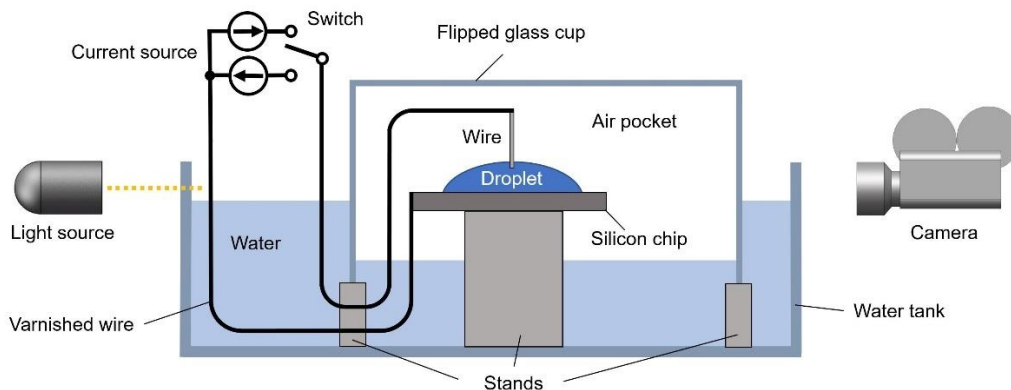


Figure 2-7. Setup for electrodedwetting longevity test. A glass cup was flipped upside down into a water tank to create an air pocket containing a wire, silicon wafer, and droplet. Two varnished wires were passed through the water to connect the wire and wafer to a current source placed outside the water tank. A relay served as a switch to toggle the polarity of the current source. The silicon wafer and glass cup were mounted

on stands and the water was adjusted to be higher outside the air pocket than inside. This setup slowed down the evaporation effectively, extending the droplet evaporation time, thus the maximum testing time, from only a few minutes to 6 hours, while allowing the replacement of the silicon chip and test droplet to be quick and easy.

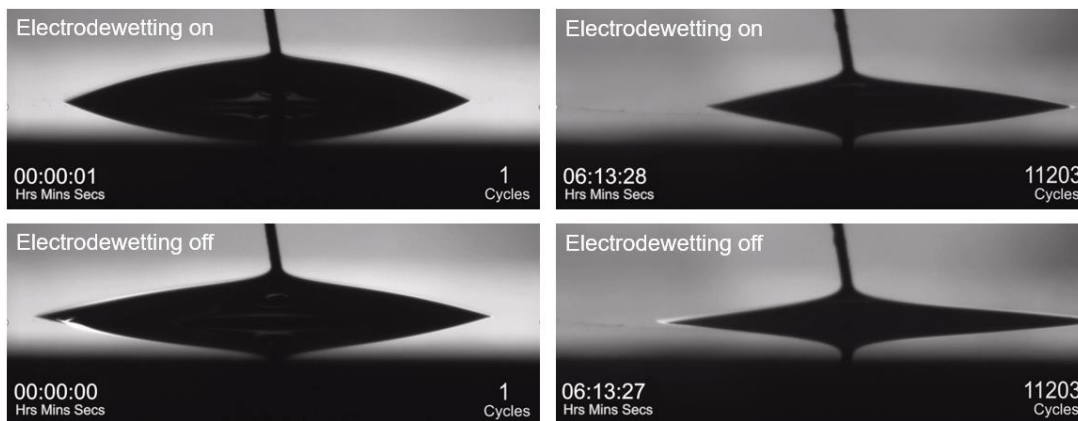


Figure 2-8. Screenshots of a droplet that was under electrodedwetting switching for over  $10^4$  cycles, or 6 hours. Left two screenshots show droplet on the first cycle and right two screenshots show the droplet on the 11203th cycle (at ~6 hours).

### 2.3.2 Resistance to high current

Electrodedwetting is normally operated at low current (usual 2.5-3.0 V and 3  $\mu$ A). We tested how excessive voltages and currents affect electrodedwetting. For cationic surfactants, at ~4 V and ~0.2 mA (i.e., well above the usual 2.5-3.0 V and 3  $\mu$ A), bubbles began to appear inside the droplet on both the wire and the substrate, indicating significant electrolysis of water. However, electrodedwetting was still found to work well and reversibly while, and after, bubbles were generated violently and even satellite droplets were shot out at ~10 V with a runaway current above 3 mA, as shown in Figure 2-9. This surprising resilience is in stark contrast to EWOD, for which even slight electrolysis by leakage current leads to a device failure.

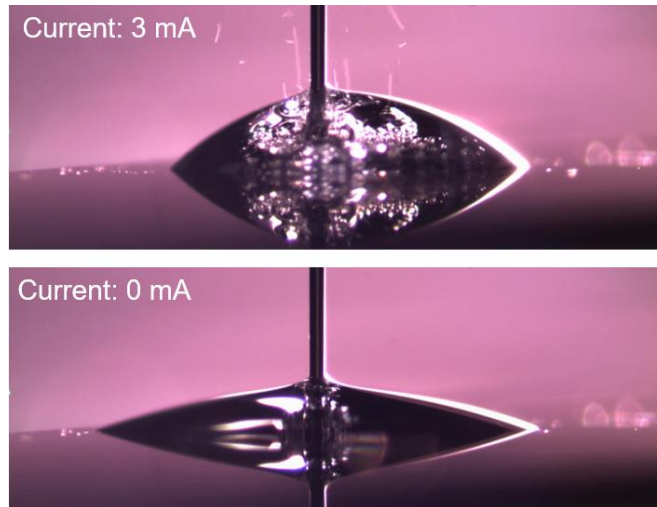


Figure 2-9. Despite usual operating current is small ( $3 \mu\text{A}$ ), electrodwetting still works under 1000X current (3 mA) when significant electrolysis occurs on the needle and the substrate. This is in stark contrast to EWOD in which case the device fails even slight electrolysis occurs.

Above difference between electrodwetting and EWOD can be explained by looking into the working principles of these two (Figure 2-10). While electrodwetting uses an electric field formed inside a droplet to manipulate the adsorption of ionic surfactant molecules on the solid surface, electrodwetting (i.e., EWOC) and EWOD use an electric field formed across EDL and the dielectric layer, respectively. Free from the reliability problems of EWOD, the electrodwetting has been confirmed to be extremely robust and durable.

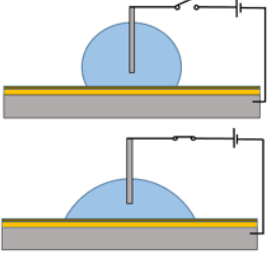
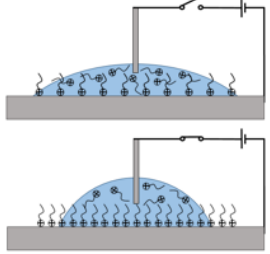
	<b>Electrowetting on dielectric (EWOD)</b>	<b>Electrodewetting</b>
<b>Setup</b>		
<b>Uniqueness</b>	Dielectric layer	Ionic surfactant
<b>Surface</b>	Hydrophobic	Hydrophilic
<b>Working principle</b>	Electric field across the dielectric	Electric field across the droplet

Figure 2-10. EWOD depends on electric field builds up across the dielectric layer while the electrodedewetting depends on electric field builds up across the droplet. This explains why electrolysis fails an EWOD device but not an electrodedewetting device.

### 2.3.3 Bistability

Bistability is a key to achieving low power consumption devices. Electrowetting is not a bistable phenomenon, thus it needs design of an extra slot or space to achieve bistable, decreasing the cell density and increasing the complexity of a device. In contrary, we found electrodedewetting is a bistable phenomenon when we tested cationic surfactant droplet at neutral pH level on a silicon surface.

While explaining the bistable mechanism of electrodedewetting, let us also look at strategy of applying external voltage to achieve electrodedewetting under various pH conditions (Figure 2-11). Since the surface of the silicon wafer (native silicon dioxide to be exact) is charged negatively when in contact with water in a pH-dependent manner [12], we can reason generally how the surface charge would affect the way electrodedewetting is applied and reversed and evaluate the reasoning through experiments. If the surfactant used is cationic, the surfactant molecules will be

automatically attracted to the solid surface by the negative surface charges on it. If enough surfactant molecules are adsorbed on the surface, dewetting will occur by itself, a process known as autophobing. In this autophobing case, an electric field (reverse of electro-dewetting, i.e., negative voltage applied to the wire) may be used to desorb the surfactant molecules from the surface and induce wetting. Note this automatic dewetting and active wetting is analogous but opposite to the previous case of anionic surfactant with active dewetting and automatic wetting. We tested DTAB (a cationic surfactant) at 0.2 mM DTAB in water and indeed observed such a switching between automatic dewetting and active wetting at  $\sim 3 \mu\text{A}$ , but only when the solution was tuned to pH 11.2, i.e., not pH 6.5 or pH 2.3. We reason that the negative surface charge density was high enough to induce significant autophobing at pH 11.2 but not at pH 6.5 and pH 2.3. For the medium charge density on the silicon surface at pH 6.5, an electric field (electro-dewetting, i.e., positive voltage to the wire) was needed to perform dewetting (migrate and deposit surfactant from droplet onto the silicon surface), and an electric field of the opposite polarity (reverse of electro-dewetting, i.e., negative voltage to the wire) was needed to perform wetting (drive the surfactant from the surface back to the liquid), thus the bistable. Lastly, for the low charge density on silicon surface at pH 2.3, an electric field (electro-dewetting, i.e., positive voltage to the wire) was needed for dewetting, and the wetting state was recovered by simply removing the electric field.

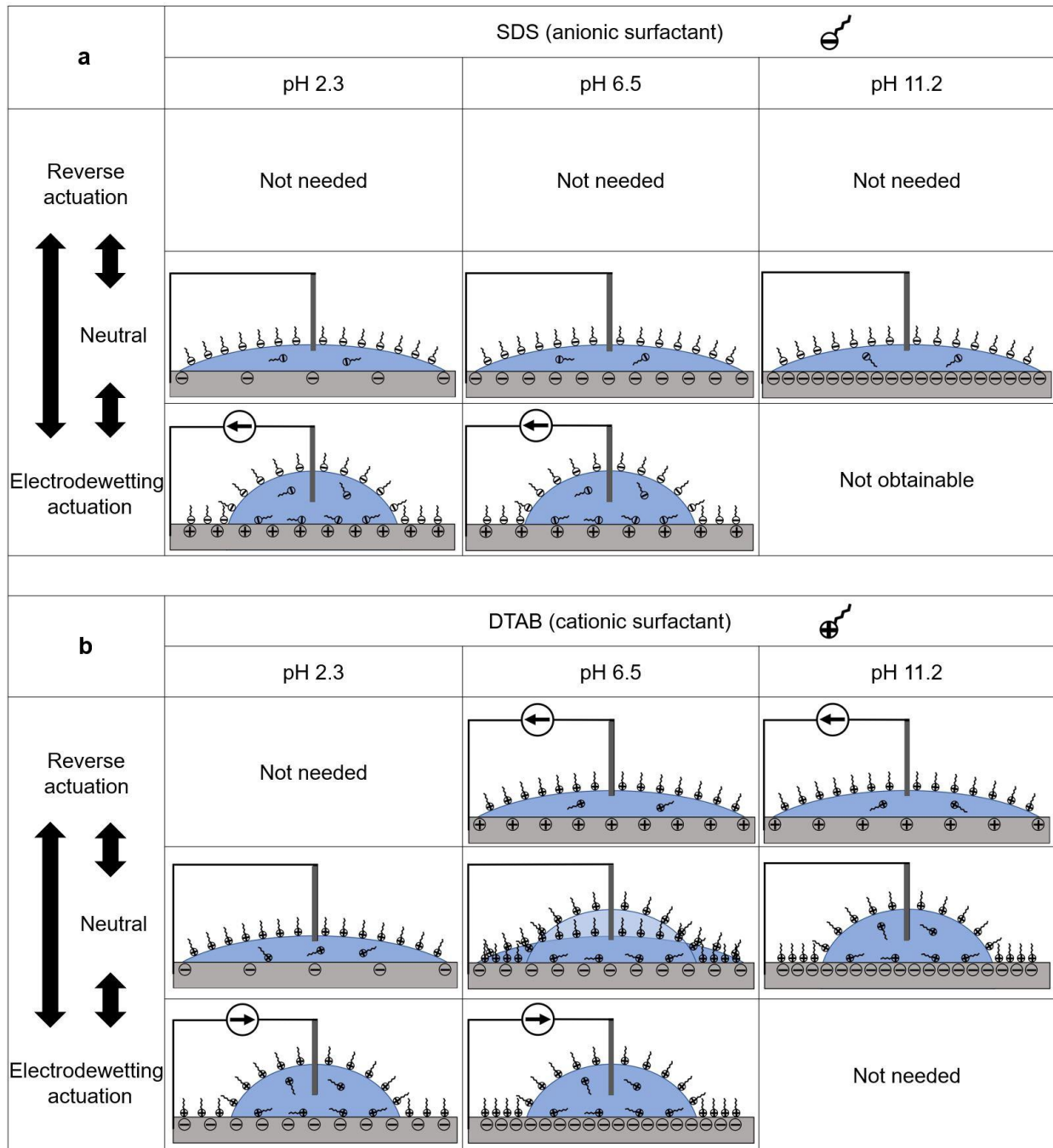


Figure 2-11. Switching between electrodedwetting, neutral, and actively-recovered wetting state experimentally confirmed for droplets containing DTAB (cationic surfactant) and SDS (anionic surfactant) on a bare silicon wafer. The working mechanisms are proposed by schematically illustrating surfactant molecules and surface charges. Bistable is achieved in cationic surfactant case at pH 6.5.



We did not observe bistable phenomenon in anionic surfactant case. If the surfactant used is anionic, the surfactant molecules will be repelled from the solid surface by the negative charges on it. After the surfactant molecules are attracted to the solid surface by an electric field for electrodedwetting (negative voltage applied to the wire), one can simply remove the electric field to desorb them from the surface (i.e. repelled by the intrinsic negative charges on the surface) for the reversal of electrodedwetting. In other words, electric actuation is needed for dewetting, and wetting is restored by simply stopping the actuation. We tested SDS (an anionic surfactant) at 0.31 mM concentration in water and confirmed electrodedwetting at  $\sim 3 \mu\text{A}$  when the solution was tuned to pH 2.3 and pH 6.5 but could not obtain electrodedwetting at pH 11.2. We reason that at pH 11.2 the high intrinsic negative charge density on the silicon surface prevented adsorption of enough SDS molecules on the surface even when this charge was counteracted to some degree by the applied electric field. After the electrodedwetting with pH 2.3 and pH 6.5, we confirmed a reversal to the wetting state by removing the electric actuation, as expected above.

The above strategy of how to switch a droplet between wetting and dewetting states, experimentally confirmed at least for DTAB and SDS on bare silicon, is summarized in Figure 2-11. Even though an electric field is not needed (i.e., simply removing the field is enough) to recover the natural state after an actuated state for many cases (e.g., recovering the wetting state for DTAB with pH 2.3 and SDS with pH 2.3 and 6.5; recovering the dewetting state for DTAB with pH 11.2), it is more practical and advisable to always switch actively like the bistable case (DTAB with pH 6.5).

## **2.4 Characterization of electrodedwetting**

### **2.4.1 Effect of surfactant type, surfactant concentration and voltage**

The degree of observed electrodedewetting may be complicated by the “autophobing” effect [13], which refers to the spontaneous dewetting of a sessile droplet as a result of electrostatic attraction of ionic surfactant to the intrinsic surface charge [14]. To characterize the “pure” electrodedewetting, we have to eliminate the autophobing effect. Luckily, studies showed that adsorption of ionic surfactants on solids can be altered by controlling pH [14], [15], [16], [17]. On the bare silica surface, increasing pH leads to deprotonation of silanol groups and increase negative surface charge. Under these conditions, cationic surfactants (e.g. CTAB) are increasingly attracted to the surface the higher the pH, resulting in increased amount of autophobing. To reduce autophobing to enable study of the electrodedewetting effect in isolation, the pH can be lowered. There is little surface charge below pH ~6, and negligible charge below pH 2. For anionic surfactants, e.g. SDS, there can be some intrinsic adsorption due to hydrophobic interactions, but this can be minimized via increase in pH which leads to electrostatic repulsion.

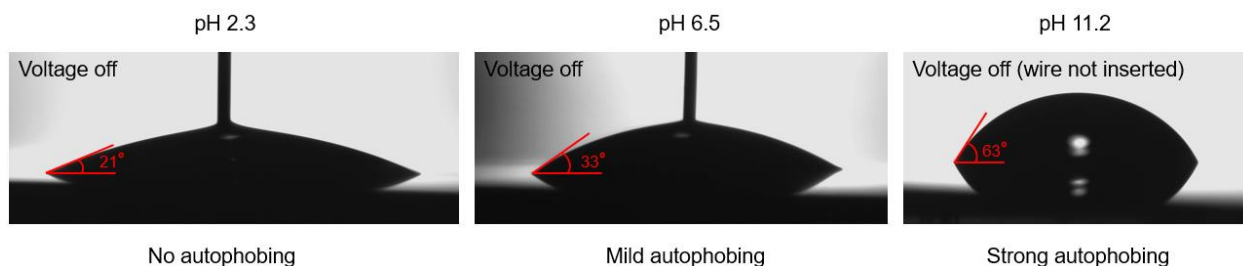


Figure 2-12. An aqueous solution with higher pH would induce more negative charges on the native oxide of silicon, autophobing by the cationic surfactant was strong for a basic solution (pH = 11.2). For a neutral solution (pH = 6.5), autophobing exists but not dominant. For an acidic solution (pH = 2.3), no autophobing was found. It is the condition we used to characterize the “pure” electrodedewetting.

We performed characterization tests on silicon surfaces using aqueous droplets of three cationic and one anionic surfactants: DTAB, tetradecyltrimethylammonium bromide (TTAB), cetyltrimethylammonium bromide (CTAB), and sodium dodecyl sulfate (SDS), respectively. To

obtain the electrodedwetting effect in isolation, i.e., without any autophobing effect, we used pH ~2.3 for all cationic surfactant solutions in this characterization study. For anionic surfactant SDS, we used pH~2.3 to make it consistent to cationic surfactants. The results summarized in Figure 2-13a, which shows only the contact-angle increase and dewetting time for clarity (full data with error bars in Figure 2-14), revealed that the four surfactants all follow a similar trend, exhibiting optimal electrodedwetting performance (i.e., large contact angle change, short dewetting time) with concentrations around 0.05 critical micelle concentration (CMC). We hypothesize that when the surfactant concentration is too low, there are too few molecules to appreciably affect the surface wettability, while when too high, the surfactant near the surface is approaching saturation, leaving little room for further increase. We note the dewetting and recovery time was around 0.5 sec, which is slower than EWOD (e.g., 0.02 sec) [18]. Likely this can be explained by the needed time for migration and assembly of surfactant molecules during electrodedwetting compared with the near instantaneous charging of the dielectric layer for EWOD. Figure 2-13b showed the contact-angle increase and corresponding current as function of the actuation voltage for the four surfactants. The current for SDS is noticeably smaller than those for the cationic surfactants because the polarity used to actuate the anionic surfactant anodize (passivates) the silicon surface. The commonly effective range found in Figure 2-13 allowed us to assess other surfactants without the full characterization. A variety of (~15 in total) surfactant types have been tested, and nearly all of them were found to facilitate the electrodedwetting at around 1/32 cmc.

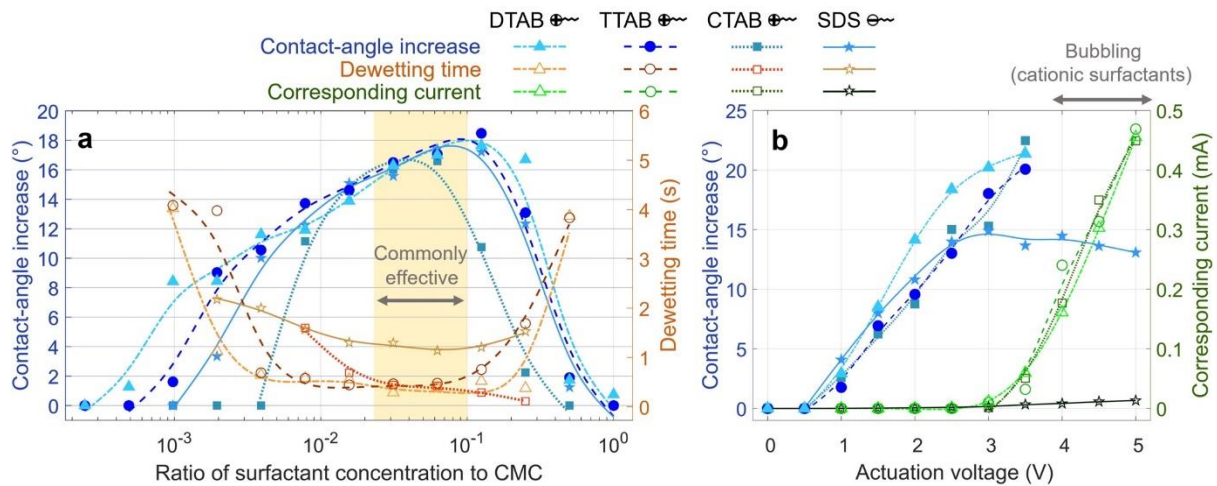


Figure 2-13. Effect of surfactant concentration and actuation voltage on electrodedwetting. **a**, Experiments using cationic (DTAB, TTAB, CTAB) and anionic (SDS) surfactants showed electrodedwetting is effective in a common range (yellow band) of concentration to CMC. The contact-angle increase was the increase from the unactuated (wetted) state to the actuated (dewetted) state, where 2.5-3.0 V (corresponding to  $\sim 3 \mu\text{A}$ ) was applied between the wire and substrate. The dewetting time was the time it took for the wetted state to reach the dewetted state upon electrodedwetting actuation. **b**, The contact-angle increase by electrodedwetting increased with applied voltage, using surfactant concentrations above  $\sim 0.015$  CMC. For cationic surfactants, the electrolytic bubbling rendered the contact-angle measurement unreliable above  $\sim 3.5$  V. In the usual actuation range ( $< 3.0$  V), the current remains below a few  $\mu\text{A}$ . (The lines are only to guide the eye and reveal the trends.)

In the characterization work (Figure 2-13), the droplet recovers to wetting state as soon as the voltage is removed. One can also use reverse voltage to speed up the wetting process. From device perspective, one can obtain better reversibility and reliability if reverse voltage is used for recovery the droplet to wetting state.

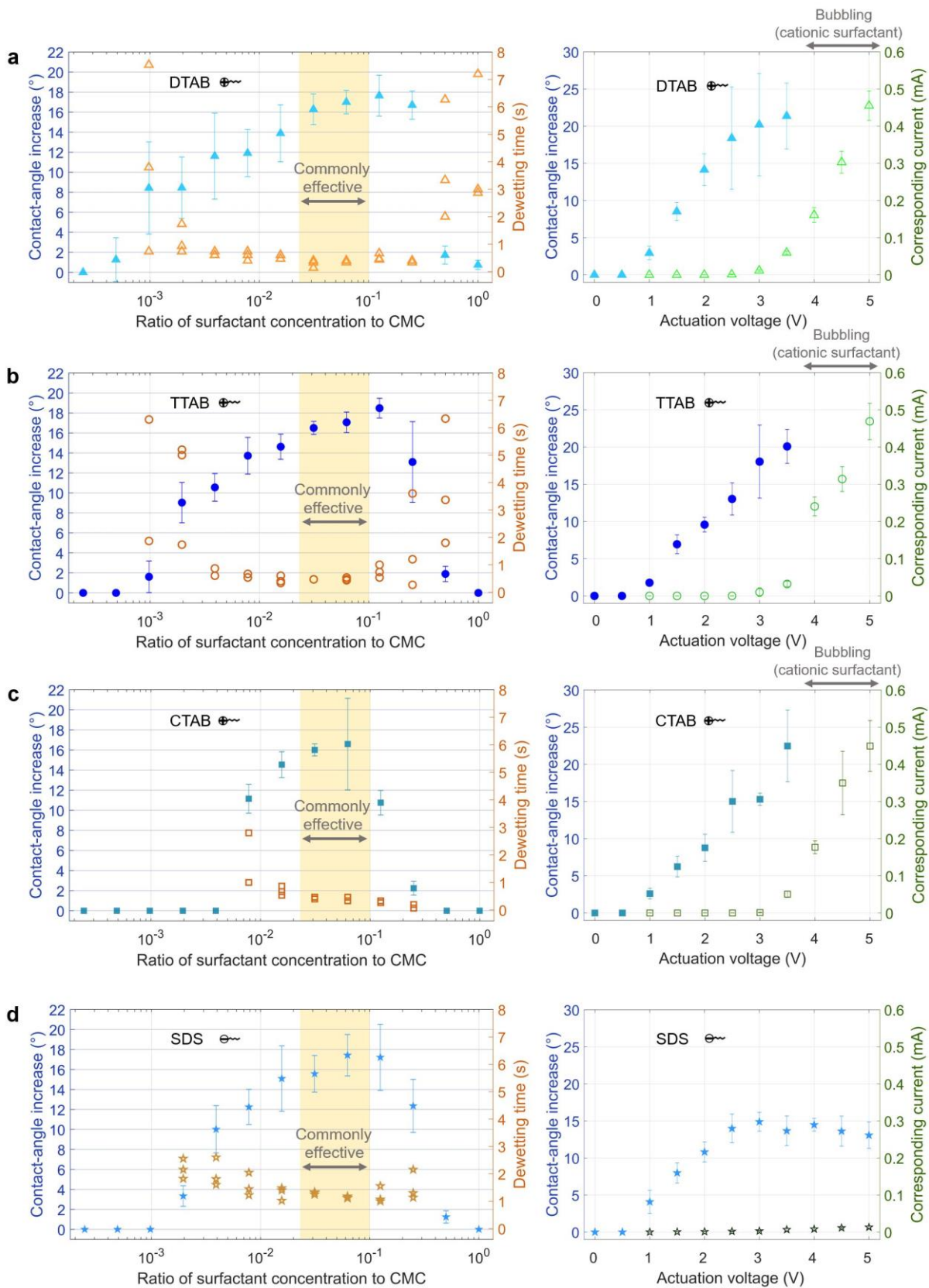


Figure 2-14. Effect of surfactant concentration and actuation voltage (i.e., Figure 2-13) shown separately for each surfactant to include error bars or all data. Each symbol and error bar are an average and standard deviation of 9 measurements (using ~180 images) made with 3 new droplets on 3 different locations across a wafer. Under the natural (unactuated) state, the contact angle was found to increase with surfactant concentration for all four surfactants. However, under the electrodedewetted state, the contact angle was found to increase with surfactant concentration at low concentrations and decrease at high concentrations, with a maximal value in between.

## 2.4.2 Other working conditions

Liquids: We have explored the validity of electrodedewetting for a variety of liquids shown in Figure 2-15.

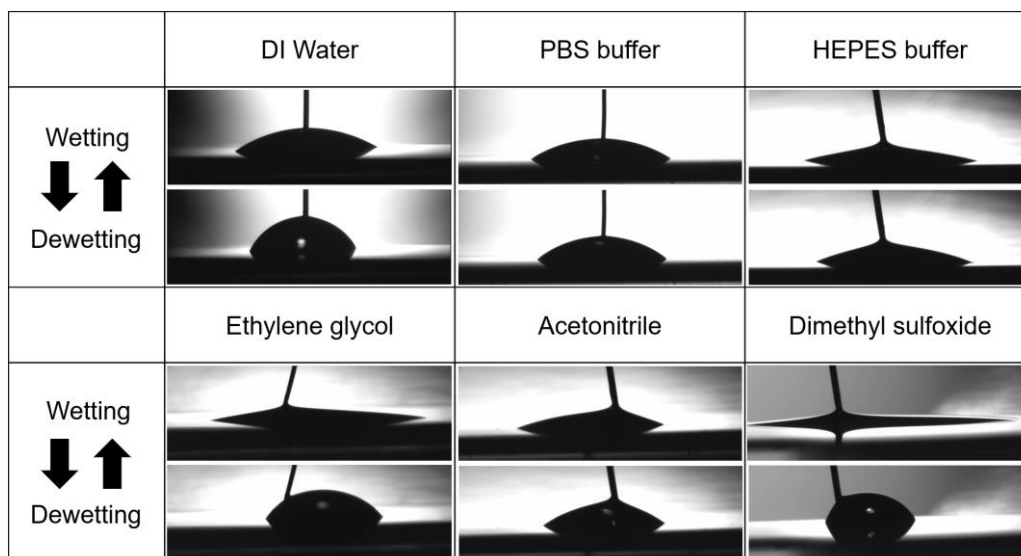


Figure 2-15. Electrodedewetting confirmed for a variety of liquids on bare silicon. DI water is included as a reference. For PBS and HEPES, we added DTAB to a concentration of 0.15 mM and obtained  $\sim 9^\circ$  and  $\sim 6^\circ$  of contact-angle changes, respectively, using  $\pm 5$  V. In the cases of ethylene glycol, acetonitrile, and DMSO, we added DTAB to a concentration of 20 mM and obtained  $\sim 40^\circ$ ,  $\sim 15^\circ$ , and  $\sim 60^\circ$  of contact-angle changes, respectively, using  $\pm 3$  V.

Surfactant type: In addition to the 4 surfactants characterized in Figure 2-13 (DTAB, TTAB, CTAB, and SDS) and the 1 fluorinated surfactant (R18) used for visualization, we have tried 10 additional (2 cationic and 8 anionic) surfactants: didodecyltrimethylammonium bromide (DDAB), dodecylamine hydrochloride (DACl), sodium decyl sulfate, sodium hexadecanesulfonate, dodecylbenzenesulfonic acid sodium salt (SDBS), dioctyl sulfosuccinate sodium salt (DOSS),

sodium laurate, sodium stearate, potassium perfluorohexanesulfonate (PFHxS), and potassium perfluorooctanesulfonate (PFOS). Out of the 9 surfactants we could test properly (sodium stearate was not dissolvable in water at room temperature and not tested for electrodedewetting), all but one (sodium laurate) showed a clear electrodedewetting effect. These additional results suggest the electrodedewetting would be applicable to most ionic surfactants and further support the trends shown in Figure 2-13, although more focused investigation will be required to establish more generalized understanding.

pH of the liquid: We have performed a set of experiments to find the effect of pH (using DTAB). As shown in Figure 2-16, pH affects the degree of autophobing (thus, the initial contact angle) and the surfactant accumulation (thus, the electrodedewetted contact angle), thus affecting the performance of electrodedewetting (i.e., contact-angle increase). It seems multiple mechanisms are in play and beyond the scope of the current manuscript, calling for focused research in the future.

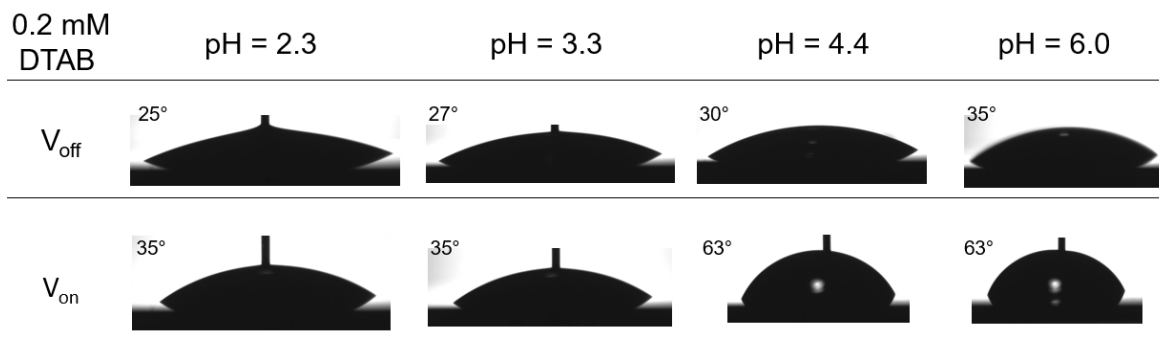


Figure 2-16. The effect of pH on electrodedewetting, obtained for DTAB. The initial contact angles (at  $V_{off}$ ) for higher pH are larger than that for pH 2.3 due to autophobing (also shown in Figure 2-12). The electrodedewetted contact angles (at  $V_{on}$ ) for higher pH are larger than that for pH 2.3 apparently because more surfactant is deposited on the surface at high pH.

Substrates: When we tried electrodedewetting on a gold surface, we did not observe the appreciable contact angle change found on the silicon surface. We believe water, which has 60-65° of contact angle on gold surface [19] is not hydrophilic enough for effective electrodedewetting.

As matter of fact, gold was used as a hydrophobic metal when electrowetting was explored for microfluidics before EWOD took its place [20]. After testing many surfaces, our experience indicated that a hydrophilic surface with contact angle  $< 25^\circ$  is desired to perform effective electrode wetting on. We have found electrode wetting working on the following surfaces: (1) LPCVD  $\text{Si}_3\text{N}_4$  layer; (2)  $\text{SiO}_2$  grown by dry oxidation and (3) sputtered  $\text{SiO}_2$  layer.

### **2.4.3 Contact angle measurement method**

For contact angle data shown in Figure 2-13, we took significant efforts to ensure the repeatability and accuracy of the measurements. First, we prepare the silicon wafer through piranha cleaning and dehydration bake to ensure identical surface condition in each test. Second, we developed an elaborate setup which keeps the wire at the center of the droplet and at a fixed distance against the substrate. Each test is performed inside a Class 1000 cleanroom where the humidity and temperature are controlled. Third, we developed an automatic contact angle measurement software which obtain an averaged contact angle value from multiple images.

Preparation of silicon wafer surfaces: For experiments in Figure 2-13, we prepared bare silicon wafer in the following manner: piranha clean with 3 parts of 98% sulfuric acid and 1 part of 30% hydrogen peroxide at  $110^\circ\text{C}$  for over 10 min; DI water rinse for 10 min; spin dry; bake on a hot plate at  $\sim 450^\circ\text{C}$  for 15 min to remove excess water and  $\text{OH}^-$  groups [21] for a consistent hydrophilicity. This process was used for all wafers including new wafers, i.e., directly out of a factory-sealed package, to ensure all characterization experiments are done on bare silicon of an identical surface condition.

The contact angle measurement setup: The test setup with the accuracy and repeatability needed to study and characterize electrode wetting is schematically shown in Figure 2-17. To



induce electrodedewetting, a platinum (to avoid oxidation and reduction) wire (100  $\mu\text{m}$  diameter) was inserted vertically into a sessile drop on a conductive ( $p^{++}$ , resistivity  $< 0.005$  ohm-cm) silicon wafer (4-inch diameter). Two cameras (Point Grey FL3-U3-13Y3M-C CCD with GO<sup>®</sup> Edmund VZM<sup>™</sup> 200i Zoom Imaging Lens), each mounted on an independent XYZ stage, were used to record the droplet side views, from which contact angles were obtained using ImageJ with DropSnake plugin [22] or an in-house code to assist measuring very low contact angles ( $< 10^\circ$ ). The wafer was placed on an XY stage, and the wire was attached to a separate Z stage. Before each test, the wire was rinsed in DI water to remove the surfactant left from the previous test. After pipetting a droplet ( $\sim 3$   $\mu\text{L}$ ) of surfactant solution onto a fresh wafer, we adjusted the XY stage to center the droplet right below the wire. We then lowered the Z stage to insert the wire into the droplet until the tip of the wire was  $\sim 85$   $\mu\text{m}$  above the substrate for all tests. The orthogonal views of the droplet by the two cameras were used to assist the user positioning the droplet and wire and later measuring the contact angles. A source measure unit (Keithley 2425 SourceMeter<sup>®</sup>) was used to apply voltage and monitor the current between the wire and substrate. All the stages were fixed on a vibration-isolation plate to obtain stable images, and all experiments were performed in a Class 1000 modular cleanroom (Terra Universal 12'x8' Class 1000 Modular Clean Room) to minimize contamination of the fresh silicon surface by the ambient air.

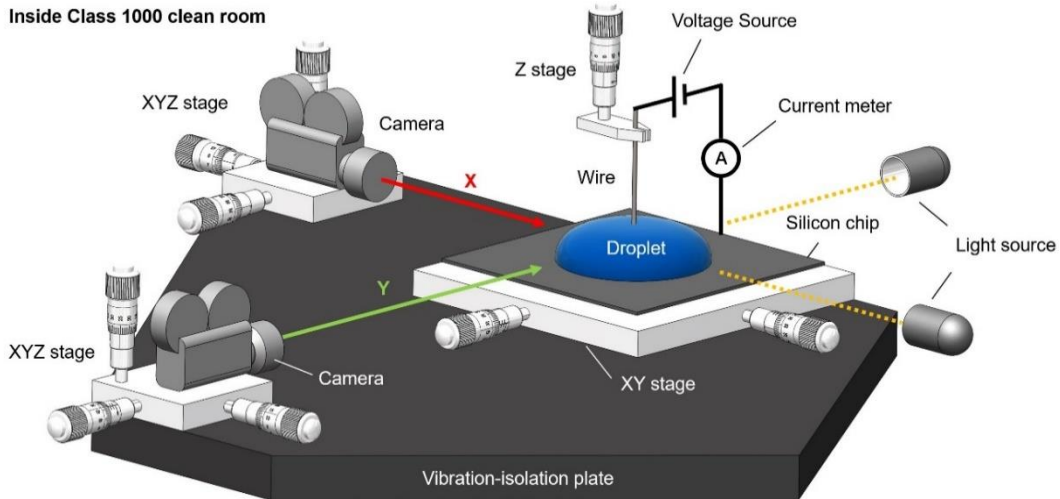


Figure 2-17. Contact angle measurement setup with a wire-droplet system for the current study. The silicon substrate sits on an XY positioning stage; the wire electrode is attached to a Z positioning stage; and two cameras, each mounted on their own XYZ stage, view two orthogonal sides of the droplet. Drawn not to scale for clarity. All the stages are fixed on a vibration-isolation plate.

Automatic droplet detection algorithm for contact angle measurement: In our contact angle measurement, a camera continuously captures the images of the droplet's side profile. Between experiments, the droplets' size, position and the tilting angle (within 1 degree) of the substrates vary. Even during one droplet's experiment, the droplet's contact line may shift when it occasionally moves closer or further from the camera under electrodedewetting. To facilitate automatic contact angle measurement, we developed a method to detect droplet-substrate-contact-line (shown in Figure 2-18).

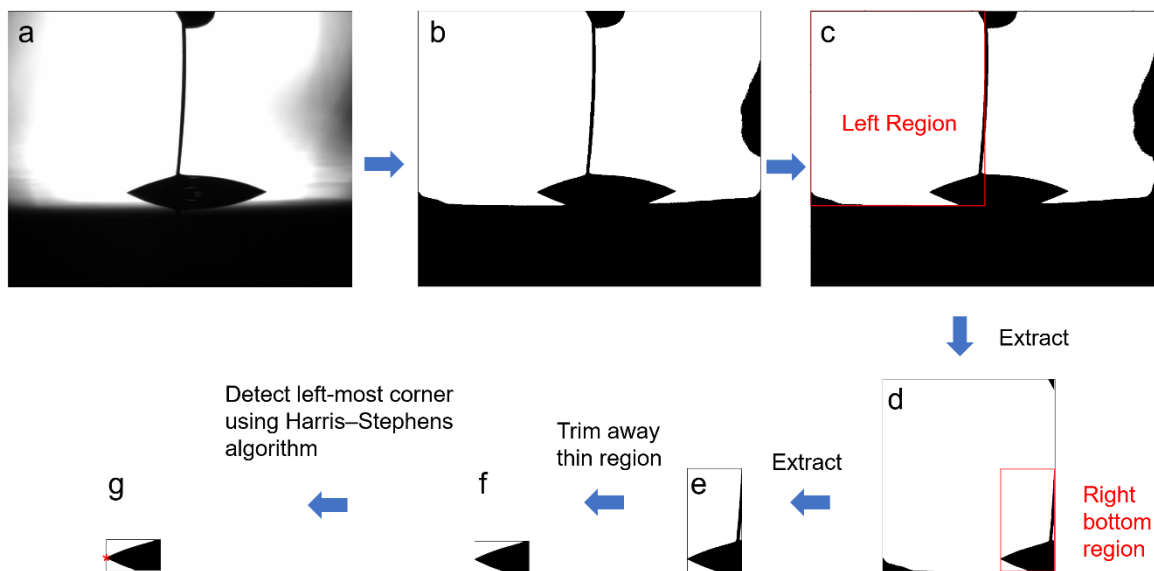


Figure 2-18. Method for detecting droplet-substrate-contact-line for automatic contact angle measurement. **a**, a grey scale image is obtained from camera recording the side profile of a droplet. If an RGB camera is used, one need to convert the RGB image into greyscale image at this step. **b**, the greyscale image is converted into a binarized image. **c**, the needle inserted in the droplet serves as a dividing line that separate the white background region. The algorithm outlines the rectangle boundary of the left region with red lines. **d**, the left region which contains the left profile of the droplet is chopped. Within **d**, it's easy to identify that the right-bottom region contains the profile of the droplet and its reflection on the substrate. The algorithm outlines the rectangle boundary of the right-bottom region with redlines. **e**, the right-bottom region is chopped from **d**. **f**, the wire's profile is further trimmed away and we finally obtained the minimized rectangle region within which the left half of the droplet and its reflection is located. **g**, the left-most corner (marked with a red asterisk symbol) is detected using Harris-Stephens algorithm. The same method applies to the right side of the droplet to obtain the right-most corner. The droplet-substrate contact line and tiling angle of the substrate is then obtained to fit following contact angle measurement algorithms.

## 2.5 Electrodeposition Device

### 2.5.1 Open air device configuration

Placed over neighboring electrodes, a water droplet containing ionic surfactant can be translated by electrodeposition in a mirror fashion of the well-known electrodeposition. As illustrated in Figure 2-19, an external voltage is applied between two electrodes in a way the resulting electric field in the liquid makes the droplet (containing cationic surfactant) dewetted on the left electrode but remain wetted on the right electrode. As result, the droplet is “repelled” (pushed) to the right.

This is conceptually similar but opposite to the droplet translation by electrowetting, where the droplet is “attracted” (pulled).

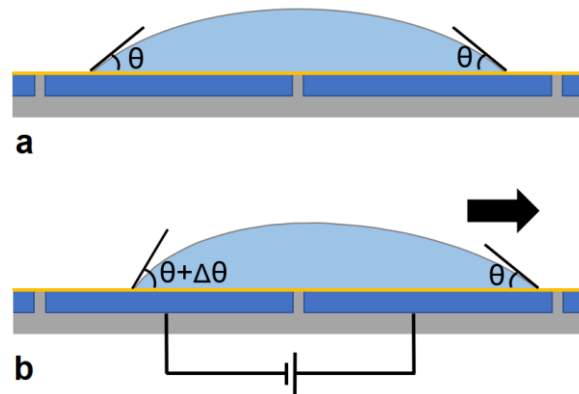


Figure 2-19. A droplet over two electrodes is moved by electrodeposition. **a**, A droplet sits across two electrodes; **b**, Electrodeposition on the left electrode repels the droplet to the right.

To relate the electrodeposition-based microfluidic device (Figure 2-19), which is free of the electrode wire, and the wire-in-droplet setup used for studying the electrodeposition mechanism (Figure 2-2), we have prepared Figure 2-20. The figure shows that the wire-free device (Figure 2-19 or Figure 2-20a) is electrically equivalent to the wire-droplet system (Figure 2-2 or Figure 2-20c). For example, characterization with a wire-droplet (Figure 2-2) shows electrodeposition works well with  $\pm 2.5$  V, and one will likely design a digital microfluidic device (Figure 2-22) to operate with DC power switching between 0 V and 5 V.

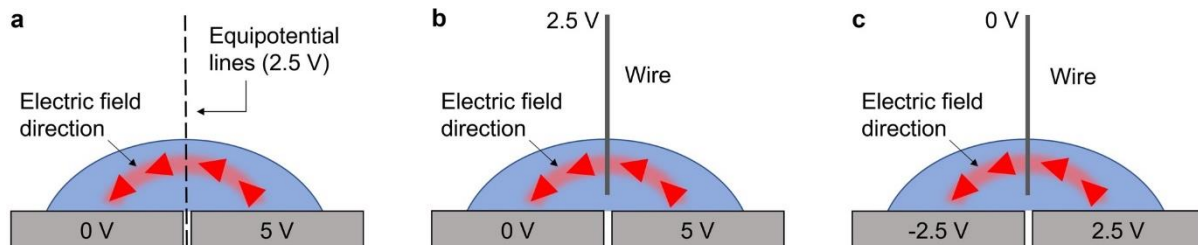


Figure 2-20. Electric actuation of a droplet at two adjacent electrodes explained with an imaginary top wire, assuming a cationic surfactant. **a**, When a droplet is actuated on the electrodeposition microfluidic device (Figure 2-22), it sits across a 0 V electrode and a 5 V electrode. For simplicity, assume the droplet is symmetric and imagine an equipotential line of 2.5 V at the center of the droplet. **b**, The case of a is electrically equivalent to having a 2.5 V wire in the droplet along the equipotential line. **c**, The case of b is

electrically equivalent to having a 0 V wire and having a -2.5 V electrode and a 2.5 V electrode. Note the left half of the droplet, where an electric field is formed from the wire (0 V) to the left electrode (-2.5 V), relates to Figure 2-2a (i.e., dewetting), and the right half of the droplet, where an electric field is formed from the right electrode (2.5 V) to the wire (0), relates to Figure 2-2b (i.e., wetting). Combining the left half (dewetting) and right half (wetting), the net effect is forcing the droplet to the right. Note the red arrows indicate the overall direction of the electric field between electrodes and do not imply electric field intensity.

### **2.5.2 Electrodeposition device made on silicon**

We found electrodeposition can be fabricated with a much simpler process flow compared with EWOD devices. We started with a silicon on insulator (SOI) wafer of a 2.5  $\mu\text{m}$ -thick top silicon layer (n<sup>++</sup>, resistivity < 0.0025 Ohm-cm) and 2.2  $\mu\text{m}$ -thick embedded silicon dioxide on  $\sim$ 500  $\mu\text{m}$ -thick base silicon wafer (n<sup>-</sup>, resistivity = 5000-10000 Ohm-cm). First, the top silicon layer was thinned down to  $\sim$ 1  $\mu\text{m}$  (ranging 0.3-1.3  $\mu\text{m}$  across the 4"-diameter wafer, measured by a surface profilometer; Veeco Dektak-8) by multiple cycles of thermal oxidation and etching of the silicon dioxide with buffered oxide etchant (BOE). This thinning would have been unnecessary if SOI wafers with desired device layer thickness were available at the time of study. The silicon electrodes were defined with a 10  $\mu\text{m}$  gap between them by patterning the top silicon layer using deep reactive-ion etching (DRIE, 90 sec, etching rate 1-2  $\mu\text{m}/\text{min}$ ) with AZ5214 photoresist as the etching mask. After removing the photoresist with acetone, we put the wafer through the process described in the "Preparation of silicon wafer surfaces" section in Chapter 2.4.3. The native oxide formed on the silicon surface is a natural state and its property does not change by itself over time. It is particularly attractive that the electrodeposition device can be easily cleaned and reused (just like glass beaker), unlike most existing microfluidic products including EWOD devices.

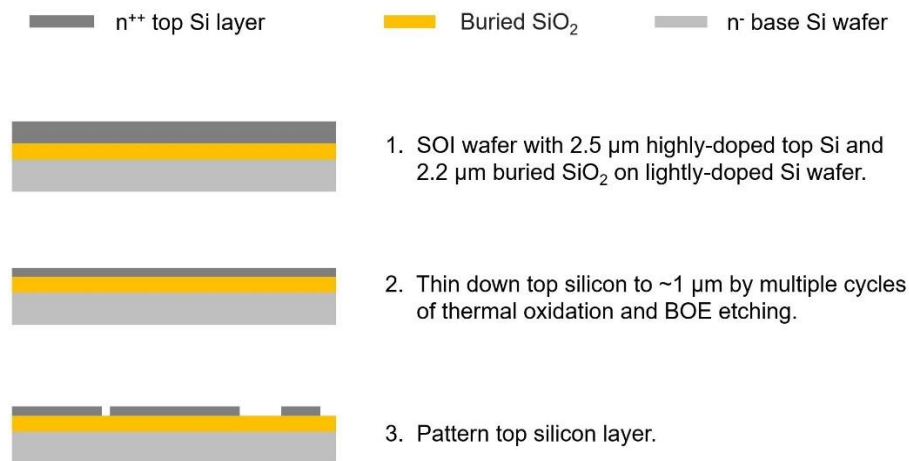


Figure 2-21. Fabrication process of the electrodedwetting device used to demonstrate the digital microfluidic operations in this study (drawn not to scale). The thin-down step was added only because SOI wafer with thin-enough top silicon layer was not available at the time of fabrication.

Using proper actuation sequences and 0.2 mM DTAB solution, we have achieved droplet generation, transportation, splitting, and merging. Although pH 2.3 solution was used for Figure 2-22 to be consistent with Figure 2-13, any pH level works as indicated in Figure 2-11. Building blocks for more complex microfluidic protocols for applications [23], these basic droplet logic operations were successfully obtained in air, i.e., without the help of the commonly-used filler oil, on an open device, i.e., without using a cover plate. While in-air operations are more difficult than in-oil but still possible, open-device operations of generating or splitting droplets is not possible with EWOD [23]. Furthermore, the droplets were transported (Figure 2-22) in a speed comparable to EWOD despite the 10-100 times slower actuation observed during sessile drop tests (Figure 2-13). This unique performance of electrodedwetting suggests its microfluidic operation comparable to EWOD in addition to the inherent reliability.

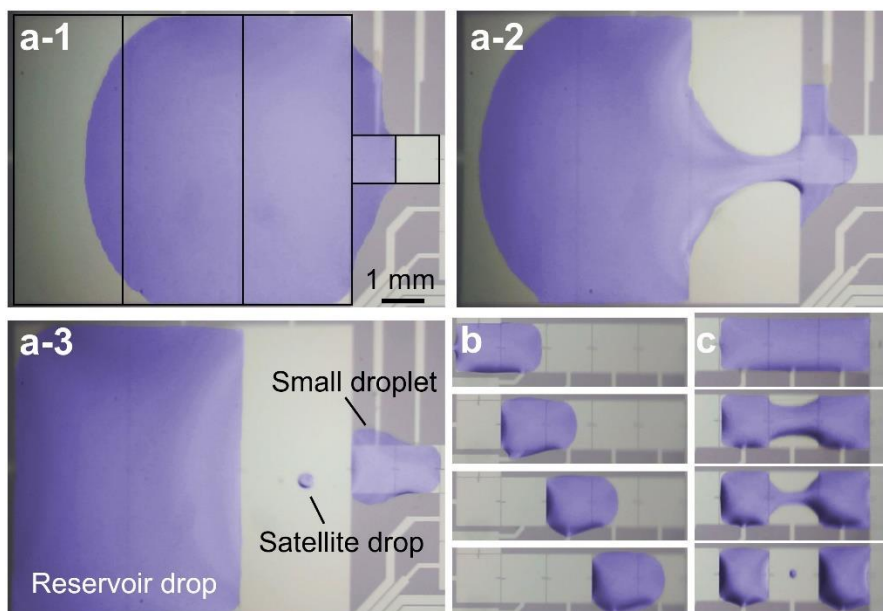


Figure 2-22. Droplet generation, transportation, and splitting realized by electrodeposition. Water droplets are operated in air on a silicon device with no cover plate, using  $\pm 2.5$  V (or 0 and 5 V). Images were captured from video and enhanced by coloring the liquid portions. **a**, Sequential images of a small ( $\sim 0.2$   $\mu\text{L}$ ) droplet generated from a reservoir droplet ( $\sim 3$   $\mu\text{L}$ ). **a-1**, The added black lines indicate the large electrodes underneath the reservoir. **a-2**, Dewetting the third reservoir electrode from left results in necking of the reservoir droplet. **a-3**, A droplet is generated on the two small electrodes to the right of the reservoir. **b**, **c**, Four sequential images showing droplet transportation and splitting. Along with **a** and merging (not shown), they establish the basis for digital microfluidics.

### 2.5.3 Electrodeposition device made on glass

For silicon device shown in Figure 2-22, the water droplet is in direct contact with native silicon oxide ( $\text{SiO}_2$ ) layer. It is reasonable to speculate that a  $\text{SiO}_2$  layer deposited on a conductive substrate may also work for electrodeposition. Our results showed a PECVD-coated  $\text{SiO}_2$  does work for electrodeposition when deposited to an ITO coated glass substrate. The device is transparent and is compatible with today's LCD manufacturing method (Figure 2-23), revealing its potential use in many optical applications. A preliminary result in Figure 2-24 shows splitting a droplet on the developed electrodeposition device with no cover plate. This enhanced ability over EWOD in open configuration is understood by recognizing the electric field is stronger near the gap between the electrodes. However, we observed noticeably stronger tendency for satellite

droplet to appear. However, we observed noticeably stronger tendency for satellite droplet to appear. Although a simple device layout was used in this proof-of-concept study, in future research we expect to design the electrode shapes that make use of the advantages and limit the drawbacks of electrodedewetting compared with EWOD.

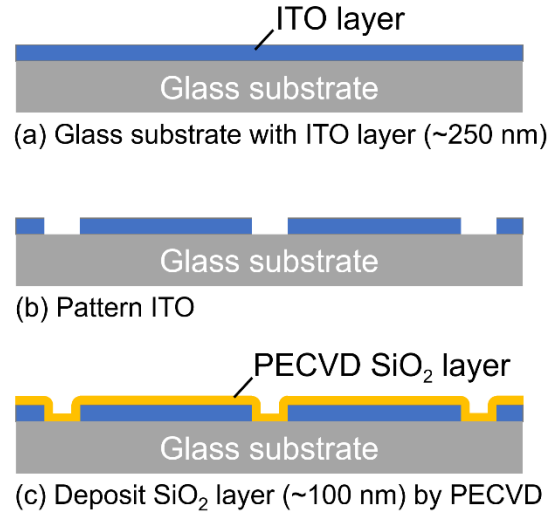


Figure 2-23. Fabrication process of transparent electrodedewetting device. (a) ITO-coated soda-lime glass as received; (b) Lithographic patterning of ITO; (c) Deposition of SiO<sub>2</sub> by PECVD.

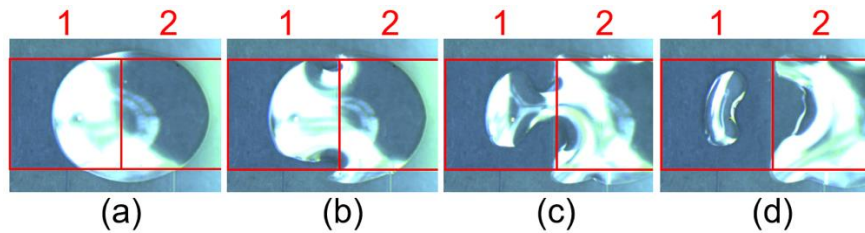


Figure 2-24. Sequential images showing a droplet of surfactant-containing DI water being split on the transparent device (with no cover plate) in air. This type of droplet manipulation was not observed with EWOD. When voltage is applied between two electrodes, electric field inside the liquid is stronger near the gap between them. This field concentration leads to early dewetting near the gap on electrode 1 and assists cutting (a, b) but also causes asymmetric cutting (c, d).

## 2.6 Summary



We report “electro-dewetting” that acts in an opposite manner to electrowetting, i.e., electrically repels a droplet on substrate reversibly. This ionic surfactant-mediated mechanism uses a hydrophilic conductive surface, eliminating the added layers along with the associated problems. This study investigates the underlying mechanism and basic characteristics of electro-dewetting needed for its implementation. Using only  $\pm 2.5$  V, a few  $\mu\text{A}$ , and  $\sim 0.015$  critical micelle concentration (CMC) surfactant, electro-dewetting is demonstrated to perform all the basic fluidic operations of digital microfluidics with water on silicon in open air. The compatibility is further validated with a variety of liquids, including common buffers and organic solvents, showing great promise for a microfluidic platform that is extremely simple and highly reliable.

## 2.7 References

- [1] Lomax, D. J. et al. Ultra-low voltage electrowetting using graphite surfaces. *Soft Matter* **12**, 8798–8804 (2016).
- [2] Monroe, C. W. et al. Electrowetting with electrolytes. *Physical Review Letters*. **97**, 136102 (2006).
- [3] Eaker, C. B., Joshipura, I. D., Maxwell, L. R., Heikenfeld, J. & Dickey, M. D. Electrowetting without external voltage using paint-on electrodes. *Lab Chip* **17**, 1069–1075 (2017).
- [4] Nave, M. I., Gu, Y., Chen-Wiegart, Y.-C. K., Wang, J. & Kornev, K. G. Is an electric field always a promoter of wetting? Electro-dewetting of metals by electrolytes probed by in situ X-ray nanotomography. *Faraday Discuss.* **199**, 101–114 (2017).
- [5] Hu, G.-H., Xu, A.-J., Xu, Z. & Zhou, Z.-W. Dewetting of nanometer thin films under an electric field. *Phys. Fluids* **20**, 102101 (2008).
- [6] Lapierre, F., Coffinier, Y., Boukherroub, R. & Thomy, V. Electro-(de)wetting on Superhydrophobic Surfaces. *Langmuir* **29**, 13346–13351 (2013).
- [7] Gallardo, B. S. et al. Electrochemical principles for active control of liquids on submillimeter scales. *Science* **283**, 57–60 (1999).
- [8] He, S., Meng, Y. & Tian, Y. Correlation between adsorption/desorption of surfactant and change in friction of stainless steel in aqueous solutions under different electrode potentials. *Tribol. Lett.* **41**, 485–494 (2011).

- [9] Cho, H. J., Mizerak, J. P. & Wang, E. N. Turning bubbles on and off during boiling using charged surfactants. *Nat. Commun.* **6**, 8599 (2015).
- [10] Xu, W., Xu, J., Li, X., Tian, Y., Choi, C.-H., & Yang, E.-H. Lateral actuation of an organic droplet on conjugated polymer electrodes via imbalanced interfacial tensions. *Soft Matter* **12**, 6902 (2016).
- [11] Nelson, W. C. & Kim, C.-J. Droplet actuation by electrowetting-on-dielectric (EWOD): a review. *J. Adhes. Sci. Technol.* **26**, 1747-1771 (2012).
- [12] Peng, L., Qisui, W., Xi, L. & Chaocan, Z. Investigation of the states of water and OH groups on the surface of silica. *Colloids Surfaces A Physicochem. Eng. Asp.* **334**, 112–115 (2009).
- [13] Hare, E. F. & Zisman, W. A. Autophobic Liquids and the Properties of their Adsorbed Films. *J. Phys. Chem.* **59**, 335–340 (1955).
- [14] Luk, V. N., Mo, G. C. H. & Wheeler, A. R. Pluronic additives: a solution to sticky problems in digital microfluidics”, *Langmuir* **24**, 6382-6389 (2008).
- [15] Goloub, T. P., Koopal, L. K., Bijsterbosch, B. H., Sidorova, M. P. Adsorption of cationic surfactants on silica. Surface Charge Effects. *Langmuir* **12**, 3188–3194 (1996).
- [16] Dick, S., Fuerstenau, D. & Healy, T. Adsorption of alkylbenzene sulfonate (A.B.S.) surfactants at the alumina-water interface. *J. Colloid Interface Sci.* **37**, 595–602 (1971).
- [17] Mugele, F. *et al.* Ion adsorption-induced wetting transition in oil-water-mineral systems. *Sci. Rep.* **5**, 10519 (2015).
- [18] Annapragada, S. R., Dash, S., Garimella, S. V. & Murthy, J. Y. Dynamics of droplet motion under electrowetting actuation. *Langmuir* **27**, 8198–8204 (2011).
- [19] Erb, R. A. Wettability of gold. *J. Phys. Chem.* **72**, 2412–2417 (1968).
- [20] J. Lee, H. Moon, J. Fowler, T. Schoellhammer, and C.-J. Kim, “Electrowetting and electrowetting-on-dielectric for microscale liquid handling”, *Sensors and Actuators*, **A95**, 259-268, (2002).
- [21] Peng, L., Qisui, W., Xi, L. & Chaocan, Z. Investigation of the states of water and OH groups on the surface of silica. *Colloids Surfaces A Physicochem. Eng. Asp.* **334**, 112–115 (2009).
- [22] Stalder, A. F., Kulik, G., Sage, D., Barbieri, L. & Hoffmann, P. A snake-based approach to accurate determination of both contact points and contact angles. *Colloids Surfaces A Physicochem. Eng. Asp.* **286**, 92–103 (2006).

- [23] Cho, S. K., Moon, H. & Kim, C.-J. Creating, transporting, cutting, and merging liquid droplets by electrowetting-based actuation for digital microfluidic circuits. *J. Microelectromechanical Syst.* **12**, 70–80 (2003).

## **Chapter 3    Cybermanufacturing Ecosystem for Digital Microfluidics**

### **3.1 The background and motivation**

Currently, most labs who perform research related to the digital microfluidics (mostly based on the electrowetting-on-dielectric or EWOD technology) need to handle everything themselves, from design and fabrication of the device (chip) to instrumentation for operation and testing of the fabricated device. Without the access to device fabrication facilities, one cannot perform digital microfluidics research. Even with the fabrication facilities, one needs to establish the device fabrication know-hows and deal with many practical difficulties, such as the reliability issues of EWOD device (shown as two bottlenecks in Chapter 1.3). Even for those who have overcome the technical barriers, i.e., those who can fabricate and operate EWOD devices, the process of developing new devices is of low efficiency and high cost. First, lacking the standardized rules and the specialized CAD tools for digital microfluidics, one has to design and draw all the electrodes on a device using a CAD developed for other purposes. Second, fabricating a small number of EWOD devices needed for a lab is much more expensive than mass production. Third, as application-unique layouts are used for each EWOD device and non-standardized components are used for the operating system, it is not possible to connect disparate parts between different groups, preventing synergistic breakthroughs via collaboration or economic development via specialization.

To lower the technical barriers for new users and make the development of EWOD device more efficient for existing players, we are building a cybermanufacturing system for EWOD digital microfluidics. The effort is to cultivate an ecosystem where a wide range of users (e.g., researchers, entrepreneurs, students, hobbyists) can focus on their own ideas and applications

without worrying about the engineering and manufacturing side of EWOD digital microfluidics. (Figure 3-1). Saved from the significant effort demanded from each user, the digital microfluidics community is expected to grow as anticipated based on its inherent potential. Further, by attracting more people from various background (for example material science, chemistry, or IC industry), the reliability problems of EWOD devices will have a better chance to be solved.

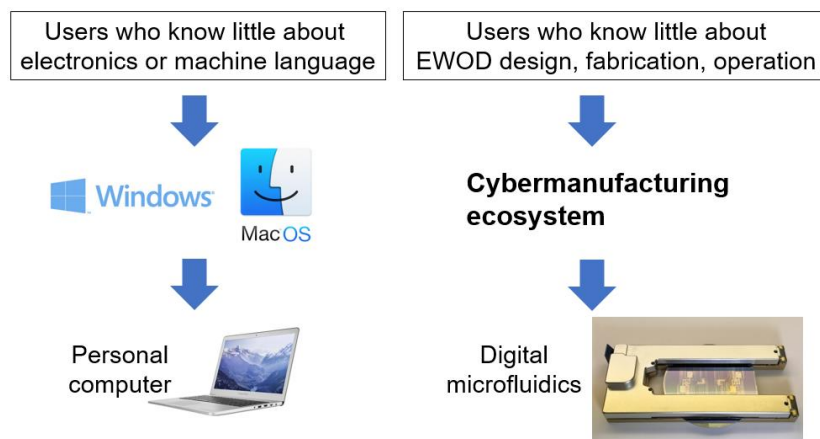


Figure 3-1. Inspired by how the operating systems (OS) of Windows and Macintosh flourished the PC industry, the cybermanufacturing ecosystem (also referred to as “cybersystem” in this manuscript) aims to boost the field of digital microfluidics by letting people, who know little about EWOD design, fabrication and operation, utilize digital microfluidics as a convenient liquid handling platform.

### 3.2 Cybermanufacturing ecosystem architecture

The cybersystem resides on a cloud server, and its web services link users to various resources. Figure 3-2 shows its architecture with blue arrow indicating the workflow between entities. A user (may be a researcher, entrepreneur, student, or hobbyist from various fields) initiates the workflow with an idea. It could be a simple neutralization reaction, a complex DNA library preparation protocol [1], or a lab-on-a-chip research topic. Sketching how the liquid droplets should be generated from reservoir, transported, split, or merged [2], the user can design own digital microfluidics chips inside a dedicated CAD which enforces the design rules. The

design files are, then, sent to one of the EWOD device foundries. During device fabrication, different users share the same fabrication process using only standard materials and specifications in a way printed circuit board (PCB) business is run today. This limitation is necessary to keep the cost under control and ensure device reliability. Users may also order an electronic operating system developed to drive EWOD devices and accessory modules (e.g., cameras, heaters, and magnetic actuators) as needed for own applications. Lastly, users are encouraged to share their design files among the online community to ease replications by others and help accumulate the knowledge for the entire community.

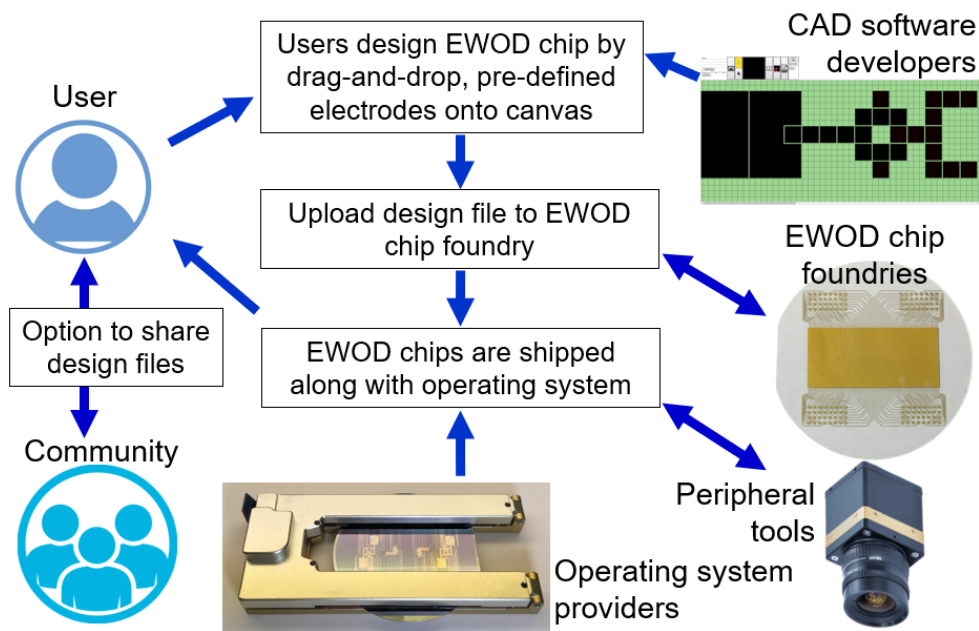


Figure 3-2. The architecture of cybermanufacturing ecosystem. The blue arrows represent the work flow of web services that links users, CAD providers, foundries, operating system and peripherals providers.

The cybersystem aims to serve the mass and, thus, is required to provide highly flexible services to accommodate various different needs. On the other hand, in order to keep the cost under control and ensure device reliability, the cybersystem needs to impose certain restrictions in device

layout, device configuration, and hardware implementation. These trade-offs are considered and balanced during the implementation of CAD tools, the foundry service, and the electronic operating system.

### **3.3 The EWOD CAD**

With no dedicated CAD tools available, most users are using existing design software packages, including those developed for PCB design or IC layout, to design EWOD devices – mostly drawing the electrode patterns and traces. Since the design rules necessary for successful EWOD device are not embedded in the above software, users have to rely on their experience and effort to design an error-free EWOD device. It would take days to complete one design and weeks or months of iterations (of design, fabrication, and testing) to obtain working devices. In order to increase the design efficiency and empower anyone to design own EWOD devices, we have developed a CAD tool for EWOD and made it available for the cybersystem.

Imagining how the liquid droplets should move, split, merge, and be generated and where special regions, such as the sample entries and reservoirs or waste collectors and exits, should be located, the user can drag and drop various electrodes on a blank canvas using the EWOD CAD software. Several shapes are available for the EWOD electrodes and the minimum gap between the electrodes are predefined to ensure successful fabrication and operation of the EWOD digital microfluidic devices. After the user finishes drawing all the EWOD electrodes, the CAD performs auto-trace-routing and generates a mask file needed for device fabrication. The CAD assists users to perform repetitive tasks such as drawing EWOD electrodes and saves them from the difficult task of mapping and drawing traces between EWOD electrodes and the contact pads, which connect the EWOD device to the electronic operating system. For a common practice, a new user

will likely finish drawing a new EWOD device in just a few hours. Most importantly, the imbedded design rules would guarantee the new design is free from common errors.

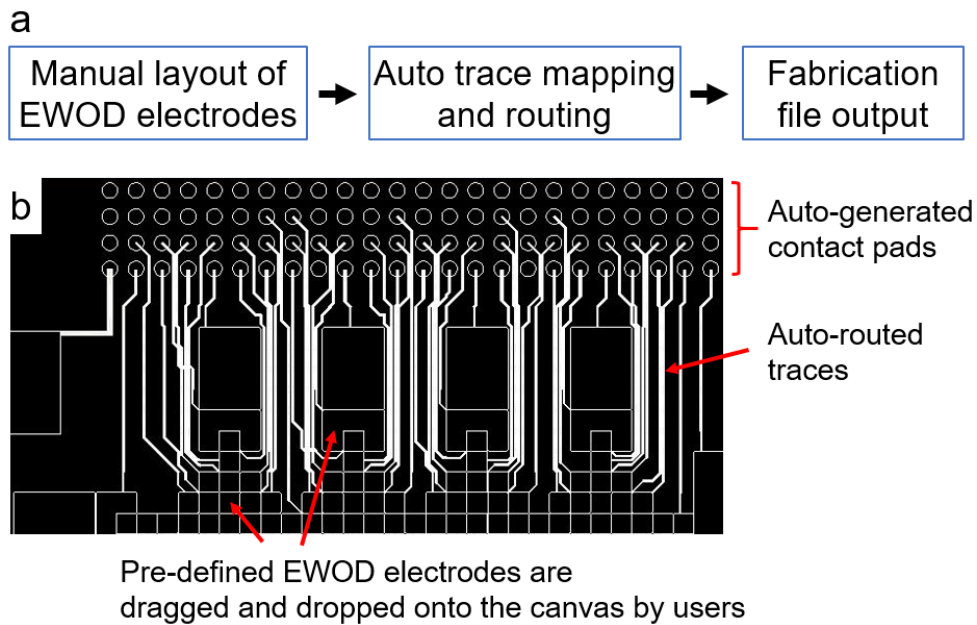


Figure 3-3. Our current version of EWOD CAD greatly reduces the time needed in designing an EWOD device by offering pre-defined EWOD electrode shapes and auto-routing of the traces. **a**, A user designs the layout of the EWOD electrodes by dragging and dropping predefined electrodes on a canvas. The position data of these electrodes are then fed into an auto-routing program which generates mapping and traces between EWOD electrodes and contact pads (The contact pads are used for electrically interfacing with an EWOD control system). The CAD then outputs fabrication file which a foundry can directly use. **b**, Partial image of the fabrication file (in DXF format) generated by our CAD for single layer EWOD device.

The CAD, in the current version (with auto-routing algorithm from Professor Tsung-Yi Ho at National Tsing Hua University), will serve design of EWOD devices with single electrode (typically metal) layer made typically on glass or paper. Because the EWOD electrodes and the traces are made in the same layer, the single-layer devices can accommodate a limited number of EWOD electrodes that can be accessed and controlled independently. As a result, one cannot design a “general” or “universal” EWOD device that would require hundreds of independently controllable electrodes in order to serve multiple applications. Multi-layer EWOD devices made of PCB [3] or TFT [4] would be needed for complex tasks that require many independently



controllable EWOD electrodes. However, there are ample needs for the single-layer EWOD devices [5] for numerous users, and their low cost of fabrication is most important, especially at the early stage of development for both the individual users and the cybersystem. As the cybersystem stabilizes and the need for the multilayer EWOD device grows, the EWOD CAD will be advanced to accommodate the design of multilayer EWOD devices.

### **3.4 The EWOD foundry service**

Users can upload their design files, generated from the EWOD CAD in the cybersystem or other CAD programs, to the cybersystem and have their design fabricated by a foundry linked to the cybersystem. The services to fabricate the EWOD devices would open the field to a wide range of individuals and labs who do not have an access to the fabrication facilities and would not have considered using digital microfluidics without the cybersystem. The quality control expected from foundry services as well as the saving of cost and time would be attractive also to many labs who are capable but would shy away from the burden. The standardized fabrication protocols, along with the operating guidelines, would also alleviate the users from the reliability issues of EWOD, such as the notorious failure by electrolysis.

Design files are sorted and fed to one of the foundry services depending on the device type – glass, paper and PCB. The trade-offs between the three types are listed in Table 3-1. The glass EWOD devices are fabricated in an IC-fabrication cleanroom, taking full advantage of the traditional IC microfabrication facilities. The device has a flat surface, a small gap between electrodes (e.g.,  $< 10 \mu\text{m}$ ), and a quality dielectric layer and would perform the best among the three types. The glass EWOD would make generation, movement, splitting, and merging of water droplets possible in air as well as in oil environment. In comparison, the PCB EWOD would make

generation, movement, splitting, and merging of water droplets possible in oil environment but not in air. Instead, the number of directly addressable electrodes can be high for the PCB EWOD device due to the multilayer interconnection capability of PCB. The paper EWOD device requires higher actuation voltages due to its low-resolution patterns but has the lowest fabrication cost and shortest fabrication time. Except above methods, a low cost and low topography fabrication method for multilayer EWOD devices is present in Chapter 5.

Table 3-1. Comparison between EWOD devices made of various substrates. The advantages of each type are shaded in green.

Substrate material	Surrounding / Device configuration	Interconnection	Substrate transparency	Cost
Glass	<ul style="list-style-type: none"> <li>• Air / Cover plate</li> <li>• Air / Open device</li> <li>• Oil / Cover plate</li> </ul>	Single layer	Transparent	High
Paper	<ul style="list-style-type: none"> <li>• Air / Open device</li> </ul>	Single layer	Opaque	Low
PCB	<ul style="list-style-type: none"> <li>• Oil / Cover plate</li> <li>• Air / Open device</li> </ul>	Multilayer	Opaque	Medium

### 3.5 The online portal (the design)

Users (including researchers, entrepreneurs, students, and hobbyists) interact with the cybersystem through webpages. Without physically building instruments or fabricating EWOD devices, companies and start-ups will be efficient in developing EWOD related products without hiring or training specialists in digital microfluidics. In academia, if one group successfully performs experiments using their EWOD device design, then other groups can order the same EWOD device from the cybersystem and replicate or build upon the existing design. Through the online forum of the cybersystem, users will post electrowetting related questions and make

discussions. The online forum will help new users and those not specializing in electrowetting learn common issues and all users keep abreast of ongoing issues so that the community grow together without much duplications and re-inventions.

To achieve above goals, the online portal will play a major role. Residing on the cloud server, it performs the following tasks: 1) hosting a portal site with all major services listed; 2) enables user to download CAD software and hosts the online version of the CAD; 3) manages users' orders for the EWOD device fabrication and keeps track of the fabrication status; 4) manages stock of the EWOD operating systems and ensures they are shipped and delivered; 5) hosts library where user can share design files and post testing results; 6) hosts forum where experts and starters meet; 7) hosts a wiki which contains study materials for digital microfluidics from various levels.

Learning from mature industry such as PCB manufacturing industry as well as emerging 3D printing industry while infusing the cybersystem with the traits of digital microfluidics, we designed the webservices are as follows:

Hosting a portal website: A portal website is a welcome page for the users. It serves the big picture of the cybersystem by listing all major services: 1) the online EWOD CAD; 2) the foundry service and 3) the EWOD electronic control system as well as other services such as the online community, support, and login/out of their account etc. A mock up portal page is shown as following:

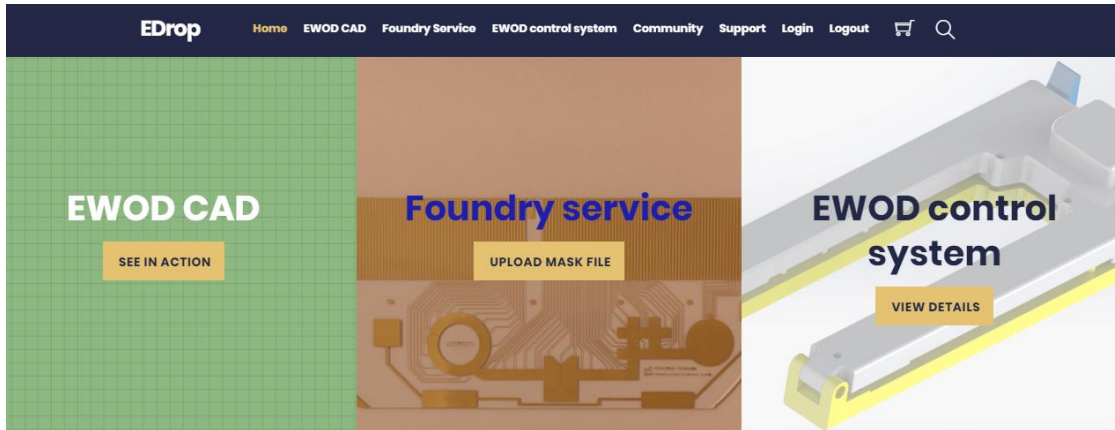


Figure 3-4. A mock page for the portal website which clearly lists and links to the major services of the cybermanufacturing system: the EWOD CAD, foundry service and EWOD electronic control system.

Hosting an online EWOD CAD: The EWOD CAD is a dedicated CAD tool aiming to expediate the design cycle of the EWOD device while enforcing design rules to increase success rate and facilitate design reuse. The main function of the EWOD CAD is described in Chapter 3.3. Except hosting the EWOD CAD to allow users access it through a webpage, the webservice also manages the following related aspects:

- 1) Account management. Without an account, user can design EWOD devices online and then save the design file to their local machine. However, in order to keep copies of their design files on the cloud and access them anywhere later, users need to create an account or associate their Gmail/Facebook account to the cybersystem. Like many mature e-commerce accounts, the account also maintains a user's other information such default shipping and billing address, history of quotes and orders, communication history between users and foundry services etc.
- 2) EWOD device design file management. Users are encouraged to share EWOD device design files generated from EWOD CAD within the online community. If one design proves to be successful, other users could benefit from it by directly ordering the same chip using the foundry service or they could improve further from existing design. Each design file will be further

integrated with droplet actuation sequence file and they together facilitate duplications of electrowetting experiments between users.



Figure 3-5. A mock page displaying the thumbnails of the design files generated by different users. By clicking on other people's design file, a user is directed to the EWOD CAD interface where he/she can design his/her own device on top of others'. This utility was widely used in many online CADs (such as Gallery view in TINKERCAD).

Manage the online foundry service: Depending on the type of substrate (an EWOD device can be made either on a glass, paper or PCB substrate), the corresponding manufacturing facilities are different and they are located on different site. There is at least one worker working on each site managing the fabrication process. The cybersystem managed the online foundry service in the following aspects:

- 1) User configures online foundry services. The cybersystem allows users to upload fabrication files generated from the EWOD CAD or from any third-party CAD software such as L-Edit or Altium designer. With the fabrication file uploaded, the user configures how the EWOD device should be made through a webpage mocked in Figure 3-6.

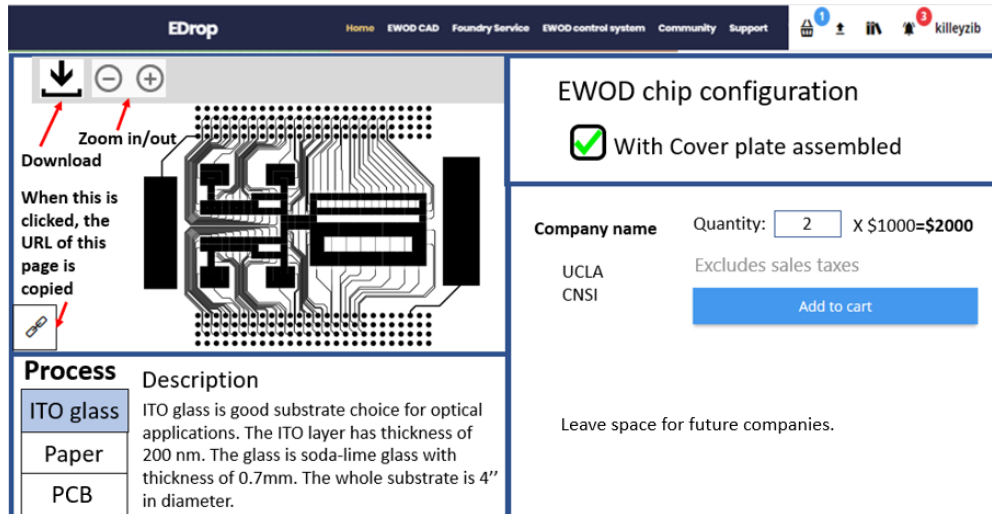


Figure 3-6. A mock page where a user is able to configure the order before sending it for manufacturing. The left top window shows the thumbnail of the fabrication file, the URL of this webpage can be copied and sent to other users for duplicating EWOD devices. The left bottom window shows the selection of fabrication processes. The trade-offs between processes (quality, cost, limitations) are listed. The right bottom window lists the instant quote for this design. Multiple quotes may appear from different manufacturers. After user confirms the order, the rest of the procedures (filling shipping address, payment methods and tracking packages etc.) are similar to today's e-commerce site.

2) Order management. Orders are sent to foundries once they are confirmed by the user. Meantime, the administrator of the cybersystem will be notified through email and by text messages. The administrator does the review work and initiates the photomask fabrication process for glass EWOD device and initiates the PCB board fabrication for PCB EWOD device. Then the fabrication file, the photomask and the bare PCB board will be sent to foundry workers who start the fabrication processes. If unexpected design flaws happen during the review processes or during the fabrication process, the administrator is responsible to contact the user immediately to advise design changes. The incident will be recorded and feedback to the CAD design team who updates the EWOD CAD to ensure future similar incident will be automatically caught by the CAD. Through the cybersystem, the administrator oversees all orders and all workers' progress in multiple manufacturing sites. For the foundry workers, they are well trained and are fully focused on fabricating the EWOD devices according to stand

operational procedures. An EWOD device fabrication process contains steps including dielectric coating, hydrophobic coating and baking, top plate assembly, quality check and packaging. Steps such as depositing metal layer and etching are also required for glass EWOD device. The worker updates the order status when they finish each step. The user can view the record of the order status and gets notified once the order is complete.

Manage distribution of EWOD control systems and general-purpose EWOD devices: The EWOD control system is for operating and debugging EWOD devices. It includes hardware and software which need to be distributed through the cybersystem. The general-purpose EWOD device is a premade EWOD device that has maximum numbers of electrodes possibly patterned on a substrate, its goal is to help users verify application before designing their own chip for mass fabrication. The concept is similar to a FPGA which is used to verify chip design before users transfer the design into an ASIC. Today's e-commerce site is sufficient for distributing both EWOD control system and EWOD devices, the major parts are designed as follows:

- 1) An online storefront where users manage orders and download software/user manuals. Figure 3-7 shows the mocked storefront for distributing the EWOD control system and the general-purpose EWOD devices.



Figure 3-7. A mock page of the online storefront for the EWOD control system and the general-purpose EWOD device made on glass (bottom left) and on silicon substrate (bottom right).

- 2) Case-study pages for the general-purpose EWOD device and examples for customized designed EWOD devices. Each case study provides step-by-step instructions which are carefully written by administrator of the cybersystem. The instructions are in uttermost detail, ensuring users without any former training can perform the same experiment with little support.

Knowledge accumulation of the cybersystem: We are infusing our current knowledge of EWOD device and control system into the cybersystem. Once the cybersystem starts to operate normally, it should be able to keep itself accumulated with new knowledges. This is to be implemented in the following methods:

- 1) The cybersystem holds an online library where shared design files are stored.
- 2) The cybersystem holds an online forum where users demand support when encountering difficulties and share experience for successful implementations.
- 3) The cybersystem also holds an online feedback channel for users to report issue and suggest ideas directly to the administrator of the cybersystem.



- 4) The knowledge accumulated in the online forum and feedback channel are unsorted data which need to be further summarized and categorized for better readability for the mass. An administrator working for the cybersystem will periodically sort the gained knowledge and summarize it in an online wiki.

### 3.6 Summary

We have conceived a cybermanufacturing ecosystem that allows users (including researchers, entrepreneurs, students, and hobbyists) use EWOD digital microfluidics with little training and low cost. Within the cybersystem, we infused our expertise of electrowetting and EWOD to arrange a dedicated EWOD CAD, prepare foundry services to fabricate EWOD devices, provide an EWOD operating system that has high flexibility, and construct an online portal that accumulates and shares knowledge and designs. With a few clicks on their computers, it is envisioned that users will be able to have their EWOD designs fabricated as devices and delivered to them for digital microfluidic operations. We expect the cybermanufacturing system will serve as an accelerator to explore applications and develop new products of digital microfluidics.

### 3.7 References

- [1] Kim, H. et al. A Microfluidic DNA Library Preparation Platform for Next-Generation Sequencing. *PLoS One* **8**, e68988 (2013).
- [2] Cho, S. K., Moon, H. & Kim, C.-J. Creating, transporting, cutting, and merging liquid droplets by electrowetting-based actuation for digital microfluidic circuits. *J. Microelectromechanical Syst.* **12**, 70–80 (2003).
- [3] Jian Gong & Chang-Jin Kim. Direct-Referencing Two-Dimensional-Array Digital Microfluidics Using Multilayer Printed Circuit Board. *J. Microelectromechanical Syst.* **17**, 257–264 (2008).

- [4] Hadwen, B. et al. Programmable large area digital microfluidic array with integrated droplet sensing for bioassays. *Lab Chip* **12**, 3305 (2012).
- [5] Jang, I. et al. Application of paper EWOD (electrowetting-on-dielectrics) chip: Protein tryptic digestion and its detection using MALDI-TOF mass spectrometry. *BioChip J.* **11**, 146–152 (2017).

## **Chapter 4 A USB-Powered Smartphone-Size Electronic Control System for Digital Microfluidics Devices**

### **4.1 The market need**

As a major part of the cybermanufacturing ecosystem (shown in Figure 3-2), an EWOD device control system is needed to break down the technical barrier (Chapter 1.3) which hinders the growth of the EWOD community. It is simple and fast to make an electronic board that can demonstrate droplet manipulations by electrowetting actuation [1], [2]. However, building a device operating system, which allows users from different disciplines (including non-engineering) to efficiently develop and debug EWOD devices, would require considerable time and efforts unless already experienced. Currently, companies with EWOD products possess well-developed control systems, but they are highly customized for their own devices. Efforts have been made to provide an electronic control system for the public [3], but it is also developed to operate their own devices. Considering many EWOD researchers make their own microfluidic devices [4], [5], [6], [7] using different materials, sizes, peripherals, and protocols due to their diverse needs, we designed a control system with a goal of accommodating the majority of users. To lower the barrier further and allow people in a wide range of disciplines and technical levels (including even high school students and hobbyists) to exercise EWOD, the electronic control system will serve as an important part of the cybermanufacturing ecosystem, which allows users to design and obtain EWOD devices. We believe such an electronic system is possible at a reasonable price if the control circuits are compact and the chassis is made of a minimum number of parts. Although the development took multiple iterations and was challenging and expensive, the resulting system reported here fits the bill with a unit cost expected to plunge when mass-produced.

## 4.2 Approaches for EWOD control circuits

During electronic operation, the EWOD control circuits should between switch tens or even hundreds of electrodes independently between ground and high voltage (over 50 V most times and over 100 V quite often). The key for building EWOD control circuits is implantation of high voltage switches. A straightforward and common approach is to build circuits on a PCB board with arrays of discrete relays [2], [8], [9]. This first approach has its advantage of wide selection of relays in different voltage-current ratings and speeds. Electromechanical relays or opto-solid-state relays allow not only high voltages but also analog signals. Furthermore, they allow high currents, giving the circuits the highest flexibility, such as integrating sensors, heaters, etc. However, they are usually not fast (switching time  $> 1$  ms) and not suitable for low power applications. Besides, a system that contains over 200 electrodes requires wiring of hundreds of relays on one or multiple PCBs, making the whole system bulky, complex, and expensive [2], [8], [9].

The second approach of implementing the circuits is to use commercially available serial-to-parallel high-voltage converter with push-pull outputs. High voltage CMOS chips, such as HV3418 and HV507 packed with 64 output channels, are attractive for their compact size, ease of implementation, and low cost (~\$20 per chip). They are commonly found in commercial products (e.g., Mondrian SP Workstation of NuGEN) and some open source platforms (e.g., Open Drop V2 of Gaudi Lab). To illustrate the working principle, we drew an EWOD device in the left top of Figure 4-1 with its electrodes on the substrate plate (as well as the reference electrode on the cover plate) connected to switches (which represent the push-pull CMOS output inside the chip). Each of the switches toggles independently between ground and a high DC voltage. For AC actuation, which is more popular in practice for more reliable EWOD performance, all the switches continue

to toggle periodically with Electrode 1 and Electrode 2 in 180-degree phase difference, as shown in the left bottom of Figure 4-1. This is electrically equivalent to feeding Electrode 2 with a square wave that has both positive and negative amplitude while keeping Electrode 1 (as well as the top electrode) grounded, as shown in the bottom right of Figure 4-1. The frequency of the square wave is determined by the toggling speed of all switches. The disadvantages of this approach lie with the limitations of converter chip themselves (HV3418 and HV507). For an example, HV3418 can only supply DC voltages in the range between ~30 V and 180 V, which means it cannot be used for electrowetting devices requiring voltages below 30 V. Similarly, HV507 can only supply DC voltages in the range between ~40 V and 300 V. Another disadvantage is that all the channels should be toggled simultaneously for AC actuation, thus the power consumption increases significantly with the frequency of the AC signals. As a result, the frequency used in this method is normally less than 10 kHz for a USB powered system.

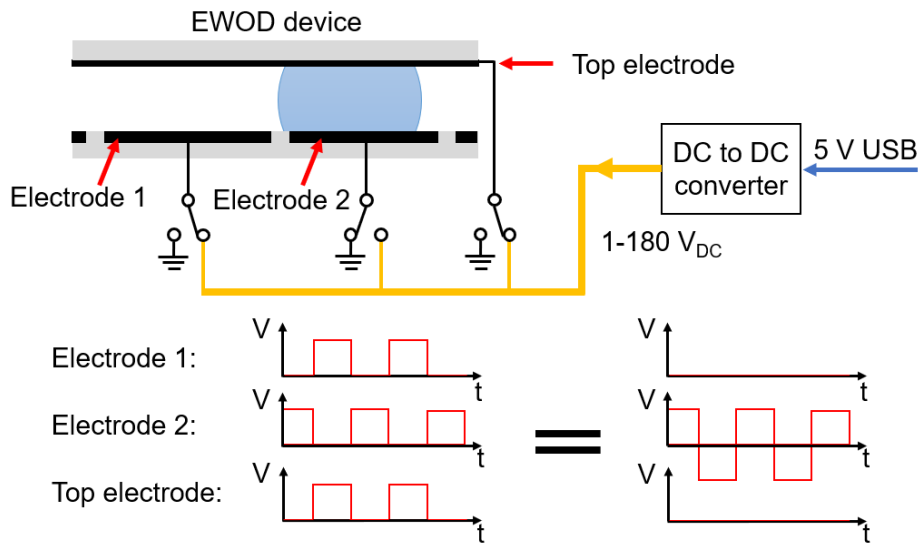


Figure 4-1. The control circuits allow users to provide DC or AC signals (with tunable amplitude and frequency) to the individual electrodes independently. Inside the control circuits, a DC-DC converter converts the 5 V voltage from USB cable to DC signals in the range of 0-180 V. The arrays of switches toggle the electrodes on EWOD device independently between DC voltage and ground. For AC actuation, the switches continue to be toggled periodically, providing square wave signals to each electrode. Note

Electrode 2 has 180-degree phase difference between Electrode 1 and Top electrode. This is equivalent to connecting Electrode 1 and Top electrode to ground while applying a square wave with twice the amplitude to Electrode 2 while grounding other electrodes.

The third approach of implementing the circuits involves building an active matrix with high voltage transistors. Using LCD manufacturing technique, thin-film transistors (TFTs) can be made directly on a glass EWOD device. Since this method can control thousands of electrodes independently, one droplet may be controlled by multiple (e.g., ~20) small electrodes underneath it. Another important advantage is that the extra room available under one droplet may be used to additional functions for each electrode, such as the impedance sensing to measure the droplet volume precisely. The disadvantage is the relatively high price of the TFT-based EWOD chip, although the economy of volume of the huge flat panel display market certainly helps.

## **4.3 The electronic control system developed**

### **4.3.1 Overall description of the system**

In general, the main control system consists of three major components: control circuits, device interface, and the graphic user interface (GUI), as shown in Figure 4-2.

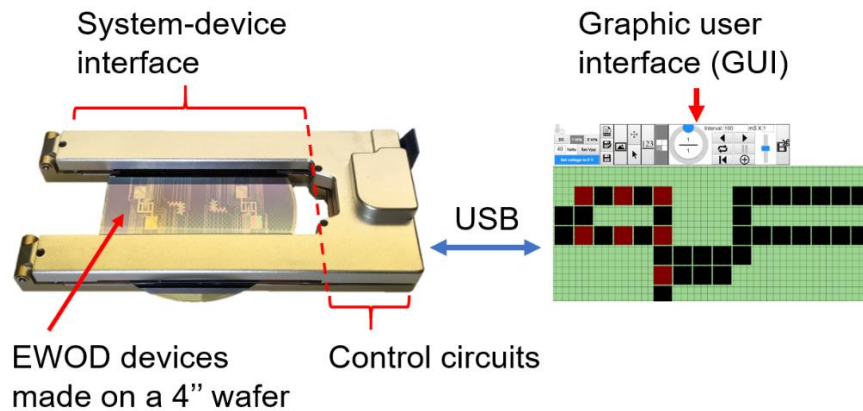


Figure 4-2. Our electronic control system for digital microfluidics consists of three major components: the control circuits, the device interface, and GUI. The U-shaped aluminum body has control circuits (footprint of 8 cm x 4.5 cm) hidden in it, and the system-device interface (8.2 cm x 20 cm) spreads along its two forks. The GUI, configurable to various electrodes layout on EWOD device, runs on a PC and communicates with the control circuits through a USB cable, which also powers the operating system.

Add-on peripherals, such as heater, cooler, magnetic actuator, and cameras, can be integrated around the main system, for particular applications in need. To fit our purpose of serving the mass, we focused on the main system, leaving room for different labs and users to add their own add-ons if desired. To help the add-ons access the device loaded in the system, the device interface (see Figure 4-2 left) is arranged in a way to leave the spaces above, below, and sides of the device open and unobstructed. Combined with a compact control circuits, the device interface is housed within an aluminum alloy chassis, which has a footprint of a cell phone. The housing is less than 3 cm in thickness, which allows users to put the system into their carrying bag or even a pocket for portable applications. Because our goal is to develop the operating system as a versatile tool rather than a click-and-run product, we designed our current GUI to run on PC (supporting both Windows and Mac OS) rather than on a phone or a tablet for maximum functionality. The GUI in the PC communicates with the circuits in the control system through a USB-C cable, which also powers the control system.

### 4.3.2 The control circuits and PCB

For the control system shown in Figure 4-2, we implemented the second approach described in the previous section, using HV3418 to produce 30-180 V in DC or 60-360 V<sub>pp</sub> in AC with the maximum frequency of 5 kHz for all electrodes.

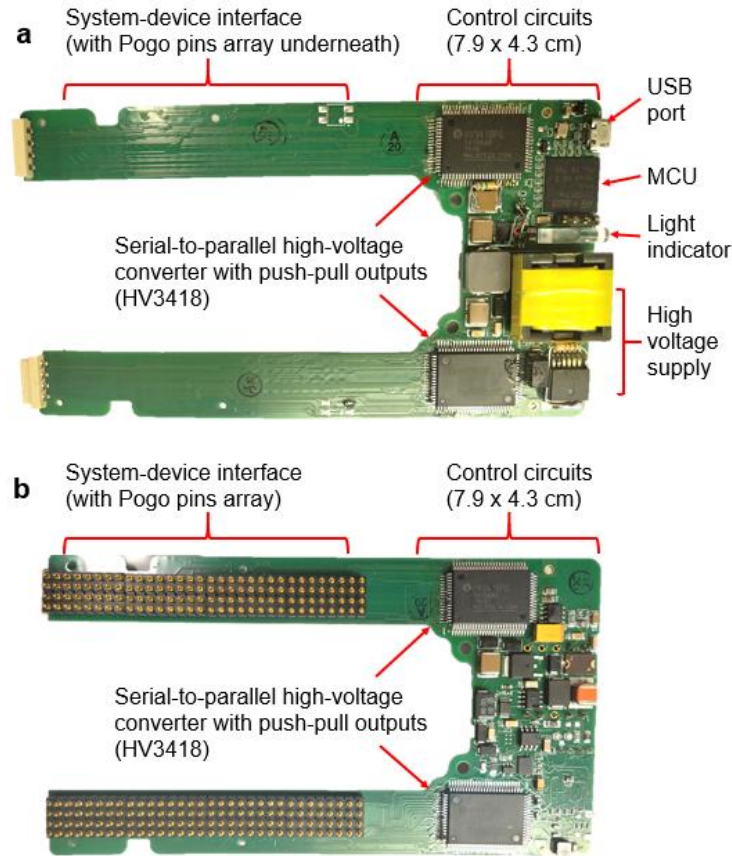


Figure 4-3. The electronic circuits and device interfaces revealed by removing the aluminum chassis from the system. **a**, The circuits utilized commercially available serial-to-parallel high-voltage converter HV3418 to supply 30-180 V in DC or 60-360 V<sub>pp</sub> in AC to 240 output channels. The footprint of the circuits (7.9 cm x 4.3 cm) is in the size of a credit card. **b**, The PCB substrate (the side facing the EWOD device) is extended to the left in the picture to implement the system-device interface, where an EWOD device is loaded.

It is useful to add extra functions, such as position sensing, feedback control, and on-chip heating, as implemented in our previous version of the control circuits [12]. However, these functions require a dedicated EWOD device, which does not align with our current goal of serving



the mass. As a result, we decided not to implement the above add-on functions in the current control circuits.

### **4.3.3 The alignment and interfacing of EWOD device**

When operating EWOD devices, especially disposable ones, a user needs to load and unload the devices into and off the control system frequently. During the loading step, the user should accomplish electric connections between the arrays of electrodes on an EWOD device and the hundreds of output channels of the control circuits effortlessly without alignment error. The connector technologies of the PC industry were borrowed for the EWOD systems from the early days [13], [14]. The use of a memory edge connector can achieve a small form factor in the system [15], but it requires machining a precise outline of the EWOD device. An LGA connector can make routing of the EWOD device ease [16], but it hinders installation of components (such as a heater) underneath the EWOD device. It is also feasible to assemble through-hole pins (header) on an EWOD device [17], if the number of connections is relatively small; if not small, the pins would make the EWOD devices expensive. Pogo pins are spring-loaded metal pins compatible with various EWOD devices including ones made from soft materials. These convenience and versatility led us to adopt Pogo pins for our interface. Furthermore and importantly, to achieve alignment without machining the EWOD device for precise outlines or alignment holes/slots, we developed a unique manual alignment mechanism [18] shown in Figure 4-4 (with the detailed working principle in the caption). As result, if preferred, a whole 4'' wafer containing several EWOD devices can be directly tested in the current system without dicing the wafer into individual devices. This convenient alignment method not only saves the user's efforts, but the use of whole wafer also eliminates the chance of device contamination during dicing.

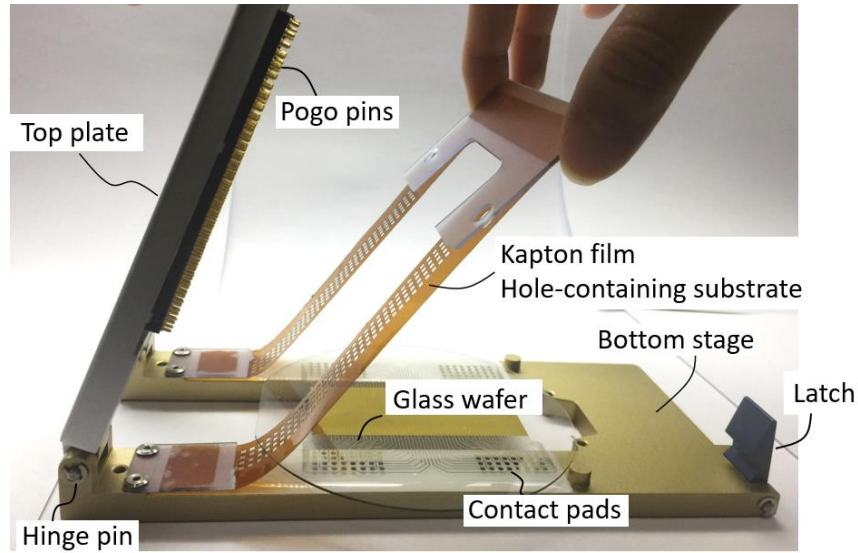


Figure 4-4. The system includes a unique mechanism to align the device to system quickly and conveniently for accurate interfacing [14]. This method utilizes a Kapton (transparent) film with arrays of holes. After a user places an EWOD device (shown: 4" glass wafer) on the bottom stage, the user lets the Kapton film rest over the EWOD device. While looking through the holes in the film, the user shifts the device on the bottom stage until all the contact pads on the EWOD device are seen through the holes. This manual alignment is easy and takes only a couple of seconds. Then, the user lowers the top plate, making all the Pogo pins travel through the holes and land on the contact pads on the device. With one simple push by the user, the latch locks the first substrate onto the bottom stage, securing the EWOD device in place with all the electric connections made and ready for electronic operation.

The device interface is also adaptable to EWOD devices made as small pieces. Figure 4-5 shows the use of three different types of EWOD devices: **a)** glass-based, **b)** silicon-based, and **c)** paper-based.

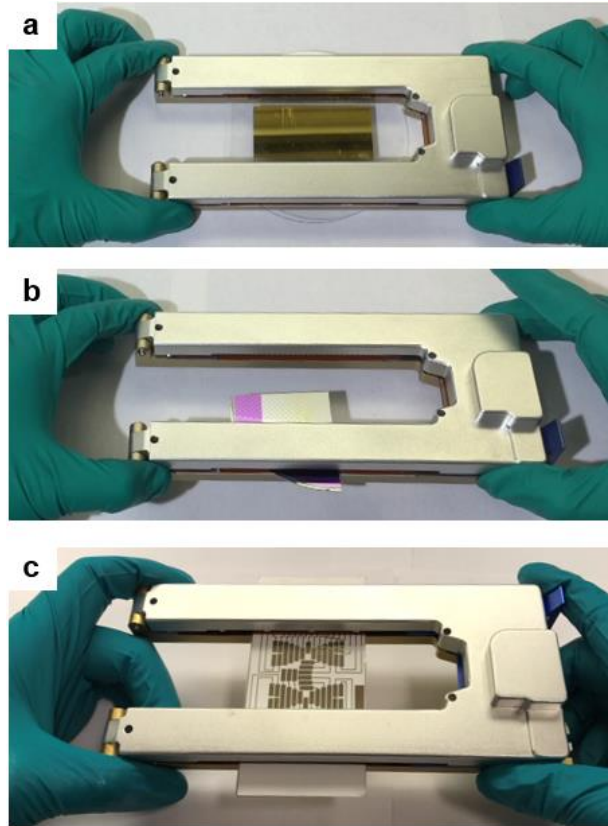


Figure 4-5. The system can operate devices with a range of thicknesses and sizes. The Pogo pins have a travel distance large enough to accommodate from the thin paper-based to the thick PCB-based EWOD devices. The unique alignment mechanism eliminates the need to dice the wafer to precise dimension or multiple pieces. The aluminum housing is designed in a U shape to open the space for transparent devices and facilitate add-on tools, such as heaters, coolers, cameras, and sensors, from the sides, top, or bottom of the system. Loading of different devices are shown: **a**, Whole 4'' glass wafer. **b**, A quarter piece of a silicon wafer. **c**, A paper device (courtesy of Prof. K. Shin's lab at Sogang University).

#### 4.3.4 The graphic user interface (GUI)

In most commercial EWOD product [19], [20], a GUI is built for click-and-run operations. The end-user chooses a pre-defined command file and runs actuation sequences without knowing the on/off status of electrodes and the routing details of droplets. In comparison, the GUI for the current system is more of a developing and debugging software, which allows researchers and developers to (i) change the layout of the GUI based on the electrode layout and wire routing of their EWOD device and (ii) program the actuation sequences and save them into a command file.

To maximize its functionality, the GUI is implemented on a PC running on either Windows or Mac OS.

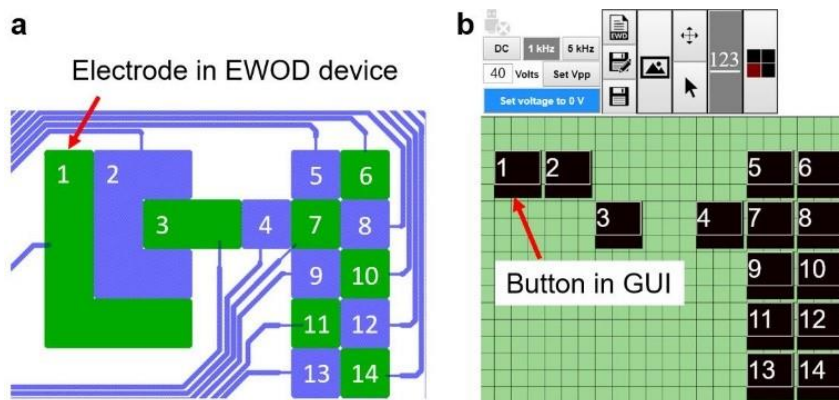


Figure 4-6. **a**, An electrode on an EWOD device is electrically connected to a numbered channel of the control system. **b**, A clickable button inside a GUI can be assigned to a number corresponds to an electrode on the EWOD device. The button controls the on/off status of the electrode.

The circuits in the current electronic control system contains 248 independent output channels, which correspond to the 248 Pogo pins in the device interface numbered from 1 to 248. On an EWOD device, an electrode that is electrically connected to a Pogo pin should be assigned with that Pogo pin's number (shown in Figure 4-6). The toggling of each electrode's on/off status is realized by clicking buttons that carry the same numbers in the GUI. Depending on the layout of the electrodes, user can arrange the locations of the buttons of the GUI by simple "drag and drop" actions. The number shown inside the button can be easily changed by the user, enabling the user to move the EWOD device to any preferred locations in the device interface. The above features make the GUI in the current system highly adaptable to various electrode layouts and wire routings in different EWOD devices.

Besides clicking the buttons manually, users can also let the system run by itself according to a preprogrammed actuation sequence. Users can directly program an actuation sequence inside

the system’s GUI, or they can use Excel or their own droplet routing algorithm [21] to generate an actuation sequence file according to the given GUI format. The ability to import and export a file containing actuation sequences not only makes programming more flexible but also facilitates users to share experimental protocols or repeat the experiments.

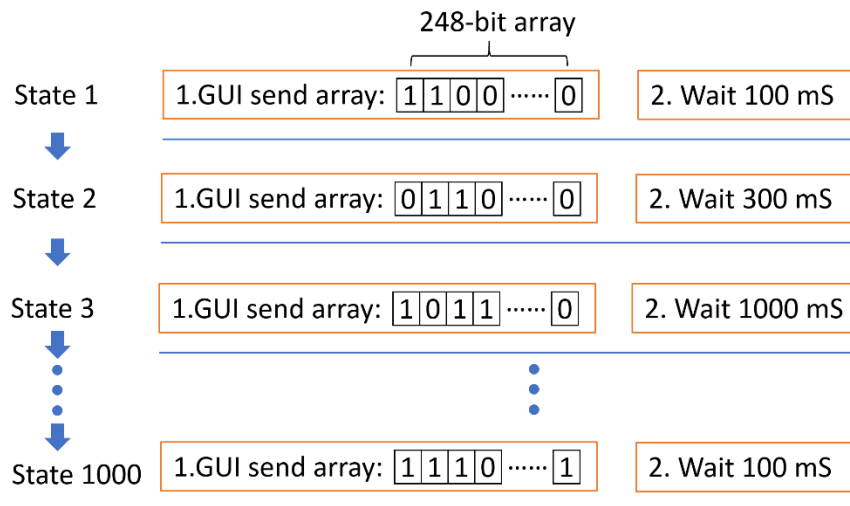


Figure 4-7. An actuation sequence contains thousands of states. The states are executed sequentially. At each state, two events occur: (1) The GUI immediately sends a 248-bit array to the control circuit through USB. According to the value of each bit inside the array (“1” or “0” means on or off status), the control circuit updates all the 248 channels. (2) The GUI waits for a predefined time before executing the subsequent state. During this waiting time, the channels’ on/off status remains unchanged.

## 4.4 Summary

We have built an operating system for (mostly EWOD-based) digital microfluidics with a goal of serving the mass, including various labs with own EWOD devices and people new to digital microfluidics. The system has been designed for adaptability and flexibility while keeping the final cost low. The device interface was designed to ensure the system can accept EWOD devices made of various thicknesses (i.e., materials) and sizes quickly and easily, while leaving rooms for add-on tools by the users. The GUI can be easily customized for different electrode layouts and wire routings. The control circuits based on CMOS chips allowed the whole system to keep a low profile

(2 cm-thick mostly and 3 cm at the thickest region) and a small footprint (19 cm x 8 cm or about a cell phone size), giving users a possibility even for portable applications.

## 4.5 References

- [1] <http://www.gaudi.ch/OpenDrop/?p=261>
- [2] Lee, J., Moon, H., Fowler, J., Schoellhammer, T. & Kim, C.-J. Electrowetting and electrowetting-on-dielectric for microscale liquid handling. *Sensors Actuators A Phys.* **95**, 259–268 (2002).
- [3] <https://sci-bots.com/>
- [4] Dixon, C., Ng, A. H. C., Fobel, R., Miltenburg, M. B. & Wheeler, A. R. An inkjet printed, roll-coated digital microfluidic device for inexpensive, miniaturized diagnostic assays. *Lab Chip* **16**, 4560–4568 (2016).
- [5] Kim, H. et al. Automated Digital Microfluidic Sample Preparation for Next-Generation DNA Sequencing. *J. Lab. Autom.* **16**, 405–414 (2011).
- [6] Rival, A. et al. An EWOD-based microfluidic chip for single-cell isolation, mRNA purification and subsequent multiplex qPCR. *Lab Chip* **14**, 3739–3749 (2014).
- [7] Moore, J. A. et al. Automated electrotransformation of Escherichia coli on a digital microfluidic platform using bioactivated magnetic beads. *Biomicrofluidics* **11**, 014110 (2017).
- [8] Ping-Yi, H., Hsin-Yi, L., Shih-Kang, F., Yen-Wen, L. & Lu, Y.-W. Mechatronic Systems in Digital Microfluidics. *Int. J. Autom. Smart Technol.* **4**, 216–221 (2014).
- [9] Fobel, R., Fobel, C. & Wheeler, A. R. DropBot: An open-source digital microfluidic control system with precise control of electrostatic driving force and instantaneous drop velocity measurement. *Appl. Phys. Lett.* **102**, 193513 (2013).
- [10] Gong, J. & Kim, C.-J. All-electronic droplet generation on-chip with real-time feedback control for EWOD digital microfluidics. *Lab Chip* **8**, 898 (2008).
- [11] Edwards, A. M. J., Brown, C. V., Newton, M. I. & McHale, G. Dielectrowetting: The past, present and future. *Curr. Opin. Colloid Interface Sci.* **36**, 28–36 (2018).
- [12] J. Li and C.-J. Kim, Shrinking down the electronics for handheld digital microfluidic systems, *International Meeting on Electrowetting*, Cincinnati, USA, (2014), Poster.

- [13] S.-K. Fan, C. Hashi, and C.-J. Kim, Manipulation of multiple droplets on N×M grid by cross-reference EWOD driving scheme and pressure-contact packaging. *Proc. IEEE Conf. MEMS*, Kyoto, Japan, 694–697 (2003).
- [14] J. Gong, S.-K. Fan, and C.-J. Kim, Portable digital microfluidics platform with active but disposable Lab-On-Chip. *Proc. IEEE Conf. MEMS*, Maastricht, the Netherlands, 355–358 (2004).
- [15] J. Li and C.-J. Kim, Development of handheld digital microfluidic systems, *Proc. Int. Conf. Miniaturized Systems for Chemistry and Life Sciences (μTAS)*, Gyeongju, Korea, 1199-1201, (2015).
- [16] J. Gong & C.-J. Kim. Direct-Referencing Two-Dimensional-Array Digital Microfluidics Using Multilayer Printed Circuit Board. *J. Microelectromech. Syst.* **17**, 257–264 (2008).
- [17] <https://nanoporetech.com/products/voltrax>
- [18] J. Li and C.-J. Kim, Device and method for aligning sample substrate to cover substrate having protruding pins, US Provisional No. 62/675,414 (2018).
- [19] <https://www.baebies.com/>
- [20] <https://www.genmarkdx.com/>
- [21] Cho & D. Z. Pan, A High-performance droplet routing algorithm for digital microfluidic biochips. *IEEE Trans. Comput. Des. Integr. Circuits Syst.* **27**, 1714–1724 (2008).

# Chapter 5 Low-cost and Low-topography Fabrication of Multilayer Interconnections for Microfluidic Devices

## 5.1 Introduction

Microdevices that have a large number of electrical connections require multilayer interconnections. However, there are trade-offs for the typical approaches for multilayer interconnections. The integrated circuit (IC) fabrication technique used for electrical interconnections of many MEMS devices [1] is expensive and not practical for applications that require devices of a large area (e.g., > 50 mm) and even for disposable applications, such as microfluidics devices. Printed circuit board (PCB) is often utilized for its low-cost multilayer routing [2], [3] but limits the selection of substrate material and integration with MEMS fabrication. It also adds significant bulk. Other unique interconnection techniques, such as glass-in-silicon wafer processing [4], require expensive processing. A convenient fabrication method is desired to meet general interconnection requirements. We turn our attention to the anodic process once explored for metallization for multilevel ICs [5]. For our adaption in this report, the conduction lines are made of tantalum, and insulation is tantalum pentoxide electrochemically grown from the tantalum. Other metals that can be anodized, such as aluminum, may also be used instead of tantalum. In this report, we explore successive repetition of patterned anodization to obtain multilayer interconnections.

Microdevices such as electrowetting-on-dielectric (EWOD) digital microfluidic devices require addressing hundreds of electrodes independently. Multilayer interconnections are needed for such a device. Since microfluidic devices are often disposable, the cost of fabricating a device is the limiting factor for practical use. Currently there are two types of successfully commercialized EWOD devices: one is PCB type [6], [7] and the other is active-matrix type [8]. The advantage of



the PCB type is its low cost, which allows large area devices. However, the surface topography of a PCB substrate hinders the EWOD droplet manipulations on such a device [2]. One solution is to perform planarization on the PCB device [2]. However, this method adds cost, and it is challenging to planarize evenly on large and flexible material. One could use a thick ( $> 10 \mu\text{m}$ ) dielectric layer to alleviate the transition between the areas of different thicknesses but it does not completely solve the problem. On the other hand, the emerging electrowetting products such as VolTRAX from Oxford Nanopore Technologies and the liquid handling platform from Aqdrop, a joint venture by Sharp and Foxconn, are using the thin-film transistor (TFT) liquid crystal display (LCD) substrate to fabricate active matrix EWOD devices [9]. Although the active matrix devices are free from the topography issue, the manufacturing process is still complex and expensive. Accordingly, they are designed to have a small area to compensate for the cost, limiting their applications and test throughputs (i.e., the number of experiments that can run concurrently).

Considering the above trade-offs, we adopted a method to fabricate multilayer interconnections by metal anodization [5] to obtain microdevices with minimal topography and simple manufacturing processes. The utility is demonstrated by developing and demonstrating an EWOD device.

## **5.2 Fabrication processes**

Anodized metal such as tantalum pentoxide is an electrically stable (dielectric strength = 6-7 MV/cm) material with high corrosion resistance that is used in high performance capacitors [10] and microelectronics [11]. Our multilayer metal interconnections process relies on partial or full anodization of blanket-deposited metal layers to form insulation layers between them or to define electrode patterns, respectively, eliminating the need to deposit and pattern insulation layers. The following three steps are repeated for each level of the interconnections: (1) blanket-deposition

of a valve metal layer, (2) selective, full oxidation of the metal using defined PR as the mask and through-metal anodization, and (3) selective, partial oxidation of the metal, using defined PR as the mask and time-controlled anodization. In this paper, we developed three-level interconnections designed for EWOD devices with tantalum as the valve metal, following the process flow presented in Figure 5-1.

In Figure 5-1(a), a 250 nm of tantalum was deposited by sputtering (Denton Discovery 550 Sputtering System) on 0.7 mm-thick, 10 mm-diameter glass wafer (Schott BOROFLOAT®). In Figure 5-1(b), a 12  $\mu\text{m}$ -thick PR (MicroChemicals AZ4620) was spin-coated and patterned with Mask 1 in a contact aligner (Karl Suss MA6). To prevent peeling of the PR during the subsequent anodization step, it was important to ensure good adhesion. Before the PR coating, the substrate was dipped into Piranha solution (by mixing 20 mL 30 wt%  $\text{H}_2\text{O}_2$  with 60 mL 96 wt%  $\text{H}_2\text{SO}_4$ ) quickly (only a few seconds) followed by DI water rinsing and drying on a hot plate (150°C, 2 min). To prevent any electrochemical reaction (e.g., electrolysis) on the tantalum under the PR during the anodization, a thick PR was used (12  $\mu\text{m}$  here) and hard-baked extensively (on 120°C hot plate, 30 min here). Slow cool down (turn off the hot plate with the wafer on and wait until room temperature is reached) was preferred to avoid PR cracking.

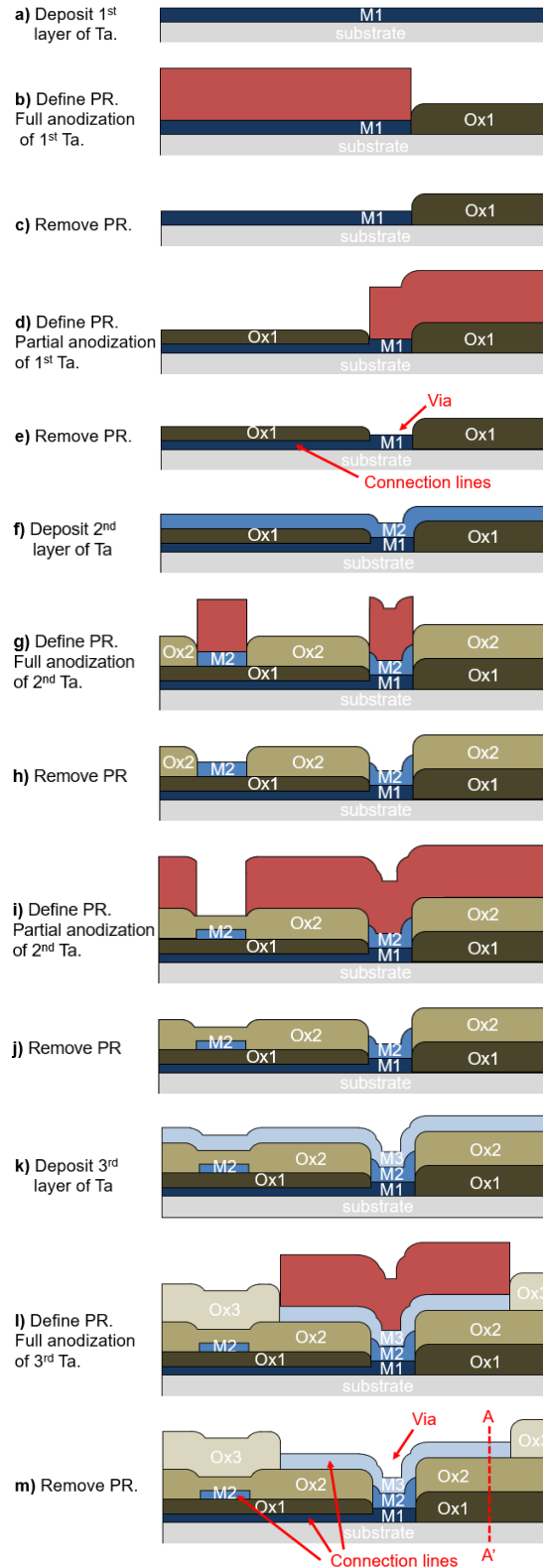


Figure 5-1. Process flow to fabricate the proposed multilevel interconnections, drawn for three layers. Each anodization step was performed while masked by defined PR. Tantalum was used in the current report for the metal layers. M1: first Ta layer; M2: second Ta layer; M3: third Ta layer; Ox1: first Ta<sub>2</sub>O<sub>5</sub> layer; Ox2: second Ta<sub>2</sub>O<sub>5</sub> layer; Ox3: third Ta<sub>2</sub>O<sub>5</sub> layer.

In Figure 5-1(c), the exposed tantalum was fully anodized in 0.01 wt% KI solution using a tantalum sheet as the cathode. The bias voltage applied between the anode wafer the cathode sheet was gradually increased to 300-350 V to obtain full anodization. The full anodization through the entire thickness of the metal layer was critical because this anodized material (i.e., insulating material) electrically separates all the electrodes within the given conductive layer. During the anodization, the region being anodized turns from opaque to translucent and to transparent, which indicated full anodization. The progress of anodization was also monitored by measuring the voltage or current between cathode and KI solution [12]; the voltage and current drop as the anodization nears completion This full anodization defined the conductive pattern on the first metal layer. In Figure 5-1(d), the existing PR was removed, and another 12  $\mu\text{m}$ -thick PR was spin-coated and defined with Mask 2, following the same PR preparation of Figure 5-1(b). In Figure 5-1(e), the exposed tantalum was partially anodized using 100 V to grow an insulation layer on top. The 100 V voltage was kept constant on for 1 hour [12]. The regions of the metal layer not anodized under the PR would become conductive vias later. The PR was, then, removed.

In Figures 5-1(f) and 5-1(j), similar steps were repeated to fabricate the second layer of interconnection. After depositing the second metal layer in Figure 5-1(f) and coating and defining PR with Mask 3 in Figure 5-1(g), the second metal layer was fully anodized to pattern the electrodes as shown in Figure 5-1(h). After coating and defining another PR with Mask 4 in Figure 5-1(i), the exposed second metal layer was partially anodized to grow an insulation layer on top, as shown in Figure 5-1(j). In Figures 5-1(k) and 5-1(m), the final, third layer of interconnection was fabricated. After depositing the third metal layer in Figure 5-1(k) and coating and defining PR with Mask 5 in Figure 5-1(l), the third metal layer was fully anodized to pattern the electrodes as shown in Figure 5-1(m).

During the anodization processes in Figures 5-1(b), 5-1(g) and 5-1(l), the PR needed to protect the underneath tantalum from being anodized at a high bias up to 300-350 V. We used AZ 4620, a general-purpose PR not designed to withstand high voltage only for convenience; a different protection material with higher electrical strength would be desired in future research. In this report, we successfully repeated deposition and anodization of 250 nm tantalum three times to obtain a total of 750 nm-thick tantalum at the thinnest and 1.5  $\mu\text{m}$ -thick tantalum pentoxide at the thickest. On the complete device, illustrated in Figure 5-1(m), the height difference between the lowest and the highest point was to be around 750 nm. This topography is good (smooth) enough for many microdevices over a wide range of applications without calling for planarization and significantly smaller compared with the rough topography ( $> 10 \mu\text{m}$ ) of PCB-based microdevices.

### **5.3 Confirmation of partial and full anodization**

Because all the insulations between the electrodes are provided by anodizing metals rather than adding insulating materials in the reported process, it is important to confirm all the anodized metals function as intended. After the partial anodization, which is to form a tantalum pentoxide layer between tantalum layers, the remaining tantalum should have a proper sheet resistance. Noting the resistance of a conduction line is determined by the thickness of the remaining tantalum after partial anodization, which is affected by various local process parameters, such as current density of anodization, ionic concentration of the anodizing solution, temperature of the process, etc., we performed a series of characterization tests. We exposed the two ends of test conduction lines to facilitate resistance measurement using a probe station. As shown in Figure 5-2(a), the conduction lines in the 1st tantalum layer were formed by turning the top half of the deposited tantalum layer into tantalum peroxide, i.e., an insulator. The situation is similar for the conduction

lines in the 2nd tantalum layer, as shown in Figure 5-2(b). The conduction line in the 3rd tantalum layer was expected to be as thick as the deposited tantalum and twice as thick as the conduction lines in the 1st and 2nd tantalum layers because no partial anodization process was needed for the top layer. Because one half of the tantalum thickness was to be consumed for the partial anodization, the resistance of the conduction lines in the 3rd tantalum layer was expected to be one half of that in the first and second tantalum layers. In the characterization tests, the resistances of the connection lines were measured to be 2.5-16 k $\Omega$  for the 1st (bottom) tantalum layer, 2.7-13.8 k $\Omega$  for the 2nd (middle) tantalum layer, and 0.6-7.3 k $\Omega$  for the 3rd (top) tantalum layer, confirming the connectivity. With the same width and thickness across the device, resistances of connection lines in the same tantalum layer varied by their lengths. After the full anodization, which is to pattern electrodes within a tantalum layer, there should be no tantalum left below the tantalum pentoxide. To test the possibility of the residual tantalum shorting adjacent conduction lines, we also measured the resistance between conduction lines designed to be isolated from each other for each of the three tantalum layers. Resistance between adjacent connection lines was measured to be infinite, confirming successful electrical isolation.

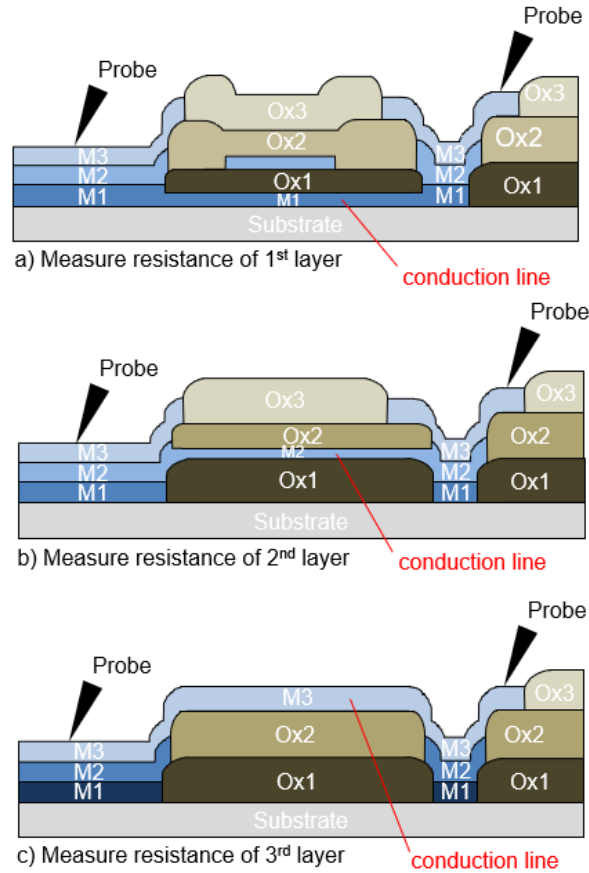


Figure 5-2. Resistance measurement for each layer. The 3rd conductive layer was thicker than the 1st and 2nd because it was not anodized. M1: first Ta layer; M2: second Ta layer; M3: third Ta layer; Ox1: first Ta<sub>2</sub>O<sub>5</sub> layer; Ox2: second Ta<sub>2</sub>O<sub>5</sub> layer; Ox3: third Ta<sub>2</sub>O<sub>5</sub> layer.

## 5.4 Application to EWOD microfluidic devices

Utility of the proposed interconnections was demonstrated by implementing the developed process for EWOD [13]. The EWOD device contained 100 independently controlled electrodes spaced as an array of 10x10 electrode pads that required a multilayer electrical connection. On a typical EWOD device, a relatively high voltage (50-100 V) is applied on each of the electrodes to manipulate droplets on them. Defect-free insulation between adjacent electrodes and their connection lines is essential for successful high voltage operation. An EWOD device with multilayer interconnection fabricated using to the process of Figure 5-1 is shown in Figure 5-3.

However, for the EWOD dielectric layer, we deposited a 1  $\mu\text{m}$  silicon nitride by PECVD rather than partially anodizing the 3rd tantalum layer because of the polarity and frequencies dependencies [14]. The fabrication was completed by spin coating Teflon to form the hydrophobic topcoat. On the device, 10x10 EWOD electrode pads were made with the 3rd tantalum layer, and each EWOD pad was exclusively connected to one of the 100 contact pads located near one edge of the device through the conduction lines of all 3 tantalum layers. To reveal the different layers on the device, we cleaved the device through an EWOD pad region and took SEM pictures (shown in Figure 5-3c) using ZEISS Supra 40VP.



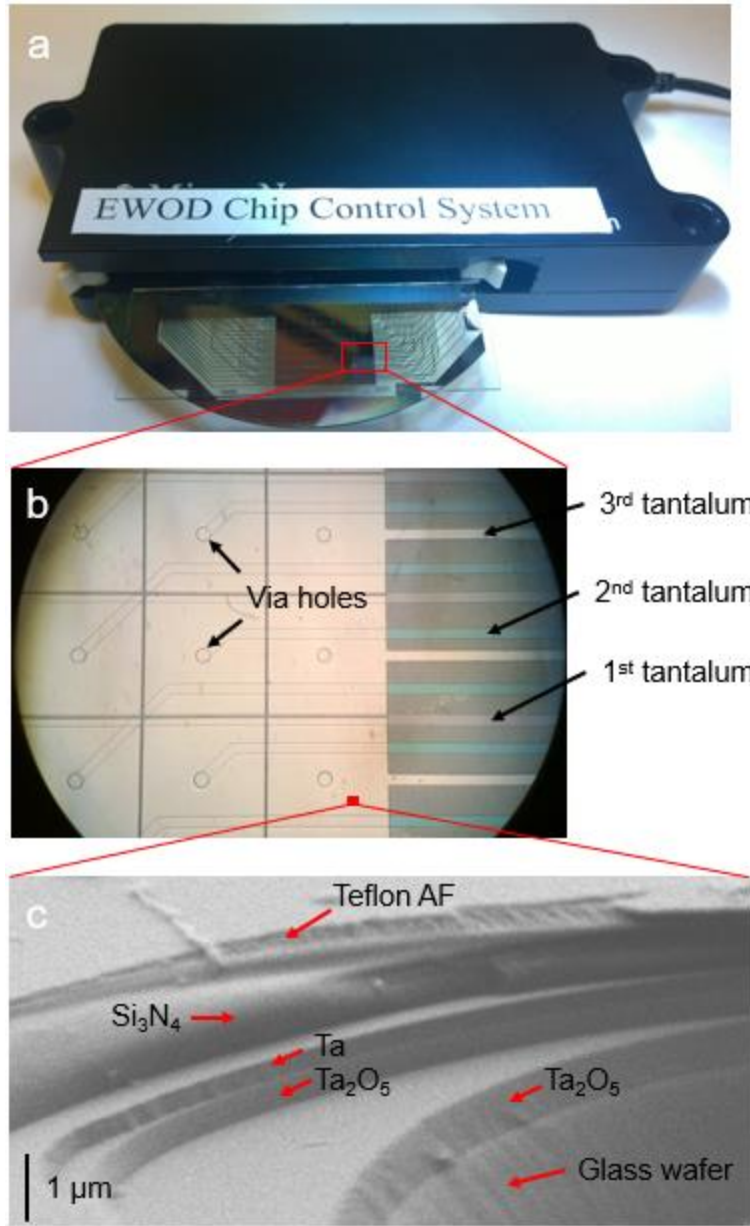


Figure 5-3. The proposed multilayer interconnection technology applied to EWOD devices as a demonstration. **a**, A fabricated EWOD device with 100 (10X10 array) independently controllable electrode pads is inserted into a custom-developed electronic control system through 244 pin socket. **b**, An optical micrograph of a portion of the EWOD device, showing 9 electrode pads with vias connected to 9 conduction lines of 3 different tantalum layers. The 1st and 2nd tantalum layers are visible through the overlaying tantalum pentoxide that is transparent. **c**, A SEM image of a broken device to reveal all the layers of A-A' in Figure 5-1(m) – Teflon,  $\text{Si}_3\text{N}_4$ , the 3rd Ta layer,  $\text{Ta}_2\text{O}_5$  from the 2nd Ta layer,  $\text{Ta}_2\text{O}_5$  from the 1st Ta layer, and glass wafer. A dielectric layer ( $\text{Si}_3\text{N}_4$ ) and hydrophobic layer (Teflon) was deposited on the multilayer interconnected device to complete an EWOD device.

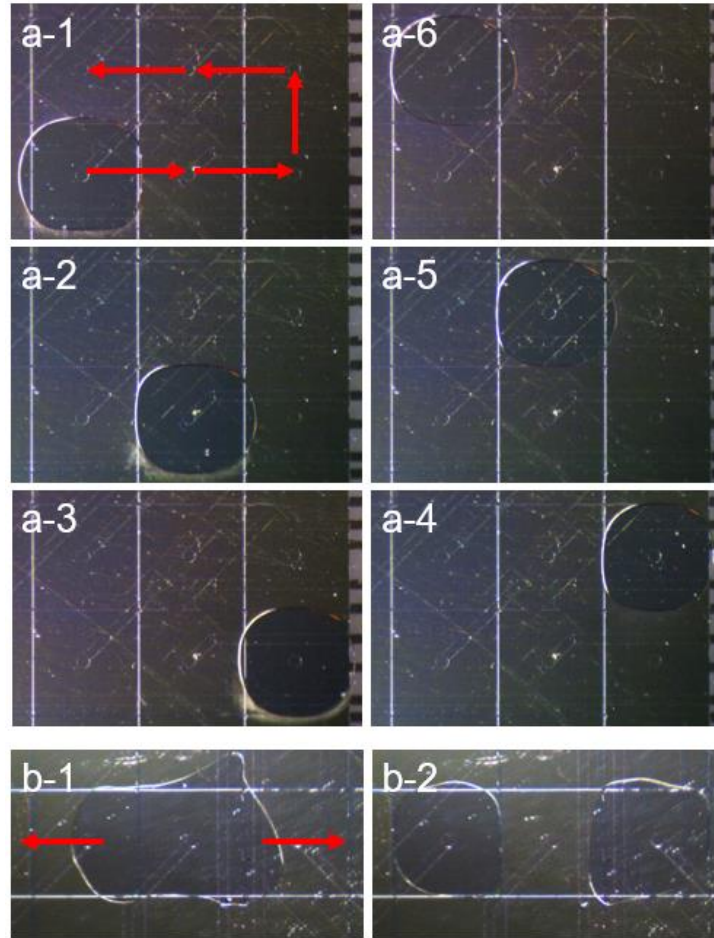


Figure 5-4. Digital microfluidic operations on an EWOD device with 3-layer interconnections. The transparent top plate is made of a glass wafer coated with ITO and Teflon. **a**, Sequential images of droplet movements. Arrows indicate the moving directions of the droplet. **b**, A droplet split into two daughter droplets.

Figure 5-4 shows the basic digital microfluidic operations (droplet translations in **a** and droplet splitting in **b**) confirmed on the fabricated EWOD device with 3-layer interconnections. The demonstration was performed using a handheld EWOD control system developed in our lab, shown in Figure 5-3a. The transparent areas in Figures 5-3a and 5-3b indicate opaque tantalum (750 nm thick) has been fully anodized to transparent tantalum pentoxide (1.5  $\mu\text{m}$ -thick) on transparent glass wafer. A sine wave of 70 V<sub>rms</sub> and 1 kHz was used to perform two basic droplet manipulation functions for digital microfluidics (i.e., moving and splitting) with DI water.

Although the 3rd metal is made of tantalum, which is non-transparent in the current device, it can be made of indium tin oxide (ITO) if fully transparent devices are desired.

One point should be noted for EWOD actuations of the above device. For successful operations, all EWOD pads should be connected to ground or high voltage and avoid floating. Since the insulation layer, i.e., the anodized metal, on the metal has a thickness comparable to the dielectric layer of a typical EWOD device, the conduction lines placed underneath the electrode pad (the 1st and 2nd metal shown in Figure 5-3b) may induce unintended electrowetting effect to the droplet if the electrode pad is floated. Another point to make is the limitation in the actuation voltage allowable for the EWOD devices made with the reported multilayer interconnection fabrication method. One cannot use voltages higher than the anodization voltage ( $\sim 100$  V) for EWOD actuation because it may trigger anodization under aqueous liquids during EWOD actuations. The proposed EWOD devices are suitable for relatively low voltage actuations.

## **5.5 Summary**

We have developed a low cost and low topography fabrication method to obtain multilayer interconnections without depositing and etching of insulating layers. We used this method to fabricate a 3-layer EWOD device. The maximum height difference for the topography on the device surface was  $0.75\ \mu\text{m}$ , and the gap between EWOD pads (i.e., feature size) was  $10\ \mu\text{m}$ , which is significantly better than an EWOD device made of a PCB substrate ( $> 10\ \mu\text{m}$  in maximum height difference and  $50\ \mu\text{m}$  gap between EWOD pads). Successful droplet manipulations were demonstrated in air (i.e., not requiring oil environment) to show its potential as a low-topography and small feature-size alternative to the PCB EWOD devices and a low-cost alternative to the active matrix TFT EWOD devices.

## 5.6 References

- [1] Van Kessel, P. F., Hornbeck, L. J., Meier, R. E. & Douglass, M. R. A MEMS-based projection display. *Proc. IEEE* **86**, 1687–1704 (1998).
- [2] C.-J. Kim and J. Gong, Chapter 6. EWOD Droplet Microfluidic Devices Using Printed Circuit Board Fabrication, in *Micro/Nano Technology Systems for Biomedical Applications*, Edited by C.-M. Ho, Oxford Press, 232-265, (2010).
- [3] J. Gong and C.-J. Kim, Direct-Referencing Two-Dimensional-Array Digital Microfluidics Using Multi-Layer Printed Circuit Board, *J. Microelectromechanical Systems*, **17**, 257-264 (2008).
- [4] Haque, R. M. & Wise, K. D. A 3D implantable microsystem for intraocular pressure monitoring using a glass-in-silicon reflow process. *IEEE 24th International Conference on Micro Electro Mechanical Systems*, 995–998 (2011).
- [5] Schwartz, G. C. & Platter, V. An Anodic Process for Forming Planar Interconnection Metallization for Multilevel LSI. *J. Electrochem. Soc.* **122**, 1508 (1975).
- [6] <https://baebies.com/products/seeker/>
- [7] <https://www.genmarkdx.com/solutions/systems/eplex-system/>
- [8] <https://nanoporetech.com/products/voltrax>
- [9] Hadwen, B. et al. Programmable large area digital microfluidic array with integrated droplet sensing for bioassays. *Lab Chip* **12**, 3305 (2012).
- [10] Byeon, S. G. & Tzeng, Y. High-performance tantalum oxide capacitors fabricated by a novel reoxidation scheme. *IEEE Trans. Electron Devices* **37**, 972–979 (1990).
- [11] Chaneliere, C., Autran, J. L., Devine, R. A. B. & Balland, B. Tantalum pentoxide (Ta<sub>2</sub>O<sub>5</sub>) thin films for advanced dielectric applications. *Mater. Sci. Eng. R Reports* **22**, 269–322 (1998).
- [12] Ueno, K., Abe, S., Onoki, R. & Saiki, K. Anodization of electrolytically polished Ta surfaces for enhancement of carrier injection into organic field-effect transistors. *J. Appl. Phys.* **98**, 114503 (2005).
- [13] W. C. Nelson and C.-J. Kim, Droplet Actuation by Electrowetting-on-Dielectric (EWOD): A Review, *Journal of Adhesion Science and Technology*, **26**, 1747–1771 (2012).
- [14] Huang, L.-X. & Koo, B. Sputtered-Anodized Ta<sub>2</sub>O<sub>5</sub> as the Dielectric Layer for Electrowetting-on-Dielectric. *J. Microelectromechanical Syst.* **22**, (2013).

## **Chapter 6    Summaries and Future Directions**

### **6.1 Dissertation summaries**

In this dissertation, we identified two bottlenecks that limit the growth of EWOD community. One is the reliability issue that originates from the dielectric layer, hydrophobic layer, and surface uniformity of an EWOD device. The other is the lack of device fabrication facilities and device control systems for the mass (researchers, entrepreneurs, students, hobbyists etc.) to perform electrowetting studies.

To solve the reliability issue, we proposed a new fluidic manipulation method - “electrodewetting”, which is free from dielectric and hydrophobic layer that caused reliability issues to EWOD. In a series of experiments, we verified electrodewetting’s working principle, demonstrated its reliability, characterized and identified its optimum working range, and finally built an electrodewetting device that can perform all four basic digital microfluidic operations (creating, moving, cutting and merging droplets) with low voltage (5 V). We further built a transparent electrodewetting device to show its potential in optical applications.

In helping the mass access to digital microfluidics, we proposed and started building a cybermanufacturing ecosystem. First, we proposed an EWOD CAD, which allows users to finish EWOD chip design within a few hours with little training. Second, we developed an electronic control system, which is compact and flexible enough to accommodate EWOD devices made with different materials, sizes, peripherals, and protocols. Third, we started arranging EWOD device manufacturers to provide EWOD devices developed under commonly useful design rules (for better reliability). In addition, we applied an interconnection fabrication method for multilayer EWOD device, which has better topography than PCB EWOD devices and lower cost than active

matrix TFT EWOD devices. Finally, we laid down the design work of the online portal, which links users to all the above services.

## **6.2 Future research directions**

As a new liquid handling method, the research directions of the electrodedewetting are wide open. It could be divided into three groups: 1) study of fundamental working principle; 2) characterization; and 3) device and applications. (1) Lippmann–Young equation explained the working principle for electrowetting and EWOD. It is worth to study if an equation or a mathematical model can be used to describe electrodedewetting. It will be useful to develop experimental setups different from the needle-droplet system adopted in this dissertation. (2) The characterization study should include exploration of various substrate materials, surface roughness, chemical treatment of the surface, various liquid combinations and surrounding environment. The goal is to optimize the electrodedewetting in action speed and contact angle change. (3) We should advance the understanding of the pros and cons of electrodedewetting against electrowetting. Various device configurations should be designed to take advantage of electrodedewetting in potential optical and biochemical applications.

The cybermanufacturing ecosystem should be implemented with continuous effort from us as well as the contributions from the EWOD community and industry. The electronic control system should be further improved to accommodate low voltage ( $< 20$  V) EWOD devices. The EWOD CAD should be improved to accommodate multilayer EWOD devices. When mature enough for public, the cybersystem should reach the mature biochemical companies to get them engage in development of EWOD products.

As for interconnection fabrication method for multilayer EWOD device, it is important to test how well other valve metals, such as aluminum, would work. Studies should be carried out to see if large area (for example 12'' x 18'') metal deposition is feasible to further reduce the manufacturing cost.